Title

Microbial and Mineral Controls over Soil Carbon Cycling and Storage: Process-based Modeling, Observational Syntheses, and Global Implications

Author

Georgiou, Katerina

Publication Date

2018

Peer reviewed|Thesis/dissertation

MICROBIAL AND MINERAL CONTROLS OVER SOIL CARBON CYCLING AND STORAGE:

Process-based Modeling, Observational Syntheses, and Global Implications

by

Katerina Georgiou

A dissertation submitted in partial satisfaction of the
requirements for the degree of

Doctor of Philosophy
in
Chemical Engineering
in the
Graduate Division
of the
University of California, Berkeley

Committee in charge:

Professor Margaret Torn, Co-Chair
Professor Ali Mesbah, Co-Chair
Professor David Schaffer
Professor John Harte

Spring 2018

MICROBIAL AND MINERAL CONTROLS OVER SOIL CARBON CYCLING AND STORAGE:

Process-based Modeling, Observational Syntheses, and Global Implications

by

Katerina Georgiou

ABSTRACT

Microbial and Mineral Controls over Soil Carbon Cycling and Storage:
Process-based Modeling, Observational Syntheses, and Global Implications

by

Katerina Georgiou

Doctor of Philosophy in Chemical Engineering

University of California, Berkeley

Professor Margaret Torn, Co-Chair
Professor Ali Mesbah, Co-Chair

Soil organic matter (SOM) is the largest actively-cycling terrestrial reservoir of carbon (C) and an integral component of thriving natural and managed ecosystems. Climate- and land-use-induced changes in plant inputs to soil may result in changes to soil organic carbon (SOC) storage with large implications for the global C balance. Despite the potential for large C feedbacks, the processes that dictate the response of SOC to changes in plant inputs are still poorly understood and inadequately represented in models, thus, limiting their predictive capability for policy and management decisions. The overarching goal of my Ph.D. research was to improve our process-level understanding of the response of SOC to changes in plant inputs, with interest in the competing microbial and mineral mechanisms that govern the decomposition and stabilization of SOC, respectively, and the capacity of soils to store C. To this end, I leveraged data collection and synthesis, meta-analysis, and process-based modeling to advance our understanding and provide predictive tools.

In Chapter 1, I provide an introduction and overview of the field of SOC modeling, and outline the trail map of my doctoral research. I then explore, in Chapter 2, the potential magnitude of the soil C sink over the last decade using remotely-sensed observations as a proxy for the rate of plant inputs. My findings suggest that soils have played a large role in the terrestrial carbon sink, especially in grassland ecosystems. This provides a strong motivation for better understanding the underlying mechanisms at play, since, as I show in Chapter 3, using simple SOC models to infer complex dynamics can lead to model artifacts and false mechanistic attribution. I highlight potential pitfalls and make recommendations for future modeling studies to include important mechanisms – e.g., microbial and mineral interactions – and to use more comprehensive data streams.

Accordingly, in Chapters 4 and 5, I focus on the representation of microbes and minerals, respectively, in process-based SOC models. Specifically, in Chapter 4, I diagnose unrealistic behaviors observed in recent mechanistic models and propose modifications by leveraging

ecological theory and analysis of long-term litter (plant input) manipulation experiments. In Chapter 5, I investigate the role of minerals in the capacity of soils to store C, and propose model formulations that match an extensive observational synthesis of mineral-associated C across soil types.

With advancements in process-based SOC models, and their widespread application, comes the need for accurate numerical methods to efficiently solve such systems of equations. Thus, in Chapter 6, I propose a novel numerical integration method that is uniquely suited for solving coupled, depth-resolved equations that arise in advection-dominated environmental systems. This class of equations is common in SOC modeling, and I present an example to that effect and assess numerical performance.

Finally, in Chapter 7, I close by discussing the broad implications of this research in the context of society. A deep understanding of soil C and nutrient cycling is essential for building predictive tools to better inform land management and conservation policy. I end by describing gaps and scaling challenges that motivate my future work.

To my parents, Efi and Tryphon,
for their love, inspiration, and unwavering support.

TABLE OF CONTENTS

LIST OF FIGURES

CHAPTER 2.

CHAPTER 3.

CHAPTER 4.

CHAPTER 5.

CHAPTER 6.

LIST OF TABLES

LIST OF ABBREVIATIONS

ABC	=	Aboveground Biomass Carbon
BBC	=	Belowground Biomass Carbon
C	=	Carbon
C_S	=	Concentration of soil organic carbon (gC/kg soil)
C_D	=	Concentration of dissolved organic carbon (gC/kg soil)
C_B	=	Concentration of soil organic carbon (gC/kg soil)
C_q	=	Concentration of mineral-associated organic carbon (gC/kg soil)
C_E	=	Concentration of enzymatic carbon (gC/kg soil)
CEC	=	Cation Exchange Capacity
CMIP	=	Community Model Intercomparison Project
CUE	=	Carbon Use Efficiency
DOC	=	Dissolved Organic Carbon
DIRT	=	Detritus Input and Removal Treatment
ECA	=	Equilibrium Chemistry Approximation
ENZ	=	Enzymatic Carbon
ESM	=	Earth System Model
FACE	=	Free-Air CO_2 Enrichment
FD	=	Finite Differences (first-order, implicit upwind scheme)
GCP	=	Global Carbon Project
HAC	=	High-activity Clay
HWSD	=	Harmonized World Soils Database
IPCC	=	Intergovernmental Panel on Climate Change
LAC	=	Low-activity Clay
LTBF	=	Long-term Bare Fallow
MAC	=	Method of Alternating Characteristics
MAP	=	Mean Annual Precipitation
MAT	=	Mean Annual Temperature
MBC	=	Microbial Biomass Carbon
MN	=	Mineral Nitrogen
MOA	=	Mineral-Organic Associations
MOC	=	Mineral-associated Organic Carbon
MSE	=	Mean-squared Error
N	=	Nitrogen
NBP	=	Net Biome Production
NPP	=	Net Primary Productivity
ODE	=	Ordinary Differential Equation
P	=	Phosphorus
PDE	=	Partial Differential Equation
SOM	=	Soil Organic Matter
SOC	=	Soil Organic Carbon
SSA	=	Specific Surface Area
τ	=	Turnover Time
TBC	=	Total Biomass Carbon (vegetation)
TN	=	Total Nitrogen

TRB = Total Reserve Bases
VOD = Vegetation Optical Depth

PREFACE

This dissertation is the product of my research between January 2014 and May 2018, funded by graduate fellowships awarded from the National Science Foundation and the Department of Energy. I have included only my own work in the chapters that follow; however, during this time I had the opportunity to engage and contribute to several fruitful collaborations which resulted in co-authored publications.

The work presented in the chapters that follow has been published or will be submitted for publications as:

> **Georgiou, K.,** C. D. Koven, W. J. Riley, M. S. Torn. Toward improved model structures for analyzing priming: potential pitfalls of using bulk turnover time. *Global Change Biology*, 21:12, 4298-4302 (2015).
>
> **Georgiou, K.,** R. Z. Abramoff, J. Harte, W. J. Riley, M. S. Torn. Microbial community-level regulation explains soil carbon responses to long-term litter manipulations. *Nature Communications*, 1-10 (2017).
>
> **Georgiou K.,** J. Harte, A. Mesbah, W. J. Riley. A method of alternating characteristics with application to advection-dominated environmental systems. *Computational Geosciences*, 22(3), 851-865 (2018).
>
> **Georgiou, K.,** et al. Evidence for the importance of soils and non-forest ecosystems in the terrestrial carbon sink. (*to be submitted*)
>
> **Georgiou, K.,** et al. The global mineralogical capacity of soils to store carbon. (*to be submitted*)
>
> **Georgiou, K.,** et al. Representing mineral-organic associations in soil carbon models: insights and ways forward. (*to be submitted*)

The following work (not described in this dissertation) has been a product of collaborations and has been published or will be submitted as follows:

> Koven, C. D., J. Q. Chambers, **K. Georgiou,** R. Knox, R. Negron-Juarez, W. J. Riley, V. K. Arora, V. Brovkin, P. Friedlingstein, C. D. Jones. Controls on terrestrial carbon feedbacks by productivity versus turnover in the CMIP5 Earth System Models. *Biogeosciences*, 12, 5211-5228 (2015).
>
> Wieder, W. R., S. D. Allison, E. A. Davidson, **K. Georgiou,** O. Hararuk, Y. He, F. Hopkins, Y. Luo, M. J. Smith, B. Sulman, K. Todd-Brown, Y-P. Wang, J. Xia, X. Xu. Explicitly representing soil microbial processes in Earth system models. *Global Biogeochemical Cycles*, 29:10, 1782-1800 (2015).

Luo, Y., A. Ahlström, S. D. Allison, N. Batjes, G. Bonan, V. Brovkin, N. Carvalhais, A. Chappell, P. Ciais, E. A. Davidson, A. Finzi, **K. Georgiou,** O. Hararuk, J. Harden, et al. Towards More Realistic Projections of Soil Carbon Dynamics by Earth System Models. *Global Biogeochemical Cycles*, 30, 40-56 (2016).

Rammensee, S., M. S. Kang, **K. Georgiou,** S. Kumar, D. V. Schaffer. Dynamics of Mechanosensitive Neural Stem Cell Differentiation. *Stem Cells*, 35, 497-506 (2017).

Castanha, C., B. Zhu, C. E. Hicks Pries, **K. Georgiou,** M. S. Torn. The effects of heating, rhizosphere, and depth on root litter decomposition are mediated by soil moisture. *Biogeochemistry*, 137: 267 (2018).

Abramoff, R. Z., M. S. Torn, **K. Georgiou,** J. Tang, W. J. Riley. Spatial gradients can hide temperature sensitivity of soil organic matter stocks. *Global Biogeochemical Cycles* (in review)

Sulman, B., J. Moore, R. Z. Abramoff, C. Averill, **K. Georgiou**, S. Kivlin, B. Sridhar, M. Hartman, G. Wang, W. Wieder, M. Bradford, Y. Luo, M. Mayes, E. Morrison, W. J. Riley, A. Salazar, J. Schimel, J. Tang, A. Classen. Multiple models and experiments underscore large uncertainty in soil carbon dynamics. *Ecology Letters* (in review)

ACKNOWLEDGEMENTS

Many individuals, institutions, and funding agencies have supported me intellectually, financially, and emotionally throughout my doctoral studies.

The NSF GRFP and DOE SCGSR programs granted me the freedom to pursue my own research questions and to think creatively. The NSF GRFP was instrumental in allowing me to find my passion in terrestrial biogeochemistry, and I am forever grateful to Prof. David Schaffer, Prof. Sanjay Kumar, and their labs for their support and encouragement during this time of introspection and exploration. I would also like to thank the UC Berkeley Graduate Division Travel Grant and the LBNL TES SFA for the opportunity to attend diverse conferences and strengthen my collaborative network. The Department of Chemical and Biomolecular Engineering at UC Berkeley has been incredibly flexible with my trajectory and I am grateful for the many opportunities they have allowed me to pursue and the teaching experiences they have facilitated. Kay Burns in the Energy and Resources Group has also gone above-and-beyond her responsibilities to help me on many occasions.

I have had several mentors and close collaborators throughout my graduate studies, who have greatly shaped my scientific thoughts and philosophy. I would first like to thank my advisor, mentor, and friend, Prof. Margaret Torn, for her unwavering encouragement, enthusiasm, brainstorming sessions, and keen attention to the scientific process, but also, for keeping an open mind when she received an e-mail four and a half years ago with the subject line “Chem. Eng. student interested in your research!” I am also grateful to Dr. Bill Riley for his contagious curiosity and passion for terrestrial biogeochemistry, for always challenging me to explore alternative hypotheses, and for the many long discussions, and to Prof. John Harte for keeping me grounded through questions that probe my understanding of the natural world, for his encouragement during difficult times and opportunities for growth, and for shaping my modeling philosophy through his inspiring quest for simplicity on the other side of complexity. I thank Prof. Ali Mesbah, Prof. Danielle Tullman-Ercek, and Prof. Teresa Head-Gordon for challenging me to grow as a scientist and as a person during my qualifying exam, and Prof. Ali Mesbah and Prof. David Schaffer for their insightful comments as part of my dissertation committee.

I have been fortunate to have a community at both UC Berkeley and LBNL, and I owe a lot to both the Harte and TES SFA lab groups. They adopted me in a time of transition, and I am fortunate to call many of them close friends in addition to colleagues. Cristina Castanha, Rose Abramoff, and Caitlin Hicks Pries have taught me so much about the practical side of soil science through many trips to the field, and Jenny Soong, Alison Hoyt, Peter Nico, Eoin Brodie, and Rachel Porras have contributed to many of my ideas on microbial and mineral dynamics. Lydia Vaughn and Danielle Svehla have been incredibly supportive and inspirational throughout my time at UC Berkeley. I would also like to recognize Charlie Koven for his deep understanding, inquisitive nature, and insightful feedback, and, beyond Berkeley, Anders Ahlström for his contagious excitement, brainstorming sessions, and generous support over the years, and Will Wieder for his encouragement and inclusivity from early in my graduate studies.

Many close friends have provided support and joined me on adventures during my time at UC Berkeley, making the experience so fun and memorable! Sukanya and Neelay have always been

there for me, from homework sessions at the very beginning to many long conversations, gardening parties, and dinners throughout. I also want to thank Cristina and Sid (for the unwavering support, quince jelly weekends, beach outings, after-work hikes, and many gourmet home-cooked meals), Karthik (my birthday buddy), Pete (for the many climbing adventures and teaching me to trad), Meredith (for her inspiring strength and support, and our climbing and brunch get-togethers), Aamod (for the random ponderings and crossing paths when we least expect it), Siobhan and Laura (for always being there for me), Grace and Ranjit (for the late night chats), Taylor, Rose, Alison, JP, Trevor, and many others for the countless happy hours, social outings, adventures, and dinners.

Above all, I'd like to thank my family. My parents, Efi and Tryphon, for their love, unwavering support, and endless inspiration, as academics themselves. They always encourage me to work hard, have fun, and believe in myself; at times, they know me better than I know myself. My brother, Thomas, has always been there for me (in his own way and when time permits!) and inspires me through his own passions. My aunt, Eleni, and late grandma, Georgia, for the many Sunday Skype sessions, luring me back to Greece every summer, and always putting things in perspective. And to the rest of my Greek family who have brought so much laughter and joy along the way. To my Mexican family, Queta, Samuel, and Paulina, for their constant love and support, and for the many nice dinners, movie nights, and family travels. And finally, to Diego, for his love and multidimensional support, his unparalleled determination to make the world a better place and endless enthusiasm to try new things, for teaching me to ride waves and accompanying me up rock walls and trees, and for reminding me to live life to the fullest.

Thank you all.

CHAPTER 1: INTRODUCTION

INTRODUCTION

"For all things come from earth, and all things end by becoming earth."
– *Xenophanes* (580 B.C.E.)

Soil organic matter (SOM) is the largest actively-cycling terrestrial reservoir of carbon, containing more than three times the *carbon* (C) present in vegetation globally (Jobbagy and Jackson, 2000; Houghton, 2007). It is an integral component of thriving natural and managed ecosystems, and provides multiple co-benefits for plants, animals, and humans – e.g., it contains nutrients that support plant growth and yields, retains water and reduces runoff, resists erosion, improves water quality, and sequesters C to reduce greenhouse gas emissions. The amount of C sequestered in soils results from the difference between plant C inputs and CO_2 released by heterotrophic respiration, a balance regulated by biological, geochemical, and hydrological factors. When the *plant inputs* that enter soil change due to anthropogenic land-use or climate-induced land-cover change, soil C storage also changes over decadal to centennial timescales as a result (Bowden *et al.*, 2014; Lajtha, Bowden and Nadelhoffer, 2014). However, the magnitude and location of such changes to *soil organic carbon* (SOC) stocks remain uncertain, due to gaps in process-level understanding, a paucity of synthesized data across soil types, and a lack of multi-scale process representation in predictive soil biogeochemical models.

Soil as a complex system and current model limitations

Soils are populated by an immense diversity of microbes, particularly bacteria and fungi, which drive SOC decomposition and formation. Plants are also a key part of this microhabitat, providing organic matter to the soil through their roots and leaves (i.e., below- and aboveground inputs, respectively). These diverse biotic components interact chemically and physically with each other, and with the surrounding heterogeneous matrix of soil minerals and aggregates, at the micro-scale to drive emergent macro-scale biogeochemical cycling. As such, soils constitute a complex and multi-scale system, where small-scale processes interact to give rise to larger-scale phenomena through hierarchical self-organization and nonlinear interactions. Yet, most of this complexity is absent from current SOC models, limiting their ability to accurately predict SOC stocks, age, and response to perturbations.

In most regional- and global-scale biogeochemical models, SOC decomposition is linearly proportional to the size of each soil C pool (i.e., first-order models) with rate modifiers that reflect environmental (e.g., temperature, moisture) controls. However, this formulation is inherently unable to reproduce potentially critical feedbacks, such as *priming* (accelerated decomposition) of native SOC stocks in response to increased plant inputs to the soil (Kuzyakov, 2010). Consequently, first-order SOC models have been challenged in recent decades, calling for process-based model formulations that reflect our current understanding (Schmidt *et al.*, 2011).

The role of microbes and minerals in SOC decomposition and stabilization

Soil microbial activity mediates SOC decomposition and, thus, increases in microbial activity following increases in plant inputs may limit SOC accumulation by stimulating decomposition (Kuzyakov, 2010; Zhu *et al.*, 2014). '*Microbial SOC models'* seek to capture this potential carbon-concentration feedback by explicitly representing microbial or enzymatic degradation of

SOC (Wieder *et al.*, 2015a). Decomposition rates thus depend not only on the size of the SOC pool, but also on the size and composition of the decomposer microbe pool (Parnas, 1975, 1976; Harte, 1982; Harte and Kinzig, 1993; Schimel and Weintraub, 2003; Wieder *et al.*, 2015a). Many macro-scale microbial models have been proposed in recent years, as part of a burgeoning effort to understand and predict soil biogeochemical dynamics (Allison, Wallenstein and Bradford, 2010; German *et al.*, 2012; Wieder *et al.*, 2014; Wieder *et al.*, 2015b). Such models have even been applied to make predictions at the global scale (Wieder, Bonan and Allison, 2013; Sulman *et al.*, 2014), despite limited mathematical analyses of their dynamics and response to long-term perturbations (Wang *et al.*, 2014, 2016; Hararuk, Smith and Luo, 2015; Sierra and Muller, 2015).

Chemical and physical limitation of microbial access to otherwise decomposable organic substrates plays a crucial role in preserving SOM (Conant *et al.*, 2011; Schmidt *et al.*, 2011; Dungait, Hopkins and Gregory, 2012; Cotrufo *et al.*, 2013; Lehmann and Kleber, 2015). Indeed, *mineral-associated organic carbon* (MOC) constitutes a large portion (30-90%) of total SOC stocks and, since such associations can protect substrates from microbial attack, MOC turnover times can be up to 100 times longer than free SOC (Kleber *et al.*, 2015). Despite the major role of *mineral-organic associations* (MOAs) in SOC stabilization and preservation, decidedly less attention has been afforded to their explicit representation in models. Most SOC models, and in particular first-order models, represent the effects of minerals implicitly using soil texture (i.e., % clay and silt) as a proxy. Recently, process-based models have implemented explicit representations of sorption, including linear (Sulman *et al.*, 2014; Wieder *et al.*, 2015) and Langmuir (Wang, Post and Mayes, 2013; Tang and Riley, 2015; Dwivedi *et al.*, 2017) isotherms. However, these formulations have yet to undergo rigorous validation and, furthermore, their parameterization at global scales remains a challenge.

Changes in plant inputs to the soil: motivation and implications

Climate and land-use change invariably affect the amount of plant C inputs that enter the soil – e.g., through changes in plant productivity, rooting depth, and allocation (Stulen and den Hertog, 1993; Hungate *et al.*, 1997; Phillips *et al.*, 2006; Lichter *et al.*, 2008; Norby *et al.*, 2016). While there is evidence that increasing C inputs to the soil can enhance C sequestration (Lichter *et al.*, 2008; Lajtha *et al.*, 2014), there are studies with contrasting results that argue otherwise (Fontaine *et al.*, 2004; Crow *et al.*, 2009; Pisani *et al.*, 2016). Thus, the net balance between C fluxes to and from the soil, and the underlying processes that dictate these responses, remain uncertain. Long-term litter manipulations are an underutilized resource for exploring these mechanisms and validating macro-scale model representations. While litter manipulations spanning diverse geographical areas have been established and maintained over the past several decades (Barré *et al.*, 2010; Fekete *et al.*, 2011; Lajtha *et al.*, 2014), a comprehensive cross-site data synthesis and analysis has yet to be performed. Two groups of long-term C-input experiments of particular interest are the *Detritus Input and Removal Treatment* (DIRT) sites, which have doubled (2x) and removed (0x) plant inputs entering the soil, and the *Long-term Bare Fallow* (*LTBF*) sites, which have removed (0x) plant inputs entering the soil over several decades. Such experiments are particularly useful for informing divergent process-based SOC model formulations, and have broad implications for both natural and managed ecosystems under a changing climate.

Dissertation trail map: research goals and questions

The overarching goal of my dissertation research is *to better understand how soil microbial processes and mineral-organic associations modulate macro-scale SOC cycling and, specifically, the response of SOC to changes in plant inputs.* Scaling dynamics – from the *micro-scale* (1 μm to 1 mm) where decomposition of SOC occurs, to the *macro-scale* (1 cm to 1 m) at which it is generally measured, to the *global-scale* (> 1 km) where *Earth System Models* (ESMs) are used to make policy-relevant predictions – is currently one of the greatest challenges for SOC modeling (Davidson, Savage and Finzi, 2014; Wieder et al., 2015a). I postulate that microbial community dynamics and mineral-organic associations are critical for understanding emergent macro-scale phenomena and better predicting SOC cycling. Given the uncertainty and potential magnitude of soil C feedbacks, it is critically important to better constrain estimates of past, current, and future SOC cycling to enhance prediction of climate and land-use scenarios and inform mitigation actions.

My driving hypothesis is that SOC models can be improved, for scientific inquiry and predictive capability, by explicitly representing coupled biotic and abiotic (i.e., microbial and mineral) processes that govern SOC decomposition and stabilization. While this is a long-term vision that will also guide my future research, much progress has been made in recent years and we are well on our way.

In the chapters to follow, I explore the overarching questions (Q):

1. How much have soils contributed to the global C sink in recent decades, and what is the potential capacity of soils to store C globally?
2. What key decomposition and stabilization mechanisms warrant representation in process-based SOC models, and how should they be represented?
3. What numerical integration methods are best suited to the unique nature of soil biogeochemical models, and what advantages do such methods confer?

To address these questions, my research was divided into five primary objectives:

Chapter 1: ***The role of soil in the global C sink***
Objective: Explore the potential magnitude of the soil C sink over the last decade using remotely-sensed observations to inform the rate of plant inputs [Q1].

Chapter 2: ***Pitfalls of simple SOC models & ways forward***
Objective: Elucidate potential pitfalls of using simple SOC models to infer complex dynamics and make recommendations for future studies [Q2].

Chapter 3: ***Microbial community dynamics in SOC models***
Objective: Diagnose unrealistic behaviors observed in recent microbial models and propose modifications based on ecological theory and analysis of long-term litter manipulation experiments [Q2].

Chapter 4: ***Mineral-organic associations in models & implications for C storage***
Objective: Investigate the role of minerals in the capacity of soils to store carbon, and propose mathematical formulations that match a global observational synthesis of mineral-associated carbon across soil types [Q1, Q2].

Chapter 5: ***Numerical tools for environmental modeling***
Objective: Propose a novel numerical integration method that is uniquely suited for solving coupled, depth-resolved equations that arise in advection-dominated environmental systems [Q3].

In my research, I have leveraged data collection and synthesis, meta-analysis, dynamical and complex systems theory, and process-based modeling to address gaps in process-level understanding and propose mechanistic SOC model formulations that better predict soil C cycling and storage. The novelty of this research rests on integrating empirical and computational insights across disciplines – *from chemical engineering and mathematics to soil and earth system science* – and across spatiotemporal scales to improve process-based biogeochemical models and, thereby, further our quantitative understanding of the microbiological and geochemical contributions to large-scale terrestrial C cycling.

References

Allison, S. D., Wallenstein, M. D. and Bradford, M. A. (2010) 'Soil-carbon response to warming dependent on microbial physiology', *Nature Geoscience*. Nature Publishing Group, 3(5), pp. 336–340. doi: 10.1038/ngeo846.

Barré, P., Eglin, T., Christensen, B. T., Ciais, P., Houot, S., Kätterer, T., Van Oort, F., Peylin, P., Poulton, P. R., Romanenkov, V. and Chenu, C. (2010) 'Quantifying and isolating stable soil organic carbon using long-term bare fallow experiments', *Biogeosciences*, 7(11), pp. 3839–3850. doi: 10.5194/bg-7-3839-2010.

Bowden, R. D., Deem, L., Plante, A. F., Peltre, C., Nadelhoffer, K. and Lajtha, K. (2014) 'Litter Input Controls on Soil Carbon in a Temperate Deciduous Forest', *North American Forest Soils*, pp. S66–S75. doi: 10.2136/sssaj2013.09.0413nafsc.

Conant, R. T., Ryan, M. G., Ågren, G. I., Birge, H. E., Davidson, E. a., Eliasson, P. E., Evans, S. E., Frey, S. D., Giardina, C. P., Hopkins, F. M., Hyvönen, R., Kirschbaum, M. U. F., Lavallee, J. M., Leifeld, J., Parton, W. J., Megan Steinweg, J., Wallenstein, M. D., Martin Wetterstedt, J. Å. and Bradford, M. a. (2011) 'Temperature and soil organic matter decomposition rates - synthesis of current knowledge and a way forward', *Global Change Biology*, 17(11), pp. 3392–3404. doi: 10.1111/j.1365-2486.2011.02496.x.

Cotrufo, M. F., Wallenstein, M. D., Boot, C. M., Denef, K. and Paul, E. (2013) 'The Microbial Efficiency-Matrix Stabilization (MEMS) framework integrates plant litter decomposition with soil organic matter stabilization: Do labile plant inputs form stable soil organic matter?', *Global Change Biology*, 19(4), pp. 988–995. doi: 10.1111/gcb.12113.

Crow, S. E., Lajtha, K., Bowden, R. D., Yano, Y., Brant, J. B., Caldwell, B. A. and Sulzman, E. W. (2009) 'Increased coniferous needle inputs accelerate decomposition of soil carbon in an old-growth forest', *Forest Ecology and Management*, 258(10), pp. 2224–2232. doi: 10.1016/j.foreco.2009.01.014.

Davidson, E. A., Savage, K. and Finzi, A. C. (2014) 'A big-microsite framework for soil carbon modeling', *Global Change Biology*, 20, pp. 3610–3620. doi: 10.1111/gcb.12718.

Dungait, J. A. J., Hopkins, D. W. and Gregory, A. S. (2012) 'Soil organic matter turnover is governed by accessibility not recalcitrance', *Global Change Biology*, 18, pp. 1781–1796. doi: 10.1111/j.1365-2486.2012.02665.x.

Dwivedi, D., Riley, W. J., Torn, M. S., Spycher, N., Maggi, F. and Tang, J. Y. (2017) 'Mineral properties, microbes, transport, and plant-input profiles control vertical distribution and age of soil carbon stocks', *Soil Biology & Biochemistry*, 107, pp. 244–259. doi: 10.1016/j.soilbio.2016.12.019.

Fekete, I., Kotroczó, Z., Varga, C., Veres, Z. and Tóth, J. A. (2011) 'The effects of detritus input on soil organic matter content and carbon dioxide emission in a central European deciduous forest', *Acta Silvatica et Lignaria Hungarica*, 7, pp. 87–96.

Fontaine, S., Bardoux, G., Abbadie, L. and Mariotti, A. (2004) 'Carbon input to soil may decrease soil carbon content', *Ecology Letters*, 7(4), pp. 314–320. doi: 10.1111/j.1461-0248.2004.00579.x.

German, D. P., Marcelo, K. R. B., Stone, M. M. and Allison, S. D. (2012) 'The Michaelis-Menten kinetics of soil extracellular enzymes in response to temperature: A cross-latitudinal study', *Global Change Biology*, 18(4), pp. 1468–1479. doi: 10.1111/j.1365-2486.2011.02615.x.

Hararuk, O., Smith, M. J. and Luo, Y. (2015) 'Microbial models with data-driven parameters predict stronger soil carbon responses to climate change', *Global Change Biology*, 21(6), pp.

2439–2453. doi: 10.1111/gcb.12827.
Harte, J. (1982) 'Modeling Lake-water Mineralization Processes', *Journal of theoretical biology*, 99, pp. 553–569.
Harte, J. and Kinzig, A. P. (1993) 'Mutualism and Competition between Plants and Decomposers: Implications for Nutrient Allocation in Ecosystems', *The American Naturalist*, 141(6), p. 829. doi: 10.1086/285511.
Houghton, R. A. (2007) 'Balancing the Global Carbon Budget', *Annual Review of Earth and Planetary Sciences*, 35(1), pp. 313–347. doi: 10.1146/annurev.earth.35.031306.140057.
Hungate, B. A., Holland, E. A., Jackson, R. B., Chapin, F. S. I., Mooney, H. A. and Field, C. B. (1997) 'The fate of carbon in grasslands under carbon dioxide enrichment', *Nature*, 388, pp. 576–579.
Jobbagy, E. G. and Jackson, R. B. (2000) 'The vertical distribution of soil organic carbon and its relation to climate and vegetation', *Ecological Applications*, 10(2), pp. 423–436.
Kleber, M., Eusterhues, K., Keiluweit, M., Mikutta, C., Mikutta, R. and Nico, P. S. (2015) *Mineral – Organic Associations : Formation , Properties , and Relevance in Soil Environments*, *Advances in Agronomy*. Elsevier Ltd. doi: 10.1016/bs.agron.2014.10.005.
Kuzyakov, Y. (2010) 'Priming effects: Interactions between living and dead organic matter', *Soil Biology and Biochemistry*. Elsevier Ltd, 42(9), pp. 1363–1371. doi: 10.1016/j.soilbio.2010.04.003.
Lajtha, K., Bowden, R. D. and Nadelhoffer, K. (2014) 'Litter and Root Manipulations Provide Insights into Soil Organic Matter Dynamics and Stability', *Soil Science Society of America Journal*, 78(S1), p. S261. doi: 10.2136/sssaj2013.08.0370nafsc.
Lajtha, K., Townsend, K. L., Kramer, M. G., Swanston, C., Bowden, R. D. and Nadelhoffer, K. (2014) 'Changes to particulate versus mineral-associated soil carbon after 50 years of litter manipulation in forest and prairie experimental ecosystems', *Biogeochemistry*, 119(1–3), pp. 341–360. doi: 10.1007/s10533-014-9970-5.
Lehmann, J. and Kleber, M. (2015) 'Perspective The contentious nature of soil organic matter', *Nature*, 528, pp. 60–68. doi: 10.1038/nature16069.
Lichter, J., Billings, S. A., Ziegler, S. E., Gaindh, D., Ryals, R., Finzi, A. C., Jackson, R. B., Stemmler, E. A. and Schlesinger, W. H. (2008) 'Soil carbon sequestration in a pine forest after 9 years of atmospheric CO 2 enrichment', *Global Change Biology*, 14, pp. 2910–2922.
Norby, R. J., De Kauwe, M. G., Domingues, T. F., Duursma, R. A., Ellsworth, D. S., Goll, D. S., M, L. D., Luus, K. A., MacKenzie, A. R., Medlyn, B. E., Pavlick, R., Rammig, A., Smith, B., Thomas, R., Thonicke, K., Walker, A. P., Yang, X. and Zaehle, S. (2016) 'Model–data synthesis for the next generation of forest free-air CO2 enrichment (FACE) experiments', *New Phytologist*, 209, pp. 17–28.
Parnas, H. (1975) 'Model for decomposition of organic material by microorganisms', *Soil Biology & Biochemistry*, 7, pp. 161–169.
Parnas, H. (1976) 'A theoretical explanation of the priming effect based on microbial growth with two limiting substrates', *Soil Biology & Biochemistry*, 8, pp. 139–144.
Phillips, D. L., Johnson, M. G., Tingey, D. T., Catricala, C. E., Hoyman, T. L. and Nowak, R. S. (2006) 'Effects of elevated CO2 on fine root dynamics in a Mojave Desert community: a FACE study', *Global Change Biology*, 12, pp. 61–73. doi: 10.1111/j.1365-2486.2005.01085.x.
Pisani, O., Lin, L. H., Lun, O. O. Y., Lajtha, K., Nadelhoffer, K. J., Simpson, A. J. and Simpson, M. J. (2016) 'Long-term doubling of litter inputs accelerates soil organic matter degradation

and reduces soil carbon stocks', *Biogeochemistry*, 127(1), pp. 1–14. doi: 10.1007/s10533-015-0171-7.
Schimel, J. P. and Weintraub, M. N. (2003) 'The implications of exoenzyme activity on microbial carbon and nitrogen limitation in soil: A theoretical model', *Soil Biology and Biochemistry*, 35(4), pp. 549–563. doi: 10.1016/S0038-0717(03)00015-4.
Schmidt, M. W. I., Torn, M. S., Abiven, S., Dittmar, T., Guggenberger, G., Janssens, I. A., Kleber, M., Kogel-Knabner, I., Lehmann, J., Manning, D. A. C., Nannipieri, P., Rasse, D. P., Weiner, S. and Trumbore, S. E. (2011) 'Persistence of soil organic matter as an ecosystem property', *Nature*, 478, pp. 49–56. doi: 10.1038/nature10386.
Sierra, C. A. and Muller, M. (2015) 'A general mathematical framework for representing soil organic matter dynamics', *Ecological Monographs*, 85(4), pp. 505–524. doi: 10.1890/07-1861.1.
Stulen, I. and den Hertog, J. (1993) 'Root growth and functioning under atmospheric CO2 enrichment', *Vegetatio*, 104/105, pp. 99–115.
Sulman, B. N., Phillips, R. P., Oishi, a. C., Shevliakova, E. and Pacala, S. W. (2014) 'Microbe-driven turnover offsets mineral-mediated storage of soil carbon under elevated CO2', *Nature Climate Change*, 4(December), pp. 1099–1102. doi: 10.1038/nclimate2436.
Tang, J. and Riley, W. J. (2015) 'Weaker soil carbon-climate feedbacks resulting from microbial and abiotic interactions', *Nature Clim. Change*, 5, pp. 56–60. doi: 10.1038/nclimate2438.
Wang, G., Post, W. M. and Mayes, M. a. (2013) 'Development of microbial-enzyme-mediated decomposition model parameters through steady-state and dynamic analyses', *Ecological Applications*, 23(1), pp. 255–272. doi: 10.1890/12-0681.1.
Wang, Y. P., Chen, B. C., Wieder, W. R., Leite, M., Medlyn, B. E., Rasmussen, M., Smith, M. J., Agusto, F. B., Hoffman, F. and Luo, Y. Q. (2014) 'Oscillatory behavior of two nonlinear microbial models of soil carbon decomposition', *Biogeosciences*, 11(7), pp. 1817–1831. doi: 10.5194/bg-11-1817-2014.
Wang, Y. P., Jiang, J., Chen-Charpentier, B., Agusto, F. B., Hastings, A., Hoffman, F., Rasmussen, M., Smith, M. J., Todd-Brown, K., Wang, Y., Xu, X. and Luo, Y. Q. (2016) 'Responses of two nonlinear microbial models to warming and increased carbon input', *Biogeosciences*, 13(4), pp. 887–902. doi: 10.5194/bg-13-887-2016.
Wieder, W. R., Allison, S. D., Davidson, E. A., Georgiou, K. and Hararuk, O. (2015) 'Explicitly representing soil microbial processes in Earth system models', *Global Biogeochemical Cycles*, 29, pp. 1782–1800.
Wieder, W. R., Bonan, G. B. and Allison, S. D. (2013) 'Global soil carbon projections are improved by modelling microbial processes', *Nature Climate Change*, pp. 1–7.
Wieder, W. R., Grandy, A. S., Kallenbach, C. M. and Bonan, G. B. (2014) 'Integrating microbial physiology and physio-chemical principles in soils with the MIcrobial-MIneral Carbon Stabilization (MIMICS) model', *Biogeosciences*, 11(14), pp. 3899–3917. doi: 10.5194/bg-11-3899-2014.
Wieder, W. R., Grandy, a. S., Kallenbach, C. M., Taylor, P. G. and Bonan, G. B. (2015) 'Representing life in the Earth system with soil microbial functional traits in the MIMICS model', *Geoscientific Model Development*, 8(6), pp. 1789–1808. doi: 10.5194/gmd-8-1789-2015.
Zhu, B., Gutknecht, J. L. M., Herman, D. J., Keck, D. C., Firestone, M. K. and Cheng, W. (2014) 'Rhizosphere priming effects on soil carbon and nitrogen mineralization', *Soil Biology and Biochemistry*. Elsevier Ltd, 76, pp. 183–192. doi: 10.1016/j.soilbio.2014.04.033.

CHAPTER 2: Evidence for the importance of soils and non-forest ecosystems in the terrestrial carbon sink

CHAPTER 2: Evidence for the importance of soils and non-forest ecosystems in the terrestrial carbon sink

This chapter is being prepared for submission as the original journal article:

Georgiou, K., et al. Evidence for the importance of soils and non-forest ecosystems in the terrestrial carbon sink.

Abstract

Due to the substantial annual uptake of carbon dioxide (CO_2) by the land and oceans, the annual increase in atmospheric CO_2 concentrations constitutes approximately half of anthropogenic CO_2 emissions. However, CO_2 uptake by terrestrial ecosystems is spatially and temporally variable, and is greatly influenced by land-use and climate-induced land-cover change. While studies have sought to quantify changes in vegetation biomass via remote sensing and bottom-up inventory approaches, the relative contribution of soil organic matter to the global carbon sink is still unclear. Here we provide a novel observation- and model-based assessment of the total terrestrial C sink over the last decade, disaggregating our estimates into above- and belowground C trends for each biome. We highlight the importance of non-forest ecosystems in their ability to sequester soil C following changes to plant C inputs. Our findings suggest that the response of soil to changes in plant inputs significantly contributes to regional and global C budgets.

Introduction

Globally, soil organic matter contains more than three times the carbon (C) present in vegetation (Jobbagy and Jackson, 2000; Houghton, 2007). The amount of C sequestered in soils results primarily from the difference between plant C inputs and CO_2 released by heterotrophic respiration, a balance regulated by enviroclimatic and edaphic factors. When the amount and type of plant inputs that enter soil change due to anthropogenic land-use or climate-induced land-cover change, soil C storage will also change over decadal to centennial timescales as a result (Johnson and Curtis, 2001; Lajtha *et al.*, 2014). Globally, the size and location of such changes to soil C remain uncertain, despite better-known changes to the density and type of vegetative cover as estimated by remote sensing and inventory-based methods (Pan *et al.*, 2011; Liu *et al.*, 2015). Given the uncertainty and potential magnitude of the soil C sink, it is critically important to better constrain estimates of past, current, and future soil C cycling to support climate and land-use discussions and to inform mitigation actions.

The Intergovernmental Panel on Climate Change (IPCC) and the Global Carbon Project (GCP) estimate that, over the last decade, terrestrial ecosystems assimilated 3.0 ± 0.8 petagrams carbon per year (Pg C $year^{-1}$) (Le Quéré *et al.*, 2015). This land sink is calculated annually as the difference between the sources (e.g., emissions from fossil fuels, cement production, and land-use change) minus the ocean and atmospheric sinks from 2005 to 2014 (Le Quéré *et al.,* 2015; Canadell *et al.,* 2007). Subtracting the estimated land-use change emissions of 0.9 ± 0.5 Pg C $year^{-1}$, as calculated by inventory- and remote-sensing based methods, from the total land sink reduces the net terrestrial C sink to 2.1 ± 1.0 Pg C $year^{-1}$ (Le Quéré *et al.,* 2015). Recent studies

have sought to corroborate the magnitude of the net terrestrial sink by using ground- and satellite-based time-series of vegetation and soil C globally. However, most studies have, thus far, focused only on forest ecosystems (Pan *et al.,* 2011; Liu *et al.,* 2015), despite mounting evidence that non-forest ecosystems play a critical role in the magnitude and trend of the terrestrial C sink (Poulter *et al.* 2014; Ahlström *et al.,* 2015).

Here we provide a global observation- and model-based assessment of the net terrestrial C sink over the last decade, as driven by anthropogenic and climatic changes to vegetation and, consequently, soil. We use remotely-sensed aboveground biomass (from microwave-derived vegetation optical depth) to evaluate interannual changes in vegetation (above- and below-ground) biomass, by employing biome-specific ratios of above- to below-ground vegetation biomass from the literature (Liu *et al.,* 2011, 2015). Although many studies have focused on quantifying interannual changes in vegetation biomass, particularly in forest ecosystems (Pan *et al.,* 2011; Liu *et al.,* 2015), these changes in plant C drive lagged and substantial changes to soil C that we show are a critical component of the terrestrial C sink.

We use this remotely-sensed time-series of vegetation C as a starting point to estimate the resulting changes to soil C pools in all biomes over the same time period. We derive and apply biome-specific estimates of the ratio between vegetation and total (vegetation + soil) biomass, to determine the amount of vulnerable soil C based on observed changes in vegetation. Directly applying this ratio (e.g., Liu *et al.,* 2015) would assume that soil C is constantly in equilibrium with vegetation C, although there is likely a decade- to century-long time lag for soil to reach a biome- or region-specific steady-state. This lag is largely controlled by the soil C turnover time and varies substantially between biomes (Carvalhais *et al., 2014*; Todd-Brown *et al.,* 2013). We therefore calculate the soil turnover for each biome by a few different, yet corroborating, methods (see Methods and Supplementary Information). From these biome-specific values, we calculate the corresponding lag (proportion of steady-state achieved) as a function of time for each biome and use it to refine our estimates of interannual changes in soil C over the last two decades. This approach provides a novel assessment of the soil and total terrestrial C sink globally, regionally, and by biome, and reveals the emergent importance of soils and non-forest ecosystems to the magnitude and variability of the global C cycle.

Contribution of non-forest ecosystems to the global soil C sink

Satellite data can be used to infer global changes in vegetation biomass and type with high spatiotemporal resolution and are increasingly being used for carbon accounting, land-use monitoring, and conservation, among other applications (Hansen *et al.* 2013; Friedl *et al.* 2010; Baccini *et al.* 2012). A recent study by Liu and colleagues (2015) quantified the contribution of vegetation C uptake to the terrestrial carbon sink using satellite-derived estimates of aboveground biomass production globally across all biomes. They reported that, from 2003 to 2012, the average above- and below-ground vegetation uptake was 0.75 ± 0.15 Pg C yr^{-1}, of which 0.12 ± 0.04 Pg C yr^{-1} was attributed to forests and 0.63 ± 0.14 Pg C yr^{-1} to non-forest ecosystems. We note that the importance of non-forest ecosystems is already evident in the C balance of aboveground biomass, due in part to extensive C losses from deforestation in tropical forests (Fig. 1).

While most studies have focused on estimates of aboveground biomass, and especially in forest ecosystems, we argue that global changes in soil C that result from changes in vegetative cover are a critical part of the terrestrial C sink. We calculate net biome production (NBP; i.e., plant photosynthesis minus ecosystem respiration and other losses including harvest, deforestation, and fire) from 2003 to 2012 using remotely-sensed observations of vegetation biomass, and partition land area between major land-cover classes (boreal, temperate and tropical forests, shrublands, woody savannahs, savannahs, and grasslands, and croplands) using the MODIS MCD12C1 classification product (Friedl *et al.* 2010). We obtain a value for the magnitude of the net terrestrial C sink that is consistent with mass balance estimates from atmospheric CO_2 inversion and terrestrial biosphere models (Le Quéré *et al.,* 2015; Ahlström *et al.,* 2015).

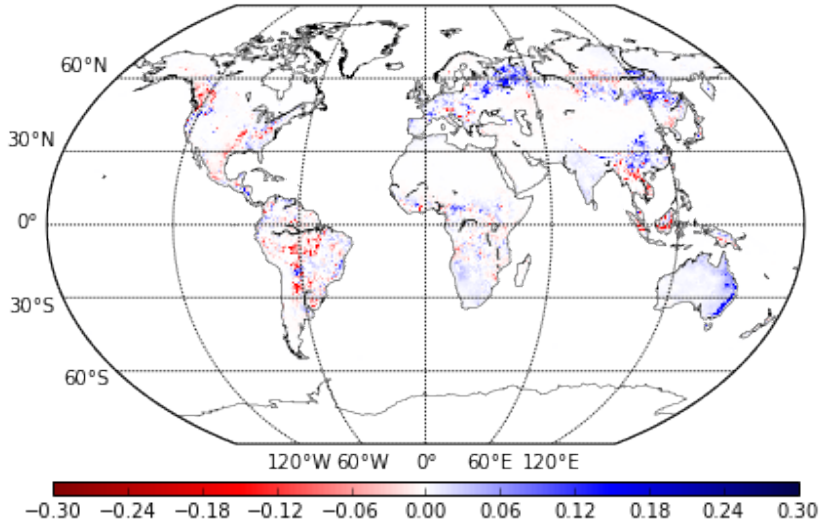

Figure 1: Average annual change in aboveground biomass carbon (kg C m^{-2} yr^{-1}) from 2003 to 2012. Aboveground biomass carbon (ABC) estimates are derived from vegetation optical depth via passive microwave observations from remote sensing (Liu *et al*. 2015). Deforestation losses in the tropics are negative (shown in red).

We derive and apply biome-specific ratios of soil C to vegetation biomass C and implement a lag based on soil turnover times to determine the change in soil C based on observed changes in vegetation (Fig. 2; Table 1). These estimates constitute the upper-limit of soil C vulnerability to changes in plant inputs, as they assume the long-term change in soil C is proportional to the change in vegetation. This formulation does not allow for non-linear priming effects (accelerated decomposition) or other indirect responses that may result from changes to the underlying mechanisms (Georgiou *et al.* 2015). We discuss the implications of this assumption and compare soil turnover times calculated in different ways; namely, we compare biome- and region-specific turnover rates from (i) empirical heterotrophic respiration and soil C stocks (Bond-Lamberty & Thomson 2010) and (ii) Community Model Intercomparison Project 5 (CMIP5) model-derived turnover rates (Carvalhais et al. 2014; Todd-Brown et al. 2014).

We find that soil constitutes nearly 58% of the global terrestrial C sink (average NBP from 2003 to 2012; Pg C yr^{-1}). The majority of this change in soil C has occurred in non-forest ecosystems (Fig. 3a), because they store proportionally more C below- than above-ground (Table 1; Fig. 2). The biome-specific ratios given herein (Table 1) are in close agreement with forest syntheses (Pan *et al*. 2011; Liu *et al.* 2015) and field studies from non-forest ecosystems (Gibbon *et al.* 2010). While recent studies have purported that these ratios were not synthesized in the literature

for all biomes, we calculate them using global observations and corroborate them with literature values.

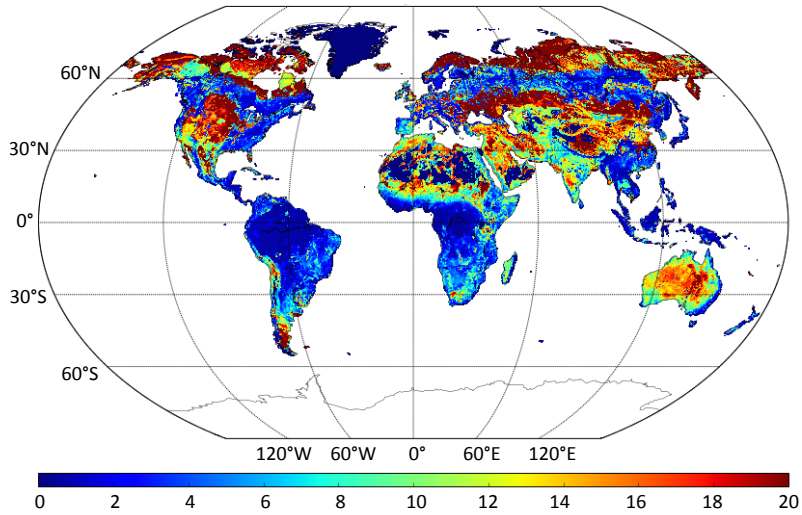

Figure 2: Ratio (unitless) of soil organic C (SOC) to aboveground biomass carbon (ABC) globally. Aboveground biomass estimates are derived from vegetation optical depth (VOD) using passive microwave satellite data (Liu *et al.* 2011, 2015) and soil C content is extracted from the Harmonized World Soils Database (HWSD).

Table 1: Ratio of total C (soil + vegetation) to TBC (total biomass carbon; only vegetation C) by biome.

	Biome type	Total C / TBC
Forest	Boreal forests	5.5
	Temperate forests	3.1
	Tropical forests	2.1
Non-forest	Shrublands	8.1
	Woody Savannahs	7.0
	Savannahs	3.9
	Grasslands	5.5
	Croplands	13.5

Non-forest ecosystems comprise 82% of the annual global terrestrial C sink (Fig. 3a), where shrublands (0.55 Pg C yr^{-1}), woody savannahs (0.46 Pg C yr^{-1}), and savannahs (0.45 Pg C yr^{-1}) account for 31%, 26%, and 25% of the terrestrial sink, respectively (Fig. 3b; Table 2). Compare this to the 0.35 Pg C yr^{-1} and 0.32 Pg C yr^{-1} sinks for boreal and temperate forests, which correspond to 20% and 18% of the total sink, respectively (Fig. 3b; Fig. S4). The relatively large importance of non-forest ecosystems results from the larger relative change in vegetation C and,

consequently, soil C of non-forest ecosystems. We note that the response of croplands is highly variable, due to a large range in soil C to vegetation C ratio, potentially due to different land management practices and departures from steady-state.

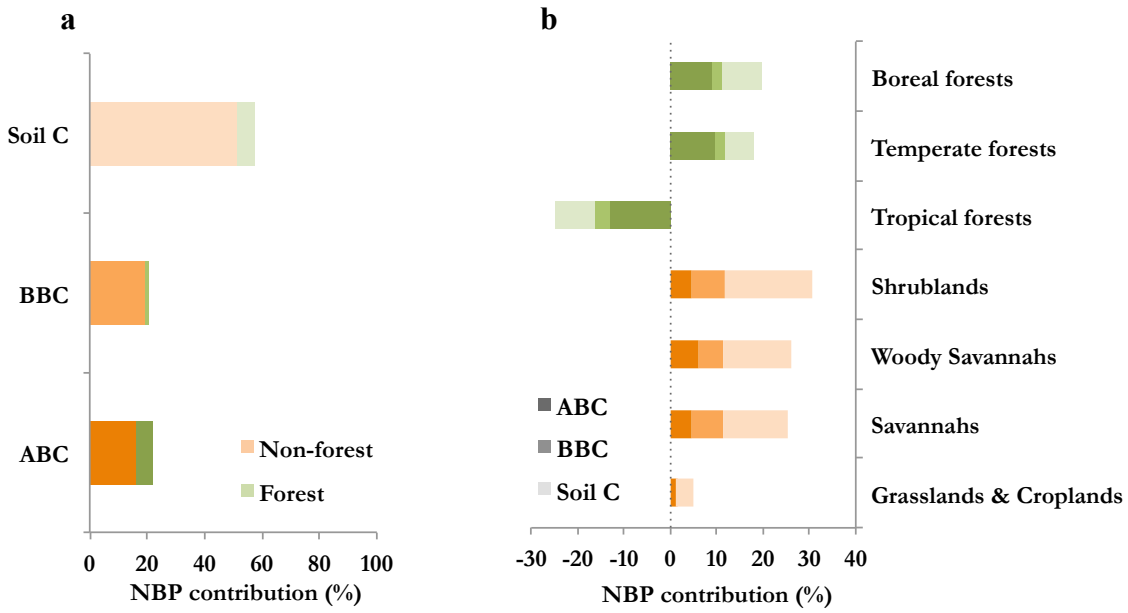

Figure 3: Contribution of above- and belowground biomass C (ABC and BBC, respectively) and soil C to annual net biome production (NBP; Pg C yr^{-1}) from 2003 to 2012.
(a) Percent contribution from forest (green) and non-forest (orange) ecosystems to above- and below-ground biomass C (ABC and BBC, respectively; dark shading) and soil C (light shading). **(b)** Percent contribution to NBP from ABC, BBC and soil C in each biome.

The importance of non-forest biomes is dominated by water-limited ecosystems, including shrublands and savannahs, which are sensitive to interannual variability in precipitation (Zhao & Running, 2010; Ahlström et al. 2015). While these non-forest ecosystems have been a large net C sink globally (Table 2), they are vulnerable to shifts in rainfall patterns and may not remain a reliable C sink.

Soil C in the global C budget

Our findings suggest that global changes to soil C content have made a considerable contribution to the magnitude (nearly 58%) and trend of the terrestrial C sink over the last two decades (Fig. 3; Table 2). The magnitude and trend of the C sinks reported herein are consistent with mass balance estimates of the total terrestrial C sink from atmospheric CO_2 inversion and within the range predicted by terrestrial ecosystem models (Le Quéré *et al.,* 2015). Furthermore, our soil C estimates provide new insights into the relative contributions of above- and belowground terrestrial components to the global carbon cycle.

We present spatially-resolved estimates of soil C change globally (Fig. 4) at a resolution of 0.25° × 0.25° across all biomes. We show that increases in aboveground shrubland, savannah, and, to a lesser extent, boreal and temperature forest biomass have driven substantial increases in soil C content. In this analysis, we account for the lag of soil C in response to changes in plant

inputs by using biome-specific soil turnover times calculated from global syntheses of soil carbon and heterotrophic respiration (see Fig. S3). We believe that for the decadal study period and the relative change of observed aboveground biomass, the model used is acceptable as a first approximation. The relative changes in soil C calculated here were found to be reasonable (see Fig. 4 and Fig. S1) and are supported by decade-long field studies that observed changes in soil C following changes in plant inputs (Lajtha *et al.* 2014). However, we note that in the long-term, as aboveground biomass continues to change, models that include explicit microbial and mineral-organic processes may be necessary to capture emergent non-linear feedbacks and soil C saturation capacity (Wieder *et al.* 2013, 2014).

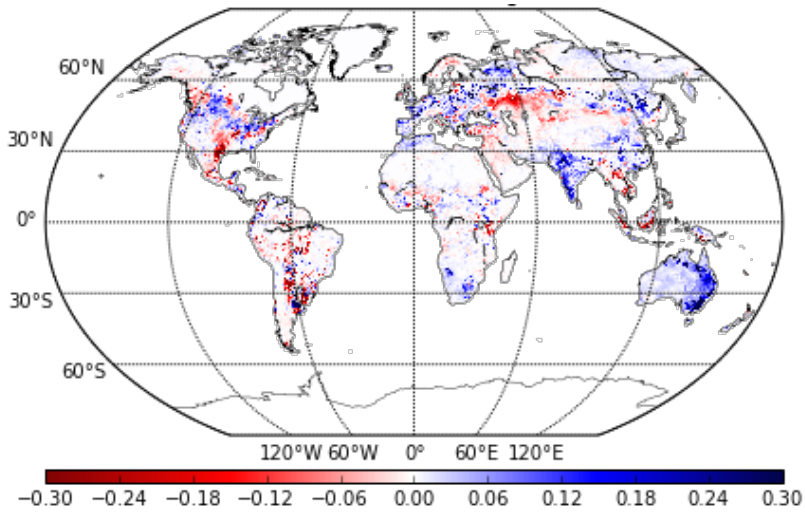

Figure 4: Average annual change in soil organic C (SOC; kg C m^{-2} yr^{-1}) from 2003 to 2012.
Changes in SOC are driven by changes to vegetation C from land-use and land-cover change globally.

Table 2: Trend in the vegetation and soil components of the terrestrial C sink globally from 2003 to 2012.
The trend is separated into aboveground biomass C (ABC), total biomass C (TBC; vegetation C), soil C, and total C (soil + vegetation) by biome. Totals are given for forest and non-forest ecosystem contributions to the total land C sink.

	Biome type	ABC trend (Pg C / yr)	TBC trend (Pg C / yr)	Soil C trend (Pg C / yr)	Total C trend (Pg C / yr)
Forest	Boreal forests	+ 0.16	+ 0.20	+ 0.15	+ 0.35
	Temperate forests	+ 0.17	+ 0.21	+ 0.11	+ 0.32
	Tropical forests	- 0.23	- 0.29	- 0.15	- 0.45
Non-forest	Shrublands	+ 0.08	+ 0.21	+ 0.33	+ 0.55
	Woody Savannahs	+ 0.11	+ 0.20	+ 0.26	+ 0.46
	Savannahs	+ 0.08	+ 0.20	+ 0.25	+ 0.45
	Grasslands	- 0.002	- 0.01	- 0.01	- 0.02
	Croplands	+ 0.02	+ 0.03	+ 0.08	+ 0.11
	Forest total	**+ 0.10**	**+ 0.12**	**+ 0.11**	**+ 0.23**
	Non-forest total	**+ 0.29**	**+ 0.63**	**+ 0.91**	**+ 1.54**
	Total	**+ 0.39**	**+ 0.75**	**+ 1.02**	**+ 1.77**

We have shown that the response of soil to changes in plant inputs significantly contributes to regional and global C budgets (Table 2). Furthermore, we highlight the importance of non-forest ecosystems in their ability to sequester C in soil. Our findings caution against studies that focus on the contributions of only forest ecosystems to the global soil and terrestrial C sinks (e.g., Pan *et al.* 2011), and support recent studies that have revealed the important contribution of non-forest ecosystems to the terrestrial C sink (e.g., Poulter *et al.* 2014; Ahlström *et al.* 2015). While the accumulation of vegetation and soil C has led to an overall C sink in the last two decades, the future terrestrial C sink may be particularly sensitive to rainfall and droughts, due to major contributions from non-forest ecosystems. Given the large spread in Earth system model predictions (Friedlingstein et al., 2006, 2014; Ahlström et al., 2012; Todd-Brown *et al.,* 2013), there is still a need to develop observational constraints for model benchmarking and validation.

Methods

To investigate the magnitude and relative contribution of soil to the terrestrial C sink in each biome, we use multiple data sources, including satellite-based vegetation products, global syntheses of heterotrophic respiration, soil C content, and ecosystem model simulations. We use aboveground biomass estimates from 1993 to 2012, derived from vegetation optical depth (VOD) using passive microwave satellite data (Liu *et al.* 2011, 2015). Soil C content from the Harmonized World Soils Database (HWSD) was used to determine biome- and region-specific ratios of soil organic C (SOC) to aboveground biomass C (ABC). In response to observed changes in aboveground biomass, and therefore litter inputs, soils undergo a lagged change in C content over decadal to centennial time scales before approaching their steady-state SOC to ABC ratio. This can be thought of as a change in SOC that is proportional to the change in ABC, as is predicted by soil C decay models commonly used in Earth system models (ESMs). The lag experienced by soils over a given time period (denoted $\alpha(t)$ in Eqn. 1) is determined from the turnover time (decay rate) of the particular location, which can vary greatly by biome and soil depth. We use global syntheses of heterotrophic respiration and soil C content (Bond-Lamberty & Thomson 2011) to estimate soil C turnover times for each biome. We calculate the lag $\alpha(t)$ based on biome-specific turnover times, as detailed in Eqn. 2 and Fig. S3. We then use Eqn. 1 to estimate the change in total C over a given time period. Since the satellite-derived estimates of ABC include disturbance (e.g., land-use, fire), the total C in Eqn. 1 is a novel estimate of NBP globally. At each grid-cell, we can calculate:

$$\Delta\,(total\ C) = \Delta\,(ABC) + \underbrace{\left(\frac{BBC}{ABC}\right)\cdot \Delta\,(ABC)}_{\Delta\,(BBC)} + \underbrace{\alpha(t)\cdot\left(\frac{SOC}{ABC}\right)\cdot \Delta\,(ABC)}_{\Delta\,(SOC)} \qquad \text{(Eqn. 1)}$$

or equivalently,

$$\Delta\,(total\ C) = \Delta\,(ABC) + \underbrace{BBC\cdot\left(\frac{\Delta\,(ABC)}{ABC}\right)}_{\Delta\,(BBC)} + \underbrace{\alpha(t)\cdot SOC\cdot\left(\frac{\Delta\,(ABC)}{ABC}\right)}_{\Delta\,(SOC)},$$

where the lag of a one-pool SOC model in response to a ramp change in inputs can be derived (see Supplementary Note) as

$$\alpha(t) = 1 - \frac{1-e^{-kt}}{kt}\,. \qquad \text{(Eqn. 2)}$$

As such, NBP estimates from the IPCC and GCP, which quantify the balance between the net uptake by plants (net primary productivity; NPP = GPP – R_a) and losses from soil respiration (R_h) and disturbance, are used here for comparison. To aggregate results by biome, we use the MCD12C1 IGBP dynamic land-cover classification.

References

Jobbágy, E. G. & Jackson, R. B. The vertical distribution of soil organic C and its relation to climate and vegetation. *Ecological Applications* **10**, 423-436 (2000).

Houghton, R. A. Balancing the global C budget. *Annual Review of Earth and Planetary Sciences* **35**, 313-347 (2007).

Johnson, D. W. & Curtis, P. S. Effects of forest management on soil C and N storage: meta analysis. *Forest Ecology and Management* **140**, 227-238 (2001).

Lajtha, K. *et al*. Changes to particulate versus mineral-associated soil carbon after 50 years of litter manipulation in forest and prairie experimental ecosystems. *Biogeochemistry* **119**, 341–360 (2014).

Pan, Y. D. *et al*. A large and persistent carbon sink in the world's forests. *Science* **333**, 988–993 (2011).

Liu, Y. Y. *et al.* Recent reversal in loss of global terrestrial biomass. *Nature Climate* Change **5**, 470-474 (2015).

Le Quéré, C. *et al.* Global Carbon Budget 2015, *Earth Syst. Sci. Data* **7**, 349–396 (2015).

Canadell, J. G. *et al.* Contributions to accelerating atmospheric CO2 growth from economic activity, carbon intensity, and efficiency of natural sinks. *P. Natl. Acad. Sci. USA* **104,** 18866– 18870 (2007).

Friedlingstein P, *et al.* Climate-carbon cycle feedback analysis: results from the (CMIP)-M-4 model intercomparison. *J. Clim.* **19,** 3337–3353 (2006).

Friedlingstein, P. *et al.* Uncertainties in CMIP5 Climate Projections due to Carbon Cycle Feedbacks. *Journal of Climate* **27**, 511-526 (2013).

Ahlström, A., Schurgers, G., Arneth, A., & Smith, B. Robustness and uncertainty in terrestrial ecosystem carbon response to CMIP5 climate change projections. *Environ. Res. Lett.* **7,** 044008 (2012).

Todd-Brown, K. E. O. *et al.* Changes in soil organic carbon storage predicted by Earth system models during the 21st century. *Biogeosciences* **11**, 2341-2356 (2014).

Ahlström, A. *et al*. The dominant role of semi-arid ecosystems in the trend and variability of the land CO2 sink. *Science* **348**, 895–899 (2015).

Poulter, B. *et al*. Contribution of semi-arid ecosystems to interannual variability of the global carbon cycle. *Nature* **509**, 600–603 (2014).

Liu, Y. Y., de Jeu, R. A. M., McCabe, M. F., Evans, J. P. & van Dijk, A. I. J. M. Global long-term passive microwave satellite-based retrievals of vegetation optical depth. *Geophys. Res. Lett.* **38**, L18402 (2011).

Carvalhais, N. *et al.* Global covariation of carbon turnover times with climate in terrestrial ecosystems. *Nature* **514**, 213-217 (2014).

Hansen, M. C. *et al.* High-resolution global maps of 21st-century forest cover change. *Science* **342**, 850-853 (2013).

Friedl, M. A. *et al*. MODIS Collection 5 global land cover: Algorithm refinements and characterization of new datasets. *Remote Sens. Environ.* **114**, 168–182 (2010).

Baccini, A. *et al.* Estimated carbon dioxide emissions from tropical deforestation improved by carbon-density maps. *Nature Clim. Change* **2**, 182-185 (2012).

Bond-Lamberty, B. & Thomson A. A global database of soil respiration data, *Biogeosciences* **7**(6), 1915-1926 (2010).

Gibbon, A. *et al.* Ecosystem carbon storage across the grassland-forest transition in the High Andes of Manu National Park, Peru. *Ecosystems* **10**, 9376 (2010).

Zhao, M. & Running, S. W. Drought-induced reduction in global terrestrial net primary production from 2000 through 2009. *Science* **329**, 940–943 (2010).
Wieder, W. R., Bonan G. B. & Allison S.D. Global soil carbon projections are improved by modeling microbial processes, *Nature Climate Change*, **3**(10), 909-912 (2013).
Wieder, W. R., Grandy A. S., Kallenbach C. M. & Bonan G. B. Integrating microbial physiology and physico-chemical principles in soils with the Microbial-Mineral Carbon Stablization (MIMICS) model, *Biogeosciences*, **11**, 3899-3917 (2014).

Supplementary Figures & Tables

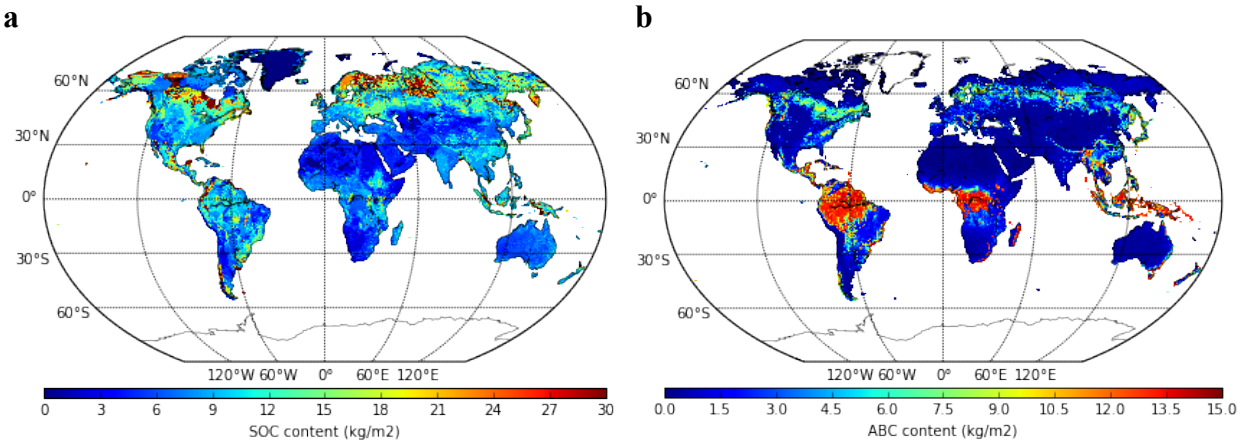

Supplementary Figure 1: Global terrestrial C stocks in soil and aboveground biomass.
(a) Global soil organic carbon to a depth of 1m from the Harmonized World Soil Database (HWSD) re-gridded to a 0.25-degree grid. **(b)** Global aboveground biomass carbon (ABC) from vegetation optical depth via passive microwave observations (Liu *et al.* 2015).

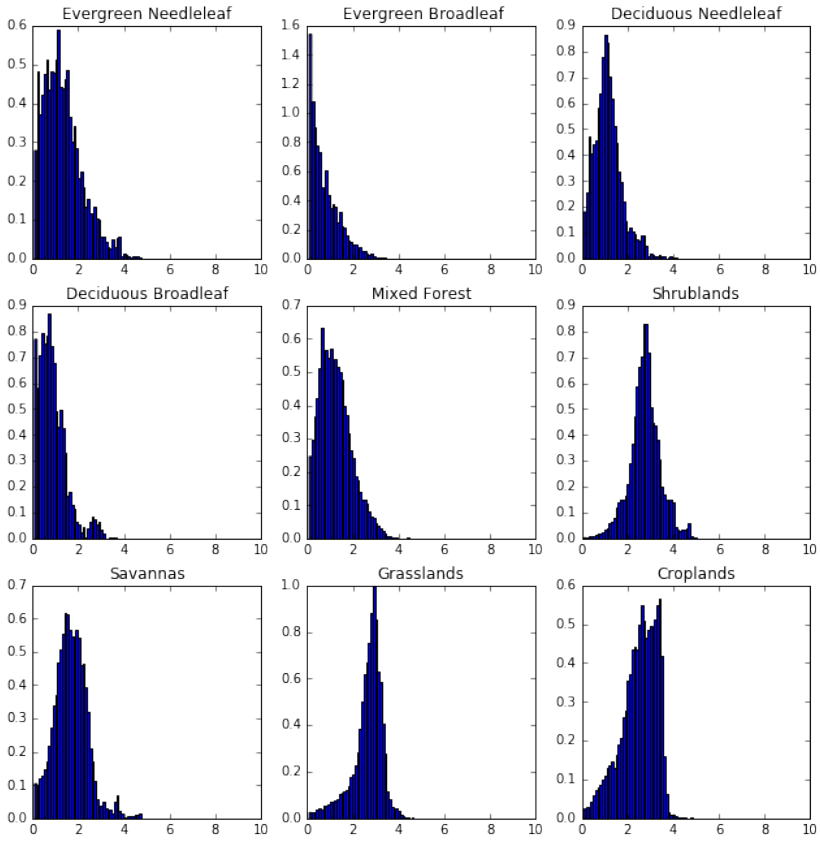

Supplementary Figure 2: Probability distribution of observing a particular soil organic C to aboveground biomass C (SOC/ABC) ratio.
Calculated globally, in each biome, and plotted as the natural log of the ratio.

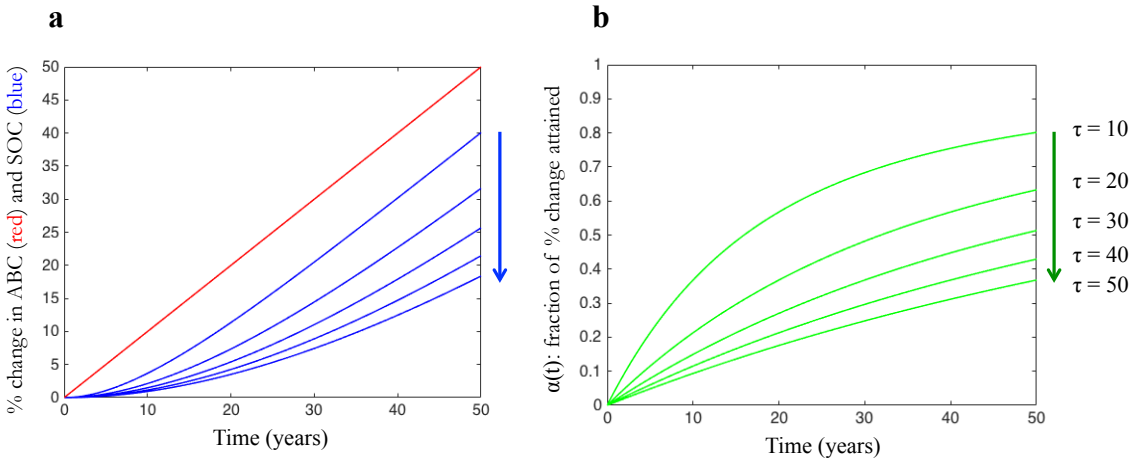

Supplementary Figure 3: Response of soil organic C (SOC) to changes in aboveground biomass carbon (ABC) as a function of soil turnover time in a one-pool model.
(a) Relative % change in SOC (blue lines) in response to a linear 1% annual increase in ABC (red line) as predicted by a one-pool exponential decay SOC model. **(b)** Fraction α(*t*) of the % change achieved by SOC at time *t*, as derived in Eqn. 2.

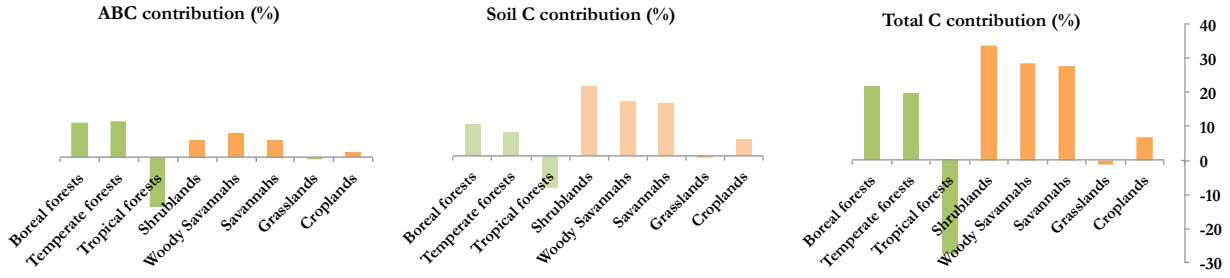

Supplementary Figure 4: Percent contribution of each biome (green = forest, orange = non-forest) to the annual terrestrial C sink.
Contribution of aboveground biomass carbon (ABC), soil C, and total C in each biome to the total annual C.

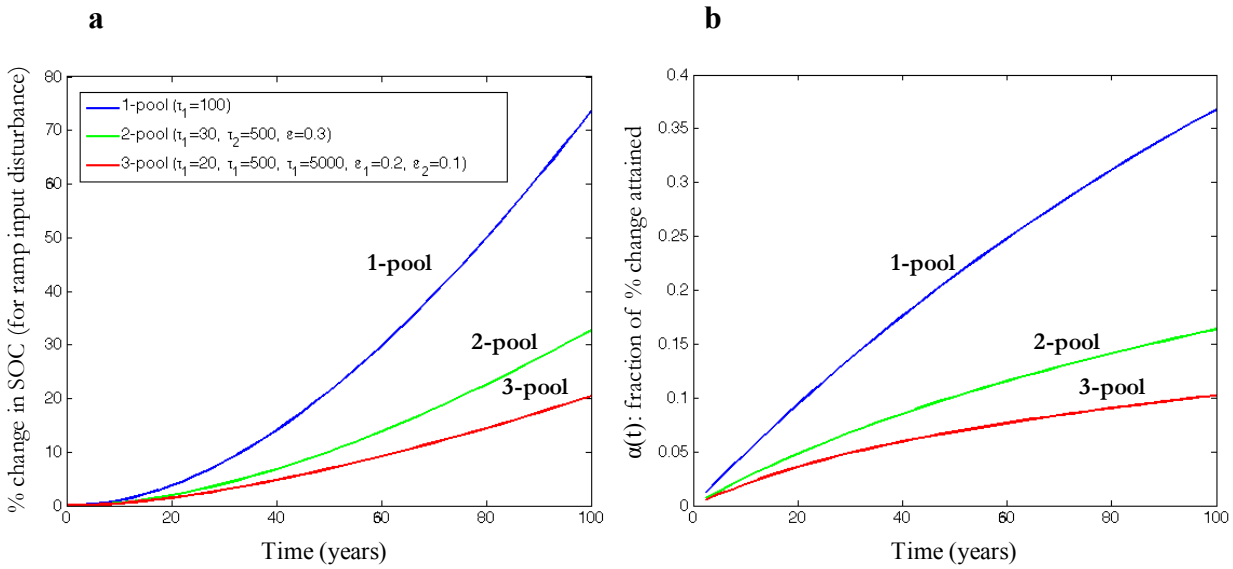

Supplementary Figure 5: Response of soil organic C (SOC) to changes in aboveground biomass carbon (ABC) as a function of soil turnover time across a range of pool-based models.
(a) Relative % change in SOC in response to a linear 1% annual increase in ABC as predicted by 1-, 2-, and 3-pool exponential decay SOC models. **(b)** Fraction α(*t*) of the % change achieved by SOC at time *t*, as derived in Eqn. 2. We observe a greater lag (lower α(*t*)) in multi-pool models, with the largest difference between 1- and 2-pool models. In future analyses, we will use global 2- & 3-pool model turnover times constrained by radiocarbon data from He *et al.* 2016.

Supplementary Note

The lag of a one-pool SOC model in response to a ramp change in inputs (Eqn. 2) is

$$\alpha(t) = 1 - \frac{1-e^{-kt}}{kt}\,.$$

The non-dimensionalization and derivation can be outlined as follows:

Consider the first-order, one-pool decomposition model

$$\frac{\mathrm{d}C}{\mathrm{d}t} = I - k \cdot C$$

where $C = \mathrm{SOC}$, $I =$ inputs from ABC, and $k > 0$ is the decomposition rate constant.

At steady state, $\frac{\mathrm{d}C}{\mathrm{d}t} = I - k \cdot C = 0$, so that $I = k \cdot C$. This system is stable for $k > 0$.

In our analysis, we are interested in perturbations from the initial ($t = 0$) steady state, where we define $C_0 = C(t = 0)$ and $I_0 = I(t = 0)$. Thus, the initial steady state is $I_0 = k \cdot C_0$ or, equivalently, $\frac{I_0}{C_0} = k$.

We then non-dimensionalize as follows, defining

$$c = \frac{C - C_0}{C_0} \text{ and } i = \frac{I - I_0}{I_0}\,.$$

Substituting these expressions into the first-order model and dividing by C_0,

$$\frac{\mathrm{d}(c \cdot C_0 + C_0)}{\mathrm{d}t} = (i \cdot I_0 + I_0) - k \cdot (c \cdot C_0 + C_0)$$

$$C_0 \frac{\mathrm{d}c}{\mathrm{d}t} = i \cdot I_0 + I_0 - k \cdot c \cdot C_0 - k \cdot C_0$$

$$\frac{\mathrm{d}c}{\mathrm{d}t} = i \cdot \frac{I_0}{C_0} + \frac{I_0}{C_0} - k \cdot c - k$$

then recalling that $\frac{I_0}{C_0} = k$, we can simplify further to obtain

$$\frac{\mathrm{d}c}{\mathrm{d}t} = i \cdot k + k - k \cdot c - k$$

and finally,

$$\frac{\mathrm{d}c}{\mathrm{d}t} = k \cdot i - k \cdot c = k(i - c)$$

where at steady-state, $c = i$.

For a ramp input in time, $i(t) = t$, we can solve the system

$$\frac{\mathrm{d}c(t)}{\mathrm{d}t} = k \cdot t - k \cdot c(t)$$

to obtain the solution

$$c(t) = \ t - \frac{1}{k}(1 - e^{-k \cdot t}) \ .$$

We then define the lag, $\alpha(t)$, between the relative change in inputs, $i(t)$, and concentration, $c(t)$, such that $c(t) = \alpha(t) \cdot i(t)$. For the case derived above, $c(t) = \alpha(t) \cdot t$, so

$$\alpha(t) = \ 1 - \frac{1}{k \cdot t}(1 - e^{-k \cdot t}) \ .$$

We highlight that the expression $c(t) = \alpha(t) \cdot i(t)$ corresponds to $\frac{\Delta SOC}{SOC} = \alpha(t) \cdot \frac{\Delta ABC}{ABC}$ or, equivalently, $\Delta SOC = \alpha(t) \cdot \frac{SOC}{ABC} \cdot \Delta ABC$, as in Eqn. 1.

CHAPTER 3: Towards improved model structures for analyzing priming: potential pitfalls of using bulk turnover time

CHAPTER 3: Towards improved model structures for analyzing priming: potential pitfalls of using bulk turnover time

This chapter is reprinted, with permission, from the original journal article:

Georgiou, K., C. D. Koven, W. J. Riley, M. S. Torn. Towards improved model structures for analyzing priming: potential pitfalls of using bulk turnover time. *Global Change Biology*, 21:12, 4298-4302 (2015).

Abstract

Many studies have shown that elevated atmospheric CO_2 concentrations result in increased plant carbon inputs to soil that can accelerate the decomposition of native soil organic matter, an effect known as priming. Consequently, it is important to understand and quantify the priming effect for future predictions of carbon-climate feedbacks. There are potential pitfalls, however, when representing this complex system with a simple, first-order model. Here we show that a multi-pool soil carbon model can match the change in bulk turnover time calculated from overall respiration and carbon stocks (a one-pool approach) at elevated CO_2, without a change in decomposition rate constants of individual pools (i.e., without priming). Therefore, the priming effect cannot be quantified using a one-pool model alone, and even a two-pool model may be inadequate, depending on effect size as well as the distribution of soil organic carbon and turnover times. In addition to standard measurements of carbon stocks and CO_2 fluxes, we argue that quantifying the fate of new plant inputs requires isotopic tracers and microbial measurements. Our results offer insights into modeling and interpreting priming from observations.

Introduction

Soils are a major reservoir of carbon, containing more than double the carbon currently in the atmosphere. As atmospheric CO_2 levels increase, plant productivity generally increases (Ainsworth & Long, 2005). However, increased carbon inputs to soils do not necessarily result in more soil carbon storage. An increase in plant inputs to soil may enhance microbial activity, thereby accelerating the decomposition rate of native soil organic matter (SOM) and limiting carbon storage. This 'priming effect' has been observed in field and laboratory studies of increased carbon inputs to soils (Carney *et al.*, 2007; Paterson *et al*., 2008; Cheng *et al*., 2013). Although the underlying mechanism is not well understood, this process could have a significant effect on global carbon cycle responses to climate change and rising CO_2. Direct observations are difficult so it is uncertain how widespread or large this effect is. It is therefore important to develop accurate detection and quantification of priming, and to represent this process in Earth System Models (ESMs) for better prediction of carbon-climate feedbacks.

Here we provide a quantitative examination and cautionary note on analytical approaches that use bulk soil turnover time (such as one based on a one-pool model) to infer a change in decomposition rate constants (Torbert *et al*., 2004; Prior *et al.,* 2008; Foereid *et al.,* 2014; van Groenigen *et al.,* 2014). Such methods have been used to infer priming in response to increased

soil carbon inputs. We show, numerically and schematically, why a one-pool SOM model alone is unable to infer an increase in SOM decomposition rates given observations of respiration and carbon stocks over time, and that other simple linear models (e.g., a two-pool model) may also have limited power of detection. We also discuss the minimal required model structure to support conclusions on priming and process-based representation of this potentially important carbon feedback in ESMs.

One-pool model of a multi-pool system

Soils have the property that the mean age of SOM is much older than the mean age of heterotrophic respiration, implying that a fraction of the carbon entering soils is respired on the order of weeks to months, while some persists for decades to centuries or longer. Soil carbon models have traditionally approximated this behavior by considering decomposition as a combination of two or more exponential decay terms with a broad range of time constants ("multi-pool models"). Three-pool models typically do a good job of characterizing carbon cycling in many different soils (Parton *et al*., 1987; Torn *et al*., 2009). In contrast, treating decomposition with a single exponential decay rate ("single-pool models") gives qualitatively different behavior that poorly represents the dynamics of SOM (Parton *et al*., 1987).

Since soil carbon is not one homogeneous SOM pool, the qualitative behavior of bulk turnover time (i.e., the turnover time estimated from treating the soil as one pool) may mistakenly be interpreted as priming, even without changes to intrinsic decomposition rates (k_i; or other proposed mechanisms for priming). To demonstrate this, we use a traditional two-pool model (for simplicity), with fast ($\tau_1 = 1/k_1 = 1.5$ years) and slow ($\tau_2 = 1/k_2 = 50$ years) cycling pools, to show that an increase in the overall (bulk) decomposition rate constant (k) will be inferred despite constant decomposition rate constants (k_1 and k_2) of individual pools (Fig. 1). We calculate bulk turnover time as soil carbon stocks over respiration; however, similar results would be predicted from a one-pool model where bulk turnover time is estimated by parameter fitting to observed soil carbon stocks over time constrained by plant growth (carbon inputs) and microbial respiration (carbon outputs). We perturb the soil from steady-state with a 20% step increase in carbon inputs, matching the average effect of elevated CO_2 in van Groenigen *et al.* (2014) as an example.

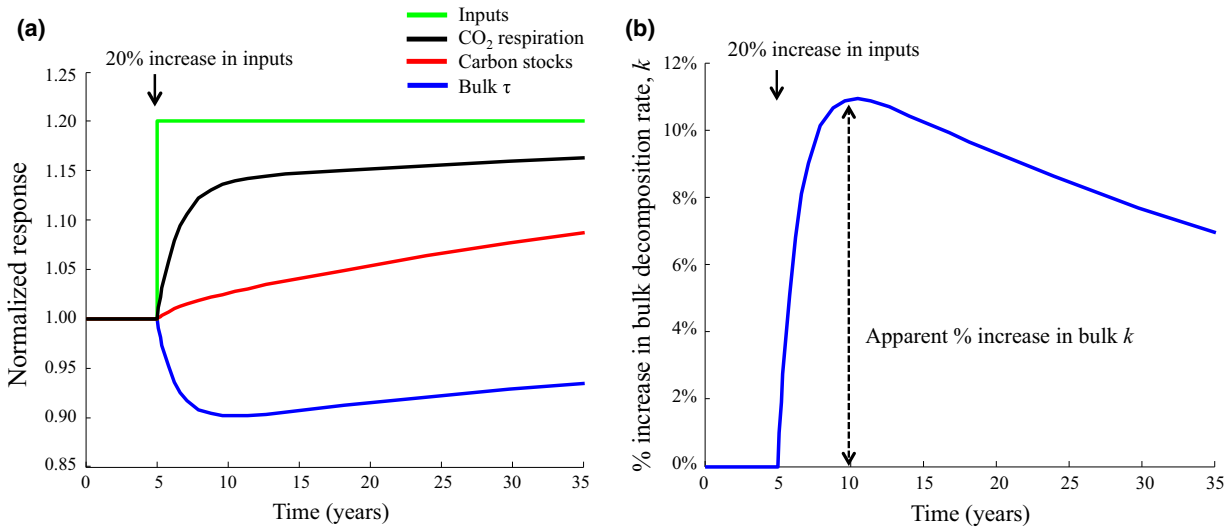

Figure 1: Results from aggregating a two-pool SOM model with fixed pool turnover times (τ_1 and τ_2) in response to a 20% increase in carbon inputs.
(a) Normalized overall (bulk) turnover time (τ), total soil carbon stocks, and CO_2 respiration from a two-pool model (τ_1 = 1.5 years and τ_2 = 50 years) in response to a 20% step increase (at year 5) in soil carbon inputs. Carbon use efficiencies of 0.30 and 0.45 (respired fractions of 0.70 and 0.55) were used for the fast and slow carbon pools, respectively, where a fraction of the carbon uptake from each pool is transferred between soil carbon pools, while the remainder is respired. **(b)** Response of the overall decomposition rate constant (k = 1/τ) as a percent increase after the disturbance.

The result is that total respiration responds more quickly than total carbon stocks, since the soil now has a larger proportion of fast versus slow cycling carbon pools because of the new inputs (Fig. 1a). As a result, a faster bulk decomposition rate is calculated when the (fast and slow) carbon pools are aggregated into a one-pool model (Fig. 1b). However, this increase in decomposition does not result from a change in individual pool decomposition rates, k_i, but rather from having more carbon in the fast-cycling pool; the increase is an artifact of treating a multi-pool system as a one-pool system and persists for decades to centuries. This effect on bulk k (and τ) in response to elevated CO_2 ('false priming') is also evident in simulations of five ESMs participating in the CMIP5 experiment, despite the fact that these models do not include mechanisms that could produce priming (Koven *et al.*, 2015).

The conceptual diagram in Fig. 2 illustrates how an aggregated one-pool model – applied to a system that has more than one carbon pool – can infer a decrease in the bulk turnover time (increase in k) as a consequence of the inappropriate model structure. We start with a two-pool model, as the simplest example of multiple carbon pools, and aggregate the outputs and carbon stocks into the structure of a one-pool model to calculate the change in bulk turnover time.

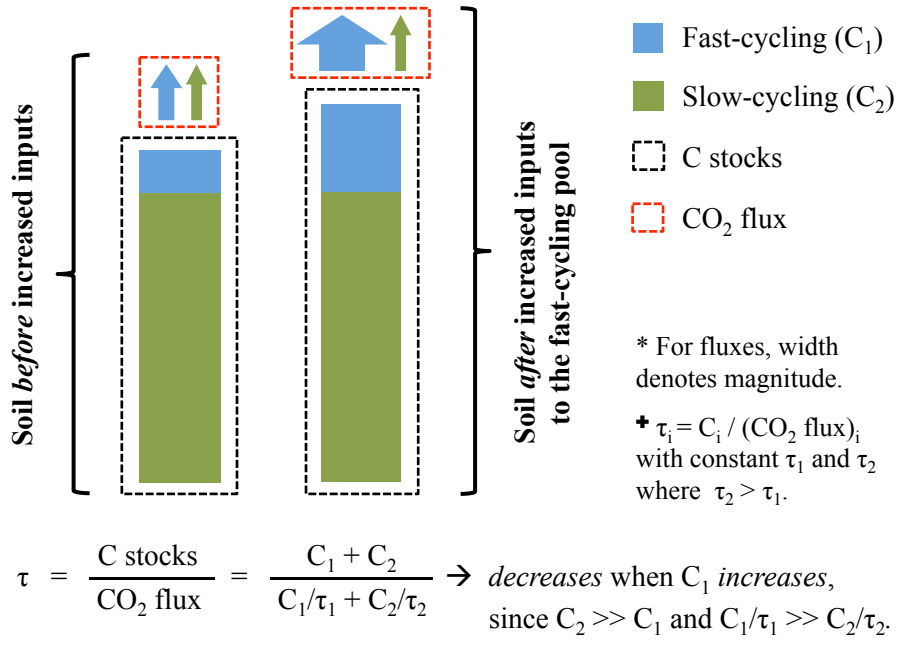

Figure 2: Conceptual diagram illustrating how aggregating a system with two SOM pools into a one-pool SOM model can exhibit a false priming response.
This appears as a decrease in the bulk turnover time (τ) without a change in the individual turnover times of the fast (C_1) and slow (C_2) cycling pools (τ_1 and τ_2, respectively). The bulk turnover time (one-pool model) of an aggregated multi-pool system is defined as the total concentration of carbon stocks divided by the total CO_2 flux respired as output. Turnover time is the reciprocal of the decomposition rate constant (k). (*Left*) Two SOM pools before an increase in carbon inputs. (*Right*) Response of the two SOM pools to an increase in carbon inputs into the fast-cycling pool. In this case, the bulk turnover time τ decreases (k increases) with time. Note, for simplicity of illustration, carbon use efficiencies equal to zero (respired fraction equal to one) are used in this figure.

For simplicity, we use a two-pool model to show the weakness of aggregating a system with multiple underlying carbon pools into a one-pool model, but even a model with two or more pools may lead to errors in assessing the effects of CO_2 fertilization or inferring SOM priming. Depending on the model parameters, a two-pool model can result in a wide range of false priming (reduction in bulk turnover time) responses to increased inputs, as shown in our sensitivity analysis (Fig. 3).

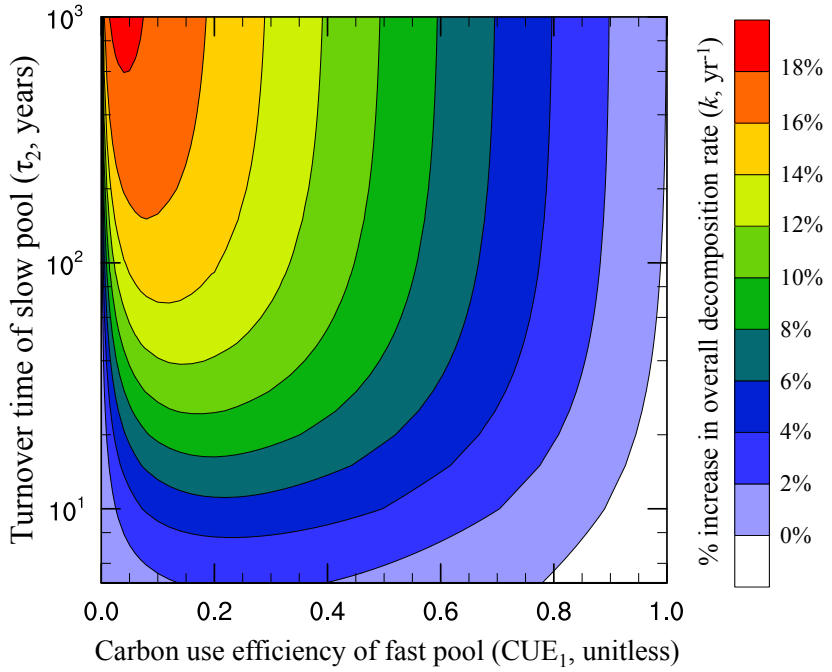

Figure 3: Sensitivity analysis depicting the potential magnitude of false priming inferred from aggregating two SOM pools with a range of parameter values into a one-pool model.
Contour plot of the percent increase in overall k [taken 5 years after a 20% increase in inputs to approximate the observational meta-analysis of van Groenigen *et al.* (2014), as an example] for a range of carbon use efficiencies of the fast pool (CUE_1) and turnover times of the slow pool (τ_2). The turnover time of the fast pool (τ_1 = 1 year) and carbon use efficiency of the slow pool (CUE_2 = 0; i.e. all carbon used for respiration) were held constant to explore the effect of CUE_1 and τ_2 only.

Bias in quantifying priming with a one-pool model

A single-pool model can be used to detect the presence of priming only when a sufficiently large change in respiration is observed, i.e., when more carbon is respired than (a) is added or (b) the bias that results from aggregating a multi-pool system. For example, if inputs increased by 20% and outputs by 25%, the additional 5% increase is clearly from faster decomposition rates of existing carbon stocks. If outputs increased by less than 20%, however, it is possible that the carbon use efficiency (CUE; defined as the fraction of carbon uptake from each pool that is allocated to microbial growth and transferred to another soil carbon pool, i.e., not respired) and shift in pool sizes of the underlying multi-pool system caused the observed change in bulk decomposition rate (Figs. 1-3).

To determine the likely range of bias due to analyzing observations with a one-pool model, we performed a sensitivity analysis using a range of carbon use efficiencies and pool-specific decomposition rate constants (Fig. 3). We again aggregated a two-pool model into a one-pool model and examined the false priming response that resulted from different parameterizations. Because the typical values of the model parameters can vary within actual soil and between models, we present the potential magnitude of false priming for a range of carbon use efficiencies of the fast pool (CUE_1) and turnover times of the slow pool (τ_2).

We infer from Fig. 3 that only respiration above the ~9-16% increase in k obtained by aggregating two SOM pools into a one-pool model can be attributed to priming, depending on the range of representative system parameters. This false priming estimate is corroborated by the ~7%-14% reduction in overall turnover time observed in the CMIP5 models in response to a 20% increase in NPP (Koven *et al*., 2015). Consequently, the magnitude of priming that can be concluded from a one-pool model alone is roughly equal to the difference between the inferred change in k and that expected from simply treating a multi-pool system as a single pool – i.e., much smaller than estimated in most of the studies cited above. In cases where the reported response of k is within the range of the response (bias) expected from using the typical range of Century-model (Parton et al., 1987) parameters (Fig. 3), an increase in intrinsic decomposition rates (priming) cannot be concluded from an analysis or meta-analysis that relies on a one-pool model.

Towards models and observations to quantify and predict priming

The mechanisms hypothesized to cause SOM priming (e.g., increased microbial production of extracellular enzymes, enhanced mycorrhizal activity, changes in microbial community structure) are absent from conventional pool-based models (Kuzyakov, 2010; Blagodatsky *et al.*, 2010). It is therefore possible that the typically rapid microbial turnover of increased exudation or fine-root necromass could explain the increase in respiration observed in litter addition and CO_2 enrichment experiments that have not traced sources of respiration, for instance, without there being a change in the original SOM pool dynamics. For example, such an increase in respiration without a change in decomposition rate constants has been observed across a tropical montane forest (Giardina *et al*., 2014). Unless the increase in respiration is significantly larger than the sum of increased inputs resulting in an overall decrease of soil carbon, or unless observations, such as isotopic tracers, are available that trace the fate of inputs and the source of respiration, inferences of enhanced degradation of existing SOM will remain highly uncertain. Analyzing observations with a model structure that includes the hypothesized mechanisms of priming (e.g., microbial and enzymatic activity) is also an important next step.

Conclusions

Soil carbon comprises a range of organic matter pools and therefore, using a simple, first-order model to infer complex carbon dynamics may lead to erroneous conclusions. Using a multi-pool soil carbon model with an imposed increase in carbon inputs, we have shown that the behavior of bulk turnover time (i.e., the turnover time estimated from aggregating multiple pools into a single pool) may mistakenly be interpreted as priming, despite constant intrinsic decomposition rates of individual SOM pools. Thus, we conclude that the priming effect cannot be quantified using measurements of bulk carbon stocks and CO_2 flux alone, but requires knowledge of the fate of new plant inputs.

To distinguish if CO_2 respiration originates from new carbon inputs or older native soil, studies using natural abundance radiocarbon or ^{13}C- or ^{14}C-labeled inputs provide useful results (Kuzyakov *et al.,* 2000; Fontaine *et al.,* 2007; Paterson *et al.,* 2013; Hopkins *et al.,* 2014). Since microbes are an active driver of carbon and nitrogen turnover in soil, microbial biomass measurements can also provide a constraint on changes to carbon dynamics (Blagodatskaya &

Kuzyakov, 2008; Blagodatsky *et al.,* 2010). These data should be used to inform estimates of priming, whether analyzed as changes in decomposition rate constants in multi-pool models or as microbial activity in microbe-enabled models (Blagodatsky *et al.,* 2010; Riley *et al.,* 2014; Tang & Riley, 2015; Wang *et al.,* 2014). Such information can then be used to parameterize this priming effect in SOM models *(*Wieder *et al.,* 2013; Guenet *et al.,* 2013; Sulman *et al.,* 2014) that can be incorporated into ESMs.

References

Ainsworth EA, Long SP (2005) What have we learned from 15 years of free-air CO_2 enrichment (FACE)? A meta-analytic review of the responses of photosynthesis, canopy properties and plant production to rising CO_2. New Phytologist, **165**, 351-372.

Blagodatskaya EV, Kuzyakov Y (2008) Mechanisms of real and apparent priming effects and their dependence on soil microbial biomass and community structure: critical review. Biology and Fertility of Soils, **45**, 115-131.

Blagodatsky S, Blagodatskaya EV, Yuyukina T, Kuzyakov Y (2010) Model of apparent and real priming effects: linking microbial activity with soil organic matter decomposition. Soil Biology and Biochemistry, **42**, 1275-1283.

Carney KM, Hungate BA, Drake BG, and Megonigal JP (2007) Altered soil microbial community at elevated CO_2 leads to loss of soil carbon. Proceedings of the National Academy of Sciences, **104**, 4990–4995.

Cheng W, Parton WJ, Gonzalez-Meler MA *et al.* (2014) Synthesis and modeling perspectives of rhizosphere priming. New Phytologist, **201**, 31-44.

Foereid B, Ward DS, Mahowald N, Paterson E, and Lehmann J (2014) The sensitivity of carbon turnover in the Community Land Model to modified assumptions about soil processes. Earth System Dynamics, **5**, 211-221.

Fontaine S, Barot S, Barré P, Bdioui N, Mary B, Rumpel C (2007) Stability of organic carbon in deep soil layers controlled by fresh carbon supply. Nature, **450**, 277-281.

Giardina CP, Litton CM, Crow SE, Asner GP (2014) Warming-related increases in soil CO_2 efflux are explained by increased below-ground carbon flux. Nature Climate Change, **4**, 822-827.

Guenet B, Moyano FE, Vuichard N, Kirk GJD, Bellamy PH, Zaehle S, Ciais P (2013) Can we model observed soil carbon changes from a dense inventory? A case study over England and Wales using three versions of the ORCHIDEE ecosystem model (AR5, AR5-PRIM and O-CN). Geoscientific Model Development, **6**, 2153-2163.

Hopkins FM, Filley TR, Gleixner G, Lange M, Top SM, Trumbore SE (2014) Increased belowground carbon inputs and warming promote loss of soil organic carbon through complementary microbial responses. Soil Biology and Biochemistry, **76**, 57-69.

Koven CD, Chambers JQ, Georgiou K *et al.* (2015) Controls on terrestrial carbon feedbacks by productivity vs. turnover in the CMIP5 Earth System Models. Biogeosciences Discussions, **12**, 5757-5801.

Kuzyakov Y, Friedel JK, Stahr K (2000) Review of mechanisms and quantification of priming effects. Soil Biology and Biochemistry, **32**, 1485-1498.

Kuzyakov Y (2010) Priming effects: interactions between living and dead organic matter. Soil Biology and Biochemistry, **42**, 1363-1371.

Parton WJ, Schimel DS, Cole CV, and Ojima DS (1987) Analysis of factors controlling soil organic matter levels in Great Plains grasslands. Soil Science Society of America Journal, **51**, 1173-1179 (1987).

Paterson E, Thornton B, Midwood AJ, Osborne SM, Sim A, Millard P (2008) Atmospheric CO_2 enrichment and nutrient additions to planted soil increase mineralisation of soil organic matter, but do not alter microbial utilisation of plant- and soil C-sources. Soil Biology and Biochemistry, **40**, 2434-2440.

Paterson E and Sim A (2013) Soil-specific response functions of organic matter mineralization to the availability of labile carbon. Global Change Biology **19**, 1562–1571.

Prior SA, Torbert HA, Runion GB, Rogers HH, Kimball BA (2008) Free-air CO_2 enrichment of sorghum: Soil carbon and nitrogen dynamics. Journal of Environmental Quality, **37**, 753-758.

Riley WJ, Maggi FM, Kleber M, Torn MS, Tang JY, Dwivedi D, Guerry N (2014) Long residence times of rapidly decomposable soil organic matter: application of a multi-phase, multi-component, and vertically respolved model (BAMS1) to soil carbon dynamics. Geoscientific Model Development, **7**, 1333-1355.

Sulman BN, Phillips RP, Oishi AC, Shevliakova E, and Pacala SW (2014) Microbe- driven turnover offsets mineral-mediated storage of soil carbon under elevated CO_2. Nature Climate Change, **4**, 1099–1102.

Tang J, Riley WJ (2015) Weaker soil carbon-climate feedbacks resulting from microbial and abiotic interactions. Nature Climate Change, **5**, 56-60.

Torbert HA, Prior SA, Runion GB, Davis MA, Pritchard SG, Rogers HH (2004) Nitrogen and carbon cycling in a model longleaf pine community as affected by elevated atmospheric CO_2. Environmental Management, **33**, 132-138.

Torn MS, Swanston CW, Castanha C, Trumbore SE (2009) Storage and Turnover of Organic Matter in Soil. In: *Biophysico-Chemical Processes Involving Natural Nonliving Organic Matter in Environmental Systems* (eds N. Senesi, B. Xing and P. M. Huang), pp. 219-272, John Wiley & Sons, Inc., Hoboken, NJ, USA.

van Groenigen KJ, Qi X, Osenberg CW, Luo Y, Hungate BA (2014) Faster decomposition under increased atmospheric CO_2 limits soil carbon storage. Science, **344**, 508-509.

Wang G, Mayes MA, Gu L, and Schadt W (2014) Representation of Dormant and Active Microbial Dynamics for Ecosystem Modeling. PLoS ONE, **9**, e89252.

Wieder WR, Bonan GB, and Allison SD (2013) Global soil carbon projections are improved by modelling microbial processes. Nature Climate Change, **3**, 909-912.

CHAPTER 4: Microbial community-level regulation explains soil carbon responses to long-term litter manipulations

CHAPTER 4: Microbial community-level regulation explains soil carbon responses to long-term litter manipulations

This chapter is reprinted, with permission, from the original journal article:

Georgiou, K., R. Z. Abramoff, W. J. Riley, M. S. Torn. Microbial community-level regulation explains soil carbon responses to long-term litter manipulations. *Nature Communications,* 1-10 (2017).

Abstract

Climatic, atmospheric, and land-use changes all have the potential to alter soil microbial activity mediated by changes in plant inputs. Many microbial models of soil organic carbon (SOC) decomposition have been proposed recently to advance prediction of climate and carbon (C) feedbacks. Most of these models, however, exhibit unrealistic oscillatory behavior and SOC insensitivity to long-term changes in C inputs. Here we diagnose the source of these problems in four archetypal models and propose a density-dependent formulation of microbial turnover, motivated by community-level interactions, that limits population sizes and reduces oscillations. We compare model predictions to 24 long-term C-input field manipulations and identify key benchmarks. The proposed formulation reproduces soil C responses to long-term C-input changes and implies greater SOC storage associated with CO_2-fertilization-driven increases in C inputs over the coming century compared to recent microbial models. This study provides a simple modification to improve microbial models for inclusion in Earth System Models.

Introduction

Understanding and quantifying the response of soil organic carbon (SOC) – the largest actively cycling terrestrial pool of organic carbon – to climatic and land-use change is imperative for projecting carbon (C) cycle dynamics. In most global- and ecosystem-scale biogeochemical models, SOC decomposition is directly proportional to the size of the soil carbon pool, with additional rate coefficients that account for soil moisture and temperature effects (i.e., "pseudo-first-order models"). This formulation is inherently unable to reproduce potentially critical feedbacks, such as priming (accelerated decomposition) of native SOC stocks due to, for example, increased plant root exudates at elevated CO_2 concentrations [1,2]. In fact, it has been widely observed that changes in plant C inputs to soils result in diverse, nonlinear responses of SOC stocks due to microbial population dynamics and competing decomposition and stabilization mechanisms [3–9]. These types of responses are particularly important in the face of atmospheric, climatic, and land-use change, which will affect the amount of plant C inputs that enter the soil – e.g., through changes in plant productivity, rooting depth, allocation, and species distributions [1,2,10–12].

Since soil microbial activity mediates SOC decomposition, increases in microbial activity following increases in plant inputs may limit SOC accumulation by stimulating decomposition [3,6,13]. Microbial models of SOC decomposition seek to capture this potential carbon-concentration feedback by explicitly representing microbial or enzymatic degradation of SOC [14]. Decomposition rates thus depend not only on the size of the SOC pool, but also on the size and

composition of the decomposer microbe pool [14–19]. Many microbial models have been proposed in recent years [14,20–22], as part of a burgeoning effort to understand and predict soil biogeochemical dynamics. Such models have even been applied to make predictions at the global scale [23,24], despite limited mathematical analyses of their dynamics and response to long-term perturbations [25–29]. These models can be grouped according to the complexity they represent (Fig. 1), and require careful theoretical and computational investigation to diagnose emergent dynamics. Within this framework, we used four archetypal models to investigate the observed divergence of model predictions from observations and the emergence of unrealistic, decadal SOC oscillations in response to changes in C input.

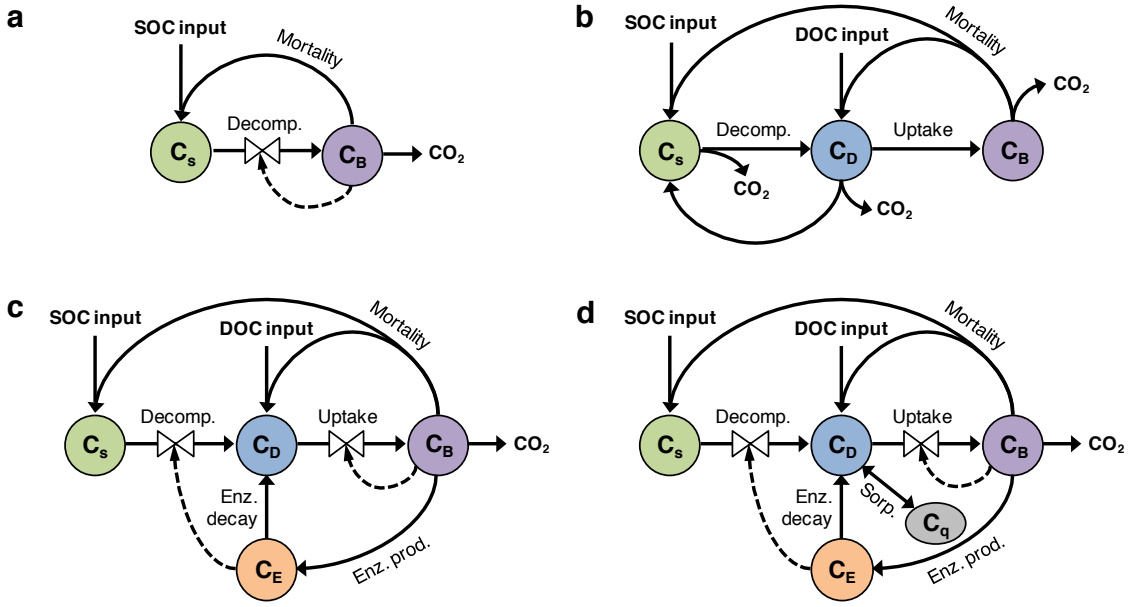

Figure 1: SOC decomposition models compared in this study.
(a) 2-pool microbial model with SOC (C_S) and microbial biomass C (MBC; C_B) pools. **(b)** 3-pool linear, first-order model with SOC, MBC and dissolved organic C (DOC; C_D) pools. **(c)** 4-pool microbial model that includes enzymatic (C_E) decomposition of SOC and subsequent assimilation (uptake) of DOC. **(d)** 5-pool microbial model that includes sorption of organic matter onto mineral surfaces to form mineral-associated organic C (C_q) that is protected from enzymatic attack.

Although oscillations of microbial biomass and activity may occur in microsites within the soil in response to a perturbation, such behavior is not commonly observed at the ecosystem scale or at daily and longer time scales [30–32]. That is, oscillations may occur in neighboring soil microsites or within hotspots, but do not appear when aggregated at the field scale because they are out-of-phase and are smoothed out by destructive interference [33,34]. However, the latter (larger) scale is that at which these oscillatory models are often applied [23,27,35]. There is also a disconnect between the timescales of observed versus predicted oscillations, where most microbial models exhibit oscillations on the decadal scale [27,35]. Thus, a key question is one of scale – the oscillations arising from microbial models are not observed at the large temporal and spatial scales at which the models are applied. Microbial models have therefore been avoided in recent studies largely on account of this unrealistic behavior [36]. While several studies have explored the emergence of decadal oscillations [26–28,35,37], a thorough analysis that diagnoses the source of this behavior and proposes modifications to remedy it is still needed.

Many microbial models consider substrate-microbe interactions at the level of individual microbes; however, at the community level, regulatory mechanisms – e.g., competition, space constraints, and other controls that depend on the density of individuals, such as disease and production of toxins – may limit microbial population sizes [34,38–42]. Indeed, representing such density-dependent processes in models is common in the field of population ecology, where the classic example is the logistic growth model that limits population size to a carrying capacity. While detailed models that include microbial community-level interactions (e.g., microbial competition, functional guilds, and stoichiometric homeostasis) do exist [34,42,43], prominent microbial models of SOC decomposition that are currently applied at regional to global scales do not impose limitations on the size of the microbial population [23,27,44]. Thus, microbial biomass in these models can grow indefinitely given a sustained increase in C inputs; whether C inputs double or increase by a factor of ten, the steady-state microbial population will change proportionally. This, consequently, drives SOC back to its pre-disturbance steady state, rendering it insensitive to long-term changes in C inputs. We thus hypothesized that including community-level regulation, via density-dependent microbial turnover, would limit both the unrealistic oscillations and SOC insensitivity to long-term changes in C input currently predicted by such microbial models.

Here we compared linear and microbial SOC models ranging in complexity to systematically diagnose their emergent behavior and attribute unrealistic characteristics to either parametric or structural differences. We incorporated density-dependent microbial turnover to explore the role of community-level regulation on projected SOC feedbacks. Specifically, we evaluated models in their response to long-term changes in plant C inputs by synthesizing observations from 24 long-term (> 5 years) litter manipulations, including the Detritus Input and Removal Treatment (DIRT) and Long-term Bare Fallow (LTBF) experiments, that span a range of soil types. These data are a unique resource for evaluating the models presented in this study and testing our hypothesis and, furthermore, constitute a powerful dataset for validating and benchmarking future SOC models. Our findings suggest that density-dependent microbial processes play an essential, but largely overlooked, role in regulating SOC dynamics. We discuss our results in the context of applying SOC models at large spatial scales and make recommendations on model features that are suitable for scaling up to Earth system models.

Methods

SOC model formulations

In this study we compare four archetypal SOC models that range in complexity (Fig. 1). Such models are common in recent literature [14,20,54,61], and require careful theoretical investigation of model behavior prior to implementation on larger spatial scales. To understand their behavior in response to C-input perturbations, we have dissected model components and added complexity incrementally, beginning from the simplest 2-pool microbial model. This 2-pool model has appeared in many studies (e.g., in refs. [21,25,35]), and here we adopt parameters from the version in ref. [35]. The C pools represented in the 2-pool model (Fig. 1a) are soil organic carbon (SOC; denoted C_S in subsequent equations) and microbial biomass carbon (MBC; denoted C_B). The 2-pool microbial model can be represented as follows,

$$\frac{dC_S}{dt} = I - \left(\frac{V_{max,U} C_B C_S}{K_{M,U} + C_S}\right) + k_B {C_B}^{\beta} \quad (3)$$

$$\frac{dC_B}{dt} = \varepsilon \left(\frac{V_{max,U} C_B C_S}{K_{M,U} + C_S}\right) - k_B {C_B}^{\beta} \quad (4)$$

where I is the carbon input rate, $V_{max,U}$ the maximum microbial assimilation rate of SOC, $K_{M,U}$ the half-saturation for assimilation, k_B the microbial mortality (turnover) rate constant, and ε the microbial C use efficiency (see Supplementary Table 1 for units and details). We also note that β (the density-dependence exponent) is proposed as a modification in this study, but has been equal to 1 (i.e., microbial mortality is directly proportional to C_B) in previous studies (e.g., refs. [21,25,35]). The condition $k_B \leq C_B^{1-\beta}$ must hold for any value of β, such that the mass balance constraint on microbial turnover, $k_B C_B^{\beta} \leq C_B$, is satisfied; for $\beta = 2$, this implies that $k_B \leq \frac{1}{C_B}$.

We compare the dynamics of this 2-pool microbe model to a 4-pool microbe-enzyme model in which we have added carbon pools for dissolved organic carbon (DOC; denoted C_D in all subsequent equations) and enzymatic carbon (ENZ; denoted C_E). This structure allows for the separation of enzymatic decomposition and microbial uptake of organic carbon (Fig. 1c). The 4-pool microbial model can then be written as

$$\frac{dC_S}{dt} = fI - \left(\frac{V_{max} C_E C_S}{K_M + C_S}\right) + a_{BS} k_B {C_B}^{\beta} \quad (5)$$

$$\frac{dC_D}{dt} = (1-f)I + \left(\frac{V_{max} C_E C_S}{K_M + C_S}\right) - \left(\frac{V_{max,U} C_B C_D}{K_{M,U} + C_D}\right) + (1 - a_{BS}) k_B {C_B}^{\beta} + r_E C_E \quad (6)$$

$$\frac{dC_B}{dt} = \varepsilon \left(\frac{V_{max,U} C_B C_D}{K_{M,U} + C_D}\right) - k_B {C_B}^{\beta} - r_p C_B \quad (7)$$

$$\frac{dC_E}{dt} = r_p C_B - r_E C_E \quad (8)$$

where V_{max} is the maximum enzymatic decomposition rate of SOC, K_M the half-saturation for decomposition, f the fraction of inputs that enters the SOC pool, a_{BS} the fraction of microbial turnover into SOC, r_E the enzyme turnover rate constant, and r_p the enzyme production rate constant.

We next include mineral sorption of DOC in a 5-pool microbial model, where DOC can reversibly bind to mineral surfaces forming a mineral-associated C pool (denoted C_q) that is protected from microbial uptake (Fig. 1d). This can be represented as

$$\frac{dC_S}{dt} = fI - \left(\frac{V_{max} C_E C_S}{K_M + C_S}\right) + a_{BS} k_B {C_B}^{\beta} \quad (9)$$

$$\frac{dC_D}{dt} = (1-f)I + \left(\frac{V_{max} C_E C_S}{K_M + C_S}\right) - \left(\frac{V_{max,U} C_B C_D}{K_{M,U} + C_D}\right) + (1 - a_{BS}) k_B {C_B}^{\beta} + r_E C_E - k_{ads} C_D \left(Q_{max} - C_q\right) + k_{des} C_q \quad (10)$$

$$\frac{dC_B}{dt} = \varepsilon\left(\frac{V_{max,U}C_BC_D}{K_{M,U}+C_D}\right) - k_B{C_B}^{\beta} - r_pC_B \quad (11)$$

$$\frac{dC_E}{dt} = r_pC_B - r_EC_E \quad (12)$$

$$\frac{dC_q}{dt} = k_{ads}C_D(Q_{max} - C_q) - k_{des}C_q \quad (13)$$

where k_{ads} is the adsorption rate constant, k_{des} the desorption rate constant, and Q_{max} the maximum DOC adsorption capacity, i.e., the mineral surface area available for organo-mineral interactions.

Finally, we compare these microbial models to a 3-pool linear, first-order model (Fig. 1b). The C pools represented include SOC, DOC, and MBC, and the transfer of C between these pools is directly proportional only to the pool where it originates [35,67]. The 3-pool linear model can be written as follows,

$$\frac{dC_S}{dt} = fI + f_Dk_DC_D + f_Bf_{B\to S}k_BC_B - k_SC_S \quad (14)$$

$$\frac{dC_D}{dt} = (1-f)I + f_Sk_SC_S + f_B(1-f_{B\to S})k_BC_B - k_{uptake}C_D - k_DC_D \quad (15)$$

$$\frac{dC_B}{dt} = k_{uptake}C_D - k_BC_B \quad (16)$$

where k_S is the SOC decay rate constant, k_D the DOC decay rate constant of DOC, k_B the MBC turnover rate constant, f_S the fraction of SOC entering the DOC pool, f_D the fraction of DOC entering the SOC pool, f_B the fraction of MBC turnover reentering the C pools (similar to a C use efficiency), $f_{B\to S}$ the fraction of retained MBC turnover C that enters the SOC pool, and k_{uptake} the DOC uptake rate constant.

Density-dependent microbial turnover

In population ecology, density-dependent processes, motivated by community-level interactions, are regulated by the size of the population itself. For example, this may take the form of density-dependent microbial turnover that effectively limits the potential size of a population. A typical formulation is logistic growth

$$\frac{dC_B}{dt} = r \cdot C_B \cdot \left(1 - \frac{C_B}{K}\right) \quad (17)$$

where r is the growth rate and K is the carrying capacity of the population. In this equation, at low populations, the unimpeded growth is modeled as the first term ($r \cdot C_B$), which results in exponential growth. As the population grows, however, the second term ($-r \cdot \frac{C_B^2}{K}$) begins to overtake the first term, thereby limiting the population size. This is an intuitive regulation of the

population size to some carrying capacity, resulting from competition, space constraints, and other density-dependent controls such as disease and toxicity.

Equation (17) can be rearranged to have the same form as the microbial models presented used in the literature. For example, from equation (4) with $\beta = 2$, we have

$$\frac{\mathrm{d}C_B}{\mathrm{d}t} = \varepsilon \cdot \left(\frac{V_{max,U} \cdot C_B \cdot C_S}{K_{M,U} + C_S}\right) - k_B \cdot {C_B}^2 \tag{18}$$

where the logistic growth parameters can be represented as

$$r = \varepsilon \cdot \left(\frac{V_{max,U} \cdot C_S}{K_{M,U} + C_S}\right) \tag{19}$$

and $\frac{r}{K} = k_B$ so that

$$K = \frac{\varepsilon}{k_B} \cdot \left(\frac{V_{max,U} \cdot C_S}{K_{M,U} + C_S}\right). \tag{20}$$

Here the growth rate and carrying capacity depend on the substrate availability (C_S) and thus, unlike most existing microbial models, microbes experience an additional constraint on population size.

We note that the parameter $\beta = 2$ gives logistic growth, but this parameter need not be equal to 2. In fact, any value greater than 1 will impart a density-dependent microbial turnover rate (i.e., more mortality when populations are large) that will limit population sizes.

Parameter values

For the 2-, 3-, and 4-pool models, we adapted parameter values from ref. [35] where the three models were fit to obtain comparable steady-state solutions among corresponding C pools in each model. We used empirical rate constants for the organo-mineral interactions in the 5-pool model [68,69] and matched the steady-state solutions of the other models. We note that a subset of the parameters from ref. [35] were derived from lab incubations in the literature and the remaining parameters were fit to attain reasonable field C pool steady-state solutions. However, rates measured in the lab may not be representative of process rates in the field or at ecosystem scales. Although we use this particular set of parameters in our numerical simulations, our analytical work shows that our conclusions about model behavior are robust to the choice of parameter values. Additional details about the parameter values are summarized in Supplementary Table 1.

Analytical and numerical evaluation

We analytically derived the steady-state solutions of each of the four models, with and without density-dependent microbial turnover, by setting all $\frac{\mathrm{d}C_i(t)}{\mathrm{d}t} = 0$ (where $C_i(t)$ is the concentration of the i^{th} component in time) and solving the corresponding algebraic equations. We then analyzed the dependence (or lack thereof) of the model steady-state solutions on the rate of C

inputs. Furthermore, we simulated all four models to analyze their diverse transient responses to increased and decreased C inputs.

We also performed a stability analysis for each of the four models to understand their behavior and explain the emergence of oscillations with select model structures and parameter sets. We linearized each model using a multivariable Taylor expansion, forming the Jacobian (*J*) matrix from the first-order partial derivatives evaluated at equilibrium. The eigenvalues (λ_j) of the matrix J characterize the stability of the system, since the solution can be written as a superposition of exponential $e^{\lambda_j t}$ terms, where t denotes time. The eigenvalues were calculated for each model to understand the dynamics near equilibrium, where for $\lambda_j = \alpha_j \pm \gamma_j i$ the following scenarios can be summarized: (1) $\gamma_j = 0$, $\alpha_j < 0$ corresponds to a stable mode and $\alpha_j > 0$ to an unstable mode; and (2) $\gamma_j \neq 0$, $\alpha_j < 0$ corresponds to a damped (diminishing) oscillation, $\alpha_j > 0$ to an unstable (increasing) oscillation, and $\alpha_j = 0$ to a persistent oscillation with a period of $\frac{2\pi}{\gamma_j}$. The damping ratio (ζ_j) can then be defined as

$$\zeta_j = \frac{-\alpha_j}{\sqrt{{\alpha_j}^2 + {\gamma_j}^2}} \tag{21}$$

for each eigenvalue λ_j, where $\zeta = 1$ signifies a stable mode, $0 < \zeta < 1$ signifies damped oscillations, and $\zeta < 0$ signifies an unstable equilibrium [29,70]. In the case of the 2-pool microbial model, there is a single complex conjugate pair of eigenvalues and the corresponding value of ζ was calculated as a function of the model parameters (Fig. 2). We assign the damping ratio of the dominant mode (smallest ζ) as the damping ratio of the linearized system and use this as a metric to illustrate the stability of the models under different parameter sets and with/without density-dependent microbial turnover.

Long-term C input simulations and observations

We simulated the response of the models to a doubling (2X; 100% increase) and removal (0X; 100% decrease) of C inputs, following the manipulations of the long-term Detritus Input and Removal Treatment (DIRT) and Long-term Bare Fallow (LTBF) experiments. We then compared the model results to our synthesis of long-term observations from DIRT and LTBF studies. We compiled DIRT and LTBF data of SOC and MBC from 18 sites with 24 total (6 doubled litter and 18 litter removal) manipulations, each across several time points ranging from 5 to 80 years (summarized in Supplementary Tables 2-3). We provide a summary of the findings across these sites, but focus our model-data comparison on experiments with over 20 years of measurements; for example, the 50+ year Noe and Wingra Woods Wisconsin DIRT experiment [30] and the 50+ year LTBF experiments [31]. We also synthesized MBC observations [55,56], which are summarized in Supplementary Fig. 12.

Results

Analytical steady-state solutions of models

For each SOC model (Fig. 1), we derived the analytical steady-state solution as a function of model parameters (Table 1). In the absence of density-dependent microbial turnover (i.e., for density-dependent exponent $\beta = 1$; see Methods), the steady-state SOC stock (denoted C_S) is not a function of total C inputs (denoted I), but only of select system parameters. For example, for the 2-pool microbial model with $\beta = 1$ (Fig. 1a):

$$C_S = \frac{K_{M,U} \cdot k_B}{\varepsilon \cdot V_{max,U} - k_B} \quad (1)$$

at steady state (Table 1), where $V_{max,U}$ is the maximum microbial assimilation rate, $K_{M,U}$ the half-saturation for assimilation, k_B the microbial turnover rate constant, and ε the microbial C use efficiency (Supplementary Table 1). Conversely, the 3-pool linear, first-order model (Fig. 1b) always predicts that the C_S steady-state solution is directly proportional to total C inputs (Table 1). In the microbial models with $\beta = 1$ and the 3-pool linear model, the steady-state microbial biomass carbon (MBC; denoted C_B) is directly proportional to the C input rate. For example, for the 2-pool microbial model with $\beta = 1$:

$$C_B = \left(\frac{\varepsilon \cdot I}{(1-\varepsilon) \cdot k_B}\right). \quad (2)$$

This implies that, for the microbial models with $\beta = 1$, the ratio of MBC to SOC (C_B/C_S) is proportional to the C input rate (Supplementary Note 1). With density-dependent microbial turnover ($\beta > 1$), however, the microbial models predict a sensitivity of the C_S steady state to C inputs and the C_B steady state remains responsive, but not proportional, to C inputs (Table 1). This allows the ratio of MBC/SOC to be largely independent of the C input rate depending on the value of β, as is also the case for the 3-pool linear model (Table 1). These are fundamental differences among the predictions of microbial models, and between microbial and linear models that are a direct consequence of model structure, and not the parameters.

Dynamic response of models to perturbations

We analytically and numerically explored the stability of each model and its response to C-input perturbations, using a change in both SOC and DOC inputs as a general case. We found that the microbial models in recent literature (i.e., the 2-, 4-, and 5-pool models with $\beta = 1$; Fig. 1a,c,d) are particularly prone to oscillations as a consequence of their model structure and parameters. For common parameter values (Supplementary Table 1), these models exhibit damped oscillations with a period of 10 to 20 years in response to an increase in C inputs (Fig. 2; Supplementary Figs. 1-3). This behavior is largely due to an imbalance between the C assimilation term, which has a positive sign and is proportional to C_B in the differential equation for $\frac{\mathrm{d}C_B}{\mathrm{d}t}$, and the microbial turnover (mortality) term. Microbial assimilation (hereafter C uptake) is represented as $\varepsilon\left(\frac{V_{max,U} \cdot C_i \cdot C_B}{K_{M,U} + C_i}\right)$, where C_i represents SOC (C_S) in the 2-pool model and DOC (C_D) in the 4- and 5- pool models. When this C uptake exceeds the mortality term, the microbial

population experiences exponential growth until it consumes too much substrate, causing a transient crash in the population until the substrate can recover – and the cycle repeats. We calculated the characteristic damping ratio (ζ; see Methods) and the period of oscillations from the eigenvalues of each linearized system and found that they strongly depend on the parameters $V_{max,U}$, $K_{m,U}$, ε, and k_B, as well as β (Fig. 2; Supplementary Figs. 2, 4 and 5; parameter details in Supplementary Table 1). A damping ratio of $\zeta = 1$ (i.e., stable system with no oscillations) is achieved for any $\beta \geq 1.5$ in the 2-pool model (Fig. 2).

Table 1: Steady-state solutions of the SOC decomposition models.

2-pool microbial model (for all β) *	$C_S = \frac{K_{M,U} \cdot k_B \cdot {C_B}^{\beta-1}}{\varepsilon \cdot V_{max,U} - k_B \cdot {C_B}^{\beta-1}}$ $C_B = \left(\frac{\varepsilon \cdot I}{(1-\varepsilon) \cdot k_B}\right)^{1/\beta}$
3-pool linear model	$C_S = \frac{fI + C_D(f_D k_D + k_{uptake} f_B f_{B\to S})}{k_S}$ $C_D = \frac{I\,[(1-f) + f f_S]}{[k_{uptake} + k_D + k_{uptake} f_B (f_{B\to S} - 1 - f_{B\to S} f_S) - f_D k_D f_S]}$ $C_B = \frac{k_{uptake} C_D}{k_B}$
4-pool microbial model (for all β) *	$C_S = \frac{K_M \cdot (f \cdot I + k_B \cdot a_{BS} \cdot {C_B}^{\beta})}{V_{max} \cdot \frac{r_p}{r_E} \cdot C_B - (f \cdot I + k_B \cdot a_{BS} \cdot {C_B}^{\beta})}$ $C_D = \frac{K_{M,U} \cdot (r_p + k_B \cdot {C_B}^{\beta-1})}{\varepsilon \cdot V_{max,U} - (r_p + k_B \cdot {C_B}^{\beta-1})}$ $k_B {C_B}^{\beta} + r_p C_B = \frac{\varepsilon \cdot I}{(1-\varepsilon)}$ (implicit equation for all β) $C_E = \frac{r_p \cdot C_B}{r_E}$
5-pool microbial model (for all β) *	C_S , C_D , C_B , C_E (same as 4-pool model for all β) $C_q = \frac{k_{ads} \cdot Q_{max} \cdot C_D}{k_{des} + k_{ads} \cdot C_D}$

* General expressions are given for any value of density-dependent microbial turnover (β), where microbial models in the literature do not include density-dependence, i.e., $\beta = 1$. Parameter definitions can be found in Supplementary Table 1.

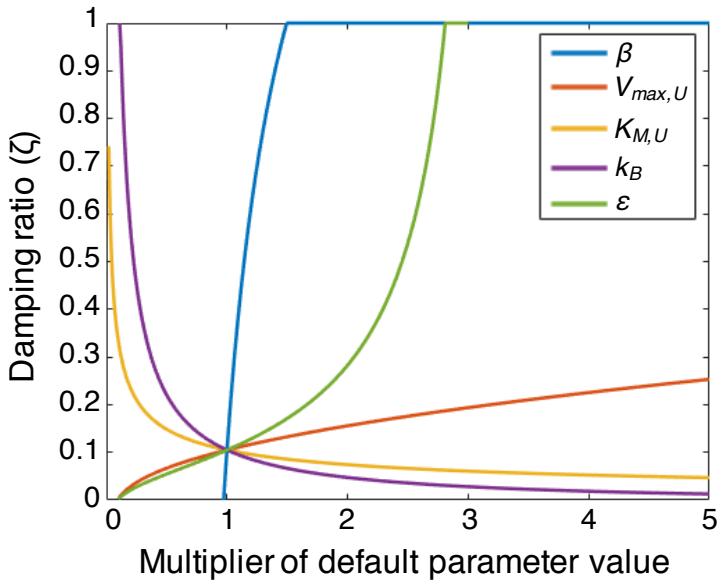

Figure 2: Damping ratio of the 2-pool microbial model as a function of the model parameters.
The damping ratio (ζ) is a metric that depicts the degree of oscillatory behavior of the linearized system near its steady state, where $\zeta = 1$ signifies a stable node, $0 < \zeta < 1$ damped (diminishing) oscillations, $-1 < \zeta < 0$ unstable (growing) oscillations, and $\zeta = -1$ an unstable node. Here all parameters were varied independently from their default value (Supplementary Table 1) by the given multiplier (x-axis) to illustrate the inherent sensitivity of the oscillations on the parameter values. The model stability is very sensitive to the density-dependence exponent (β).

We also analyzed the scenario where the change in C inputs occurs unevenly among pools, entering either the SOC pool (I_S) or the DOC pool (I_D), for example, in contrast to the change in C inputs entering both pools. That is, we performed simulations in which I_S, I_D, or both ($I = I_S + I_D$) are perturbed (Supplementary Note 2). This analysis was motivated by the potential for the fraction entering each pool (f) to change, where $I_S = f \cdot I$ and $I_D = (1 - f) \cdot I$. This numerical experiment showed that the transient dynamics and steady-state responses of all models (i.e., the microbial models and the first-order, linear model) depended on which C input (SOC or DOC) was perturbed (Supplementary Figs. 6 and 7). The response of the steady-state SOC stock to a range of C input treatments (from complete removal to doubling of I_S, I_D, or both) was compared for the 3-pool linear model and the 4-pool microbial model with and without density-dependent microbial turnover (Supplementary Fig. 7). We observed that without density-dependent microbial turnover, the 4-pool model steady-state SOC stock was insensitive to changes in the total C inputs (I), consistent with its analytical steady-state solution (Table 1).

Density-dependent microbial turnover

We evaluated the effects of density-dependent microbial turnover (i.e., setting the mortality rate proportional to $(C_B)^\beta$ with $\beta > 1$) and found that the SOC oscillations in response to changes in C inputs (as observed in the literature for $\beta = 1$) can be reduced or completely removed (Fig. 3). While an exponent of $\beta = 2$ leads to logistic growth, we note that β can take on any value > 1 to reduce SOC oscillations (Figs. 2 and 3). We further explored the effect of β on the percent change in steady-state SOC following a range of step changes in total C inputs (Fig. 4). For $\beta =$

1, the model reduces to the common microbial model where the long-term SOC is insensitive to any change in total C inputs. As the exponent ($\beta > 1$) increases, however, the long-term SOC becomes increasingly sensitive to changes in C inputs.

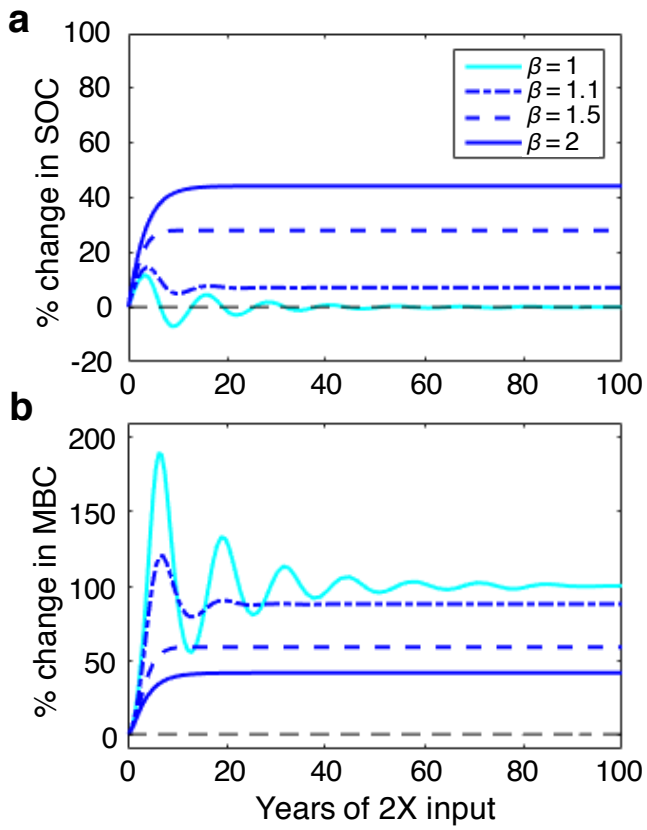

Figure 3: Response of SOC and MBC to a sustained doubling of C inputs in the 2-pool microbial model with and without density-dependent microbial turnover.
(a) Percent change of modeled SOC following a 2X step increase in total C inputs. **(b)** Percent change of modeled MBC following a 2X step increase in total C inputs. The value of the parameter β depicts the strength of density-dependent microbial turnover, where $\beta = 1$ corresponds to no density-dependence and $\beta = 2$ to a strong density-dependence.

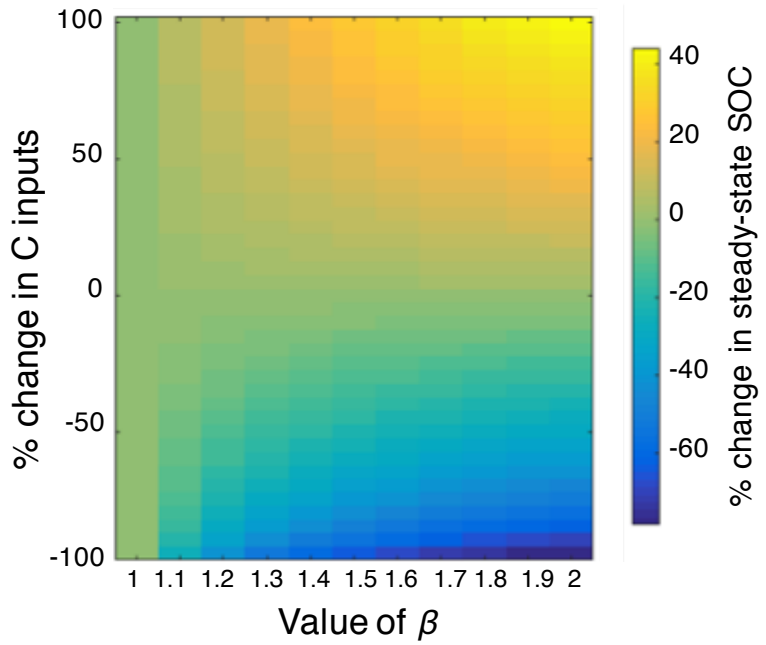

Figure 4: Percent change in the SOC steady state following a range of step changes in C inputs with a range of β values in the 2-pool microbial model.
The value of β depicts the strength of density-dependent microbial turnover, where $\beta = 1$ gives the widely used 2-pool microbial model without density-dependence and $\beta = 2$ gives a strong density-dependence.

In all models without density-dependence, heterotrophic respiration (CO_2 efflux) is always directly proportional to MBC (Supplementary Figs. 8 and 9). When density-dependence is incorporated, steady-state respiration doubles for a doubling of C inputs, but the steady-state MBC does not double due to constraints that limit population size (Supplementary Figs. 4b,c and 8b,c). This response is effectively an increase in the specific respiration rate as microbial populations increase, since there is proportionally more respiration per unit of MBC.

Doubling C inputs in models and experiments

We compared the response of all four models to a doubling of total C inputs (Fig. 5a,c) with our synthesis of DIRT experiments, in which C inputs to the soil were doubled at 6 different sites over 5 to 50 years (Fig. 6a; Supplementary Table 2). The two longest-running DIRT sites, Noe and Wingra Woods (50 years), showed similar increases in SOC stocks in response to doubling C inputs, where SOC approached a new steady state that was ~40% higher than the control (Fig. 6a). Similar SOC responses were observed at other DIRT sites, with SOC stocks varying between 0 to 60% of the pre-disturbance steady state after 5+ years of treatment (Fig. 6a; Supplementary Figs. 10a and 11).

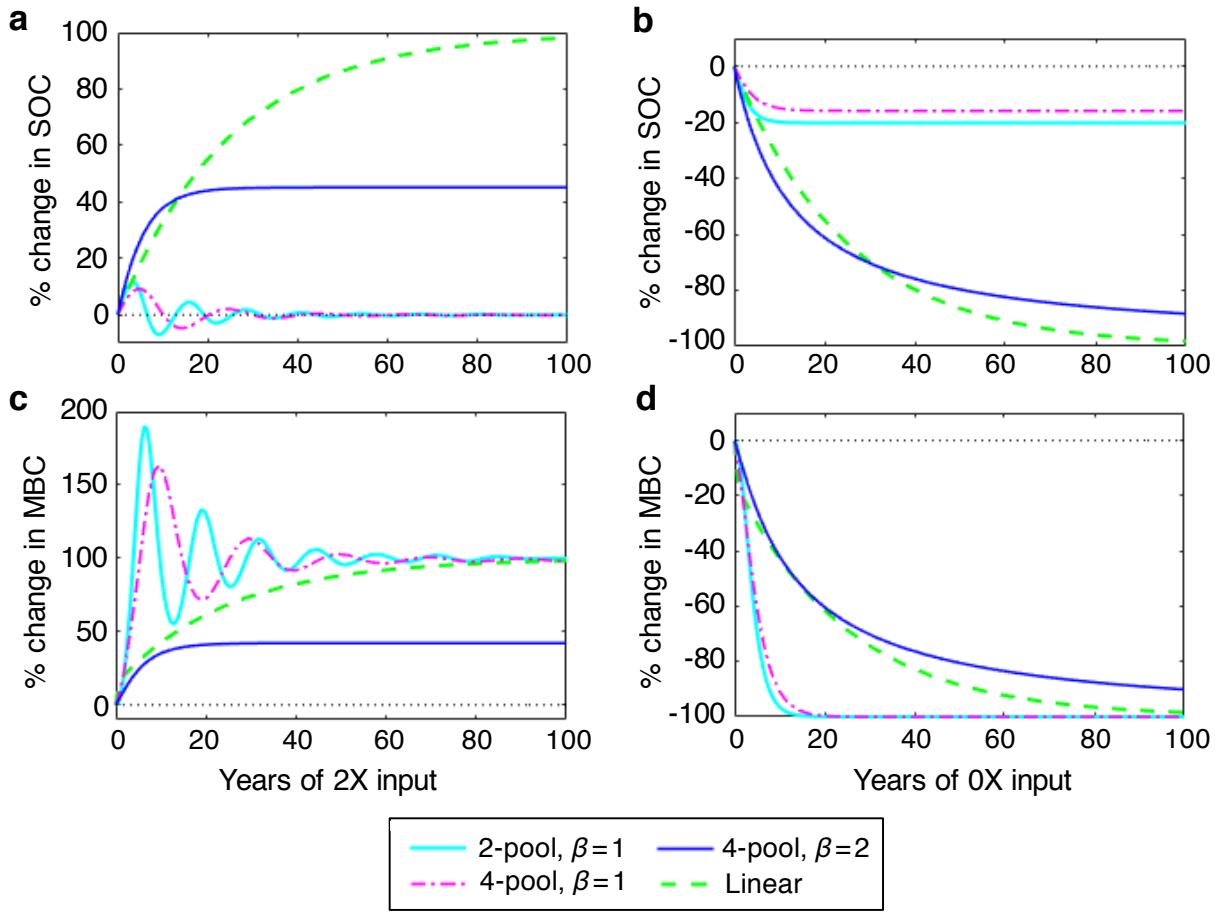

Figure 5: Response of SOC and MBC to doubling and removal of C inputs in models.
(a,c) Percent change of modeled SOC and MBC following a 2X step increase in inputs. **(b,d)** Percent change of modeled SOC and MBC following sustained 0X inputs. A value of $\beta > 1$ corresponds to a microbial model with density-dependent microbial turnover. The 5-pool microbial model overlaps with the 4-pool microbial model for the parameter set in Supplementary Table 1.

The microbial models without density-dependence are unable to capture the range of SOC responses observed in the DIRT experiments (Figs. 5a and 6a), as a direct consequence of their model structure. Similarly, the linear model structure predicts that the SOC steady state will always change proportionally to the change in C inputs. These two model formulations are thus limited in the SOC responses that they can predict, and do not match observations given an increase in total C inputs. In contrast, the microbial models with density-dependence can, depending on the value of β, capture a change in the long-term SOC stocks that is within the range observed from experiments (dark blue line, Fig. 5a; Fig. 6a). Long-term (> 5 years) MBC measurements and replicates were not available from most DIRT plots and, therefore, the comparison with MBC model output for a doubling of C inputs was inconclusive (Supplementary Table 2; Supplementary Fig. 12a).

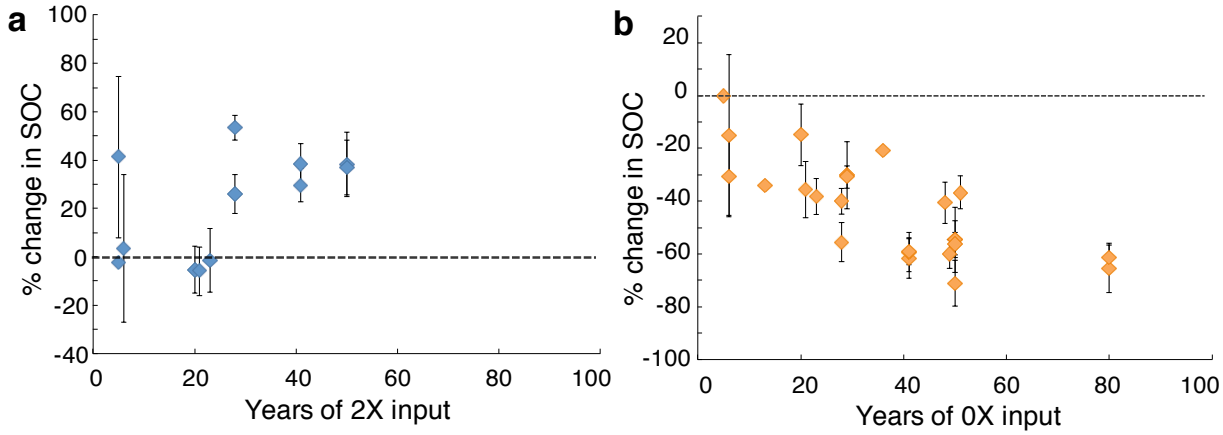

Figure 6: Response of SOC to doubling and removal of C inputs in long-term litter manipulations. **(a)** Percent change in SOC at Detritus Input and Removal Treatment (DIRT) experiments after a sustained 2X step increase in inputs. **(b)** Percent change in SOC at DIRT and Long-Term Bare Fallow (LTBF) experiments after sustained 0X inputs. Points indicate means and bars the standard error of the mean. Individual points are separated by site in Supplementary Fig. 10 and data sources are reported in Supplementary Tables 2-3.

Removing C inputs in models and experiments

We compared SOC and MBC projections for a complete removal of C inputs (Fig. 5b,d) to the analogous treatments in the DIRT and LTBF experiments (Fig. 6b; Supplementary Fig 10). We synthesized results from 18 different sites with measurements spanning 5 to 80 years (Supplementary Tables 2-3) [30,31,45–47] and summarized the observed SOC and MBC responses (Fig. 6b; Supplementary Figs. 11 and 12b). The microbial models without density-dependence ($\beta = 1$) predicted a rapid decrease in MBC, where MBC completely died out within 10 years, despite remaining SOC stocks; only ~20% of SOC stocks were lost by the time MBC declined to zero (Fig. 5b; Supplementary Fig. 13). In contrast, the linear model showed a gradual decrease in all pools, approaching zero after 80+ years. While the microbial models with density-dependent turnover ($\beta = 2$) gave similar predictions for C input removal to the linear model, they experienced a faster SOC decline in the first two decades that became more gradual over time (Fig. 5b). All of the long-term C-input removal sites showed a gradual decrease in SOC stocks (Fig. 6b), where most sites reached a period of slower decomposition by 50 years, and MBC decreased but did not die out (Supplementary Fig. 12b; Supplementary Tables 2-3).

Discussion & Conclusions

Due to the important contribution of SOC to the terrestrial C budget following changes in plant productivity, it is crucial that soil C models are able to capture the transient and steady-state dynamics of long-term C-input manipulations in the field. Our results show that, across the range of model complexities investigated, microbial models without density-dependent microbial turnover (i.e., $\beta = 1$) return to their pre-disturbance SOC steady state following a sustained increase in total C inputs, for any increase in inputs (Fig. 4; Supplementary Fig. 7). This behavior is a direct consequence of the microbial model structure, which also results in damped decadal oscillations for most parameter sets reported in the literature (Fig. 2). The decoupling of C inputs and long-term SOC stocks has been observed in several modeling studies that effectively used $\beta = 1$ [20,23,25]. The proportionality between C inputs and long-term MBC (and the resulting insensitivity of long-term SOC) implies that MBC is only limited by the C input rate

(Supplementary Fig. 7), but in fact it can also be limited by community-level regulatory mechanisms [38–41]. In microbial models with $\beta = 1$, a change in C inputs drives a proportional change in the long-term ratio of MBC to SOC (C_B/C_S; see Supplementary Note 1), in contrast to global observations that suggest this ratio is confined to a rather narrow range [48].

Increasing the density-dependence $\beta > 1$ strengthens community-level regulation of MBC, and therefore limits how large (and how quickly) the MBC pool can grow or decline (Fig. 3). The case of $\beta = 2$ has been widely used in modeling population dynamics, including past biogeochemical models [18], and it is a logical modification: microbes experience proportionally more mortality (e.g., due to competition, space-constraints, disease, and production of toxins) as their concentrations increase. We show that a value of $1 < \beta < 2$ imparts a moderate SOC sensitivity to C inputs and acts to reduce oscillations (Figs. 2 and 3). We expect the effective value of β to vary between biomes, and potentially with depth, depending on the strength of microbial community-level regulation that arises from biotic and abiotic limitations. The high sensitivity of microbial model predictions to changes in β highlights the need for experiments that quantify its value and its relation to explicit underlying regulatory mechanisms in different soils. Meta-analyses exploring MBC/SOC ratios [48,49] and emergent scaling relationships of microbial function [50–53] corroborate the density-dependent turnover ($\beta > 1$) formulation and are invaluable for constraining the value of β in future modeling studies.

Plant-input manipulation experiments show that long-term measured SOC stocks are, in fact, sensitive to C input rate in the field, contrary to the predicted SOC stocks from most microbial models (Figs. 5a and 6a). Following an increase in C inputs, microbial models without density-dependent turnover (i.e., $\beta = 1$) overestimate the response of MBC and, thus, underestimate the response of SOC (Figs. 5a,c and 6a). This suggests that a mechanism limiting the size of the microbial pool is necessary, and consistent with a density-dependent turnover formulation. Furthermore, in microbial models with $\beta = 1$, MBC disappears within 5-10 years of ceasing plant inputs (Figs. 5d), and SOC decreases too quickly to a nonzero value and is invariant once microbes die out (Figs. 5b and 6b). The complete loss of MBC after cessation of C inputs was also predicted by a microbial model (with $\beta = 1$) that included organo-mineral interactions and microbial physiology [54] (similar to the 5-pool model, Fig. 1d), but this prediction had not been compared to data. In contrast, the empirical evidence synthesized here [55–57] suggests that SOC and MBC continue to decrease slowly over decades (Figs. 6b; Supplementary Fig. 12). Density-dependent turnover in microbial models slows the decay of SOC and MBC such that they persist for 80+ years, better matching observations and further corroborating the need for a density-dependent turnover formulation.

We note that other microbial model formulations exist in the literature that behave differently than the class of models presented in this study. For example, the so-called 'reverse Michaelis-Menten' microbial model [14,19,58] – a class of Equilibrium Chemistry Approximation (ECA) kinetics [59,60] – predicts a slight sensitivity of the SOC steady state to C inputs, but the MBC steady state is again directly proportional to the C input rate [26]. While this formulation dampens oscillations [26], the decadal oscillations do persist, and the long-term response to C-input manipulations has not been evaluated. Another example is the MIcrobial-MIneral Carbon Stabilization (MIMICS) model [22,61]. Recently, the microbial turnover rate in MIMICS was modified by a factor of $\sqrt{I}$ (where I denotes C inputs) to better explain litter decomposition

observations [62]. Interestingly, explicit density-dependent microbial turnover in microbial models can be shown to impart this same modification on the microbial turnover rate over long timescales; for $\beta = 2$, $C_B \sim \sqrt{I}$ and thus microbial turnover is proportional to $\sqrt{I}\, C_B$.

Dormancy is another mechanism that has recently been incorporated in microbial models and has shown promise in better matching respiration seasonality and moisture sensitivity [63]. A dormancy formulation allows microbes to switch from an active state (in which they decompose SOC and proliferate) to a dormant state [63,64]. In the case of substrate limitation or starvation following C input removal, this mechanism may help preserve MBC, albeit in a dormant state, over longer periods of time than in microbial models without dormancy. This MBC would then be available to respond rapidly to future increases in C inputs and favorable environmental conditions, as observed in field and laboratory experiments [46,56,57]. However, if dormancy approaches zero when C inputs to the soil are increased [63,64], the resulting model approaches the microbial models without dormancy and will still be insensitive to increases in C inputs. Thus, even with dormancy, future formulations are likely to require a density-dependent turnover, either in the microbial mortality term or in the transition between active and dormant microbial states.

When connecting global change experiments to model predictions, variable changes in plant C inputs over time (as opposed to step-changes in many manipulations) may prevent SOC from reaching a steady state on relevant time scales. Thus, models must accurately capture transient dynamics, where community-level regulation (i.e., here density-dependence with $\beta = 2$) plays a key role. Step-change scenarios are also highly relevant for studying the impacts of land-use change. While we have focused on C-only manipulations in this study, more complex models that explicitly represent nutrients may be necessary to capture other biogeochemical interactions; e.g., addition/limitation of nitrogen (N) and phosphorus (P) [43]. However, our results on SOC model stability and sensitivity to C inputs are robust and relevant to more complex C-N or C-N-P models as well, since a similar representation of key processes is used in such models.

Given the significant and growing interest in developing microbial models for predicting soil C dynamics over large spatiotemporal scales, it is imperative to compare proposed models and validate model behaviors against observations. This validation is particularly important in light of the significant divergence among soil C model predictions to future temperature and C input change, which have far-reaching global implications [65,66]. Here we diagnosed structural and parametric differences between models ranging in complexity, and synthesized a novel dataset from long-term litter manipulation experiments to evaluate the models and validate our hypothesis. Analyzing the underlying mechanisms of simple microbial models allowed us to identify the source of, and potential solution to, behavior deemed unrealistic in recent studies. Namely, a model formulation with density-dependent microbial turnover ($\beta > 1$; arising from competition, space, or other community-level regulation mechanisms) reduced oscillations and resulted in a realistic sensitivity of long-term SOC stocks to (and a decoupling of the MBC/SOC ratio from) C inputs. All else equal, the proposed formulation implies larger SOC storage associated with expected CO_2-fertilization-driven increases in C inputs over the coming century compared to microbial models with $\beta = 1$. Moving forward, we encourage the validation of subcomponents of increasingly complex microbial models before they are applied at field or larger scales, and a concerted effort to identify additional metrics and datasets to benchmark mechanistic models.

References

1. Hungate, B. A. et al. The fate of carbon in grasslands under carbon dioxide enrichment. Nature 388, 576–579 (1997).
2. Stulen, I. & den Hertog, J. Root growth and functioning under atmospheric CO2 enrichment. Vegetatio 104/105, 99–115 (1993).
3. Y. Kuzyakov, J.K. Friedel, K. S. Review of mechanisms and quantification of priming effects. Soil Biol. Biochem. 32, 1485–1498 (2000).
4. Fontaine, S., Bardoux, G., Abbadie, L. & Mariotti, A. Carbon input to soil may decrease soil carbon content. Ecol. Lett. 7, 314–320 (2004).
5. Xu, S., Liu, L. L. & Sayer, E. J. Variability of above-ground litter inputs alters soil physicochemical and biological processes: A meta-analysis of litterfall-manipulation experiments. Biogeosciences 10, 7423–7433 (2013).
6. Zhu, B. et al. Rhizosphere priming effects on soil carbon and nitrogen mineralization. Soil Biol. Biochem. 76, 183–192 (2014).
7. Kallenbach, C. M., Frey, S. D. & Grandy, A. S. Direct evidence for microbial-derived soil organic matter formation and its ecophysiological controls. Nat. Commun. 7, 1–10 (2016).
8. Schmidt, M. W. I. et al. Persistence of soil organic matter as an ecosystem property. Nature 478, 49–56 (2011).
9. Cotrufo, M. F., Wallenstein, M. D., Boot, C. M., Denef, K. & Paul, E. The Microbial Efficiency-Matrix Stabilization (MEMS) framework integrates plant litter decomposition with soil organic matter stabilization: Do labile plant inputs form stable soil organic matter? Glob. Chang. Biol. 19, 988–995 (2013).
10. Lichter, J. et al. Soil carbon sequestration in a pine forest after 9 years of atmospheric CO 2 enrichment. Glob. Chang. Biol. 14, 2910–2922 (2008).
11. Norby, R. J. et al. Model–data synthesis for the next generation of forest free-air CO2 enrichment (FACE) experiments. New Phytol. 209, 17–28 (2016).
12. Phillips, D. L. et al. Effects of elevated CO2 on fine root dynamics in a Mojave Desert community: a FACE study. Glob. Chang. Biol. 12, 61–73 (2006).
13. Kuzyakov, Y. Priming effects: Interactions between living and dead organic matter. Soil Biol. Biochem. 42, 1363–1371 (2010).
14. Wieder, W. R., Allison, S. D., Davidson, E. A., Georgiou, K. & Hararuk, O. Explicitly representing soil microbial processes in Earth system models. Global Biogeochem. Cycles 29, 1782–1800 (2015).
15. Parnas, H. Model for decomposition of organic material by microorganisms. Soil Biol. Biochem. 7, 161–169 (1975).
16. Parnas, H. A theoretical explanation of the priming effect based on microbial growth with two limiting substrates. Soil Biol. Biochem. 8, 139–144 (1976).
17. Harte, J. Modeling Lake-water Mineralization Processes. J. Theor. Biol. 99, 553–569 (1982).
18. Harte, J. & Kinzig, A. P. Mutualism and Competition between Plants and Decomposers: Implications for Nutrient Allocation in Ecosystems. Am. Nat. 141, 829 (1993).
19. Schimel, J. P. & Weintraub, M. N. The implications of exoenzyme activity on microbial carbon and nitrogen limitation in soil: A theoretical model. Soil Biol. Biochem. 35, 549–563 (2003).
20. Allison, S. D., Wallenstein, M. D. & Bradford, M. a. Soil-carbon response to warming dependent on microbial physiology. Nat. Geosci. 3, 336–340 (2010).

21. German, D. P., Marcelo, K. R. B., Stone, M. M. & Allison, S. D. The Michaelis-Menten kinetics of soil extracellular enzymes in response to temperature: A cross-latitudinal study. Glob. Chang. Biol. 18, 1468–1479 (2012).
22. Wieder, W. R., Grandy, a. S., Kallenbach, C. M. & Bonan, G. B. Integrating microbial physiology and physio-chemical principles in soils with the MIcrobial-MIneral Carbon Stabilization (MIMICS) model. Biogeosciences 11, 3899–3917 (2014).
23. Wieder, W. R., Bonan, G. B. & Allison, S. D. Global soil carbon projections are improved by modelling microbial processes. Nat. Clim. Chang. 1–7 (2013).
24. Sulman, B. N., Phillips, R. P., Oishi, a. C., Shevliakova, E. & Pacala, S. W. Microbe-driven turnover offsets mineral-mediated storage of soil carbon under elevated CO2. Nat. Clim. Chang. 4, 1099–1102 (2014).
25. Wang, Y. P. et al. Oscillatory behavior of two nonlinear microbial models of soil carbon decomposition. Biogeosciences 11, 1817–1831 (2014).
26. Wang, Y. P. et al. Responses of two nonlinear microbial models to warming and increased carbon input. Biogeosciences 13, 887–902 (2016).
27. Hararuk, O., Smith, M. J. & Luo, Y. Microbial models with data-driven parameters predict stronger soil carbon responses to climate change. Glob. Chang. Biol. 21, 2439–2453 (2015).
28. Sierra, C. A. & Muller, M. A general mathematical framework for representing soil organic matter dynamics. Ecol. Monogr. 85, 505–524 (2015).
29. Sierra, C. A., Malghani, S. & Müller, M. Model structure and parameter identification of soil organic matter models. Soil Biol. Biochem. 90, 197–203 (2015).
30. Lajtha, K. et al. Changes to particulate versus mineral-associated soil carbon after 50 years of litter manipulation in forest and prairie experimental ecosystems. Biogeochemistry 119, 341–360 (2014).
31. Barré, P. et al. Quantifying and isolating stable soil organic carbon using long-term bare fallow experiments. Biogeosciences 7, 3839–3850 (2010).
32. Liu, J. et al. Metabolic co-dependence gives rise to collective oscillations within biofilms. Nature 523, 550–554 (2015).
33. Kuzyakov, Y. & Blagodatskaya, E. Microbial hotspots and hot moments in soil: Concept & review. Soil Biol. Biochem. 83, 184–199 (2015).
34. Kaiser, C., Franklin, O., Dieckmann, U. & Richter, A. Microbial community dynamics alleviate stoichiometric constraints during litter decay. Ecol. Lett. 17, 680–690 (2014).
35. Li, J., Wang, G., Allison, S. D., Mayes, M. A. & Luo, Y. Soil carbon sensitivity to temperature and carbon use efficiency compared across microbial-ecosystem models of varying complexity. Biogeochemistry 119, 67–84 (2014).
36. Lange, M. et al. Plant diversity increases soil microbial activity. Nat. Commun. 6, (2015).
37. Wang, Y. P. et al. Oscillatory behavior of two nonlinear microbial models of soil carbon decomposition. Biogeosciences 11, 1817–1831 (2014).
38. Moons, P., Michiels, C. W. & Aertsen, A. Bacterial interactions in biofilms. Crit. Rev. Microbiol. 35, 157–168 (2009).
39. Hibbing, M. E., Fuqua, C., Parsek, M. R. & Peterson, S. B. Bacterial competition: surviving and thriving in the microbial jungle. Nat. Rev. Microbiol. 8, 15–25 (2010).
40. Phaiboun, A., Zhang, Y., Park, B. & Kim, M. Survival Kinetics of Starving Bacteria Is Biphasic and Density-Dependent. PLoS Comput. Biol. 11, 1–18 (2015).
41. Kadam, S. V & Velicer, G. J. Variable patterns of density-dependent survival in social bacteria. Behav. Ecol. 833–838 (2006).

42. Kaiser, C., Franklin, O., Richter, A. & Dieckmann, U. Social dynamics within decomposer communities lead to nitrogen retention and organic matter build-up in soils. Nat. Commun. 6, 1–10 (2015).
43. Bouskill, N. J., Tang, J., Riley, W. J. & Brodie, E. L. Trait-based representation of biological nitrification: Model development, testing, and predicted community composition. Front. Microbiol. 3, 1–17 (2012).
44. Buchkowski, R. W., Bradford, M. A., Grandy, A. S., Schmitz, O. J. & Wieder, W. R. Applying population and community ecology theory to advance understanding of belowground biogeochemistry. Ecol. Lett. 20, 231–245 (2017).
45. Lajtha, K., Bowden, R. D. & Nadelhoffer, K. Litter and Root Manipulations Provide Insights into Soil Organic Matter Dynamics and Stability. Soil Sci. Soc. Am. J. 78, S261 (2014).
46. Crow, S. E. et al. Increased coniferous needle inputs accelerate decomposition of soil carbon in an old-growth forest. For. Ecol. Manage. 258, 2224–2232 (2009).
47. Nadelhoffer, K. J. et al. The DIRT Experiment: Litter and Root Influences on Forest Soil Organic Matter Stocks and Function. In: Foster DR, Aber JD (eds) Forests in time: the environmental consequences of 1000 years of change in New England. Yale University Press, New Haven, 300–315 (2004).
48. Xu, X., Thornton, P. E. & Post, W. M. A global analysis of soil microbial biomass carbon, nitrogen and phosphorus in terrestrial ecosystems. Glob. Ecol. Biogeogr. 22, 737–749 (2013).
49. Serna-Chavez, H. M., Fierer, N. & Van Bodegom, P. M. Global drivers and patterns of microbial abundance in soil. Glob. Ecol. Biogeogr. 22, 1162–1172 (2013).
50. Sinsabaugh, R. L., Shah, J. J. F., Findlay, S. G., Kuehn, K. A. & Moorhead, D. L. Scaling microbial biomass, metabolism and resource supply. Biogeochemistry 122, 175–190 (2015).
51. Sinsabaugh, R. L., Manzoni, S., Moorhead, D. L. & Richter, A. Carbon use efficiency of microbial communities: stoichiometry, methodology and modelling. Ecol. Lett. 16, 930–9 (2013).
52. Zechmeister-Boltenstern, S. et al. The application of ecological stoichiometry to plant-microbial-soil organic matter transformations. Ecol. Monogr. 85, 133–155 (2015).
53. Sinsabaugh, R. L. et al. Stoichiometry of microbial carbon use efficiency in soils. Ecol. Monogr. 86, 172–189 (2016).
54. Tang, J. & Riley, W. J. Weaker soil carbon-climate feedbacks resulting from microbial and abiotic interactions. Nat. Clim. Chang. 5, 56–60 (2015).
55. Guenet, B. et al. Metabolic capacities of microorganisms from a long-term bare fallow. Appl. Soil Ecol. 51, 87–93 (2011).
56. Brant, J. B., Sulzman, E. W. & Myrold, D. D. Microbial community utilization of added carbon substrates in response to long-term carbon input manipulation. Soil Biol. Biochem. 38, 2219–2232 (2006).
57. Veres, Z., Kotroczó, Z., Magyaros, K., Tóth, J. A. & Tóthmérész, B. Dehydrogenase activity in a litter manipulation experiment in temperate forest soil. Acta Silv. Lignaria Hungarica 9, 25–33 (2013).
58. Wutzler, T. & Reichstein, M. Priming and substrate quality interactions in soil organic matter models. Biogeosciences 10, 2089–2103 (2013).

59. Tang, J. Y. & Riley, W. J. A total quasi-steady-state formulation of substrate uptake kinetics in complex networks and an example application to microbial litter decomposition. Biogeosciences 10, 8329–8351 (2013).
60. Tang, J. Y. On the relationships between the Michaelis-Menten kinetics, reverse Michaelis-Menten kinetics, equilibrium chemistry approximation kinetics, and quadratic kinetics. Geosci. Model Dev. 8, 3823–3835 (2015).
61. Wieder, W. R., Grandy, a. S., Kallenbach, C. M., Taylor, P. G. & Bonan, G. B. Representing life in the Earth system with soil microbial functional traits in the MIMICS model. Geosci. Model Dev. 8, 1789–1808 (2015).
62. Adair, E. C. et al. Simple three-pool model accurately describes patterns of long-term litter decomposition in diverse climates. Glob. Chang. Biol. 14, 2636–2660 (2008).
63. He, Y. et al. Incorporating microbial dormancy dynamics into soil decomposition models to improve quantification of soil carbon dynamics of northern temperate forests. J. Geophys. Res. G Biogeosciences 120, 2596–2611 (2015).
64. Wang, G. et al. Microbial dormancy improves development and experimental validation of ecosystem model. Isme J 9, 226–237 (2015).
65. Todd-Brown, K. E. O. et al. Causes of variation in soil carbon simulations from CMIP5 Earth system models and comparison with observations. Biogeosciences 10, 1717–1736 (2013).
66. Todd-Brown, K. E. O. et al. Changes in soil organic carbon storage predicted by Earth system models during the 21st century. Biogeosciences 11, 2341–2356 (2014).
67. Parton, W. J., Stewart, J. W. B. & Cole, C. V. Dynamics of C , N , P and S in grassland soils: a model. Biogeochemistry 131, 109–131 (1988).
68. Ahrens, B., Braakhekke, M. C., Guggenberger, G., Schrumpf, M. & Reichstein, M. Contribution of sorption, DOC transport and microbial interactions to the ^{14}C age of a soil organic carbon profile: Insights from a calibrated process model. Soil Biol. Biochem. 88, 390–402 (2015).
69. Mayes, M. A., Heal, K. R., Brandt, C. C., Phillips, J. R. & Jardine, P. M. Relation between Soil Order and Sorption of Dissolved Organic Carbon in Temperate Subsoils. Soil Sci. Soc. Am. J. 76, 1027–1037 (2012).
70. Lallement, G. & Inman, D. A tutorial on complex eigenvalues. Proc. Int. Modal Anal. Conf. XIII 490–495 (1995).

Supplementary Note 1

In microbial models without density-dependent microbial turnover ($\beta = 1$), the steady-state ratio of microbial biomass carbon (MBC; C_B) to soil organic carbon (SOC; C_S) is proportional to the C input rate, as a result of the respective proportionality and insensitivity of long-term MBC and SOC to total C inputs. For the 2-pool microbial model with $\beta = 1$, the steady-state ratio of MBC/SOC can be written as follows

$$\frac{C_B}{C_S} = \frac{\left(\frac{\varepsilon \cdot I}{(1-\varepsilon) \cdot k_B}\right)}{\left(\frac{K_{M,U} \cdot k_B}{\varepsilon \cdot V_{max,U} - k_B}\right)}, \tag{22}$$

which is clearly proportional to the total C input rate; that is, $\frac{C_B}{C_S} \propto I^1$. In contrast, for microbial models with density-dependent microbial turnover ($\beta > 1$), the proportionality between the steady-state MBC/SOC ratio and C input rate decreases. Consider the 2-pool microbial model with $\beta = 2$, for example. In this case, the steady-state ratio of MBC/SOC can be written as

$$\frac{C_B}{C_S} = \frac{\varepsilon \cdot V_{max,U} - \left(\frac{\varepsilon \cdot I \cdot k_B}{(1-\varepsilon)}\right)^{1/2}}{K_{M,U} \cdot k_B}. \tag{23}$$

This quantity has two limiting cases of sensitivity to the total C input rate, depending on the relative magnitude of the two terms in the numerator. When $(\varepsilon \cdot V_{max,U}) > \left(\frac{\varepsilon \cdot I \cdot k_B}{(1-\varepsilon)}\right)^{1/2}$, which is the case for parameter sets used in the literature and given in Supplementary Table 1, then the steady-state MBC/SOC ratio is independent of the C input rate; that is, $\frac{C_B}{C_S} \propto I^0$. This decoupling of the steady-state MBC/SOC ratio from the C input rate in microbial models with density-dependence ($\beta > 1$) is corroborated by global observations showing that this ratio is confined to a narrow range around 1-2% [1,2]. First-order models, such as the 3-pool linear model in Fig. 1b, also predict a steady-state MBC/SOC ratio that is independent of the total C input rate; however, this is simply because each pool changes proportionally to the total C inputs. This proportionality of SOC stocks to the change in total C inputs was not observed in the DIRT experiments (Fig. 6). Comparing the predicted long-term MBC/SOC ratio, in addition to individual pool sizes, to observations can be a useful metric for validating models and constraining the value of β in future studies.

Supplementary Note 2

In the 4-pool microbial model, the SOC steady state is insensitive to changes in C inputs when both SOC inputs (I_S) and DOC inputs (I_D) – i.e., the total I in equations (5-8) – are changed by the same proportion (Supplementary Figs. 6 and 7). This perturbation in total I causes an oscillatory response in all C pools (shown for SOC and MBC) with a period of ~20 years. The case where only I_S is doubled also results in oscillations; however, an increase in the SOC steady state of $+2.9\%$ is observed (Supplementary Fig. 6). Conversely, when only I_D is doubled, we observe that oscillations are largely dampened and a decrease in the SOC steady state of -5.5% is observed (Supplementary Fig. 6). These responses were markedly different than those of the 4-pool microbial model with density-dependent microbial turnover ($\beta = 2$) and the 3-pool linear model for a doubling of I_S, I_D, or both (Supplementary Fig. 6).

Supplementary Figures & Tables

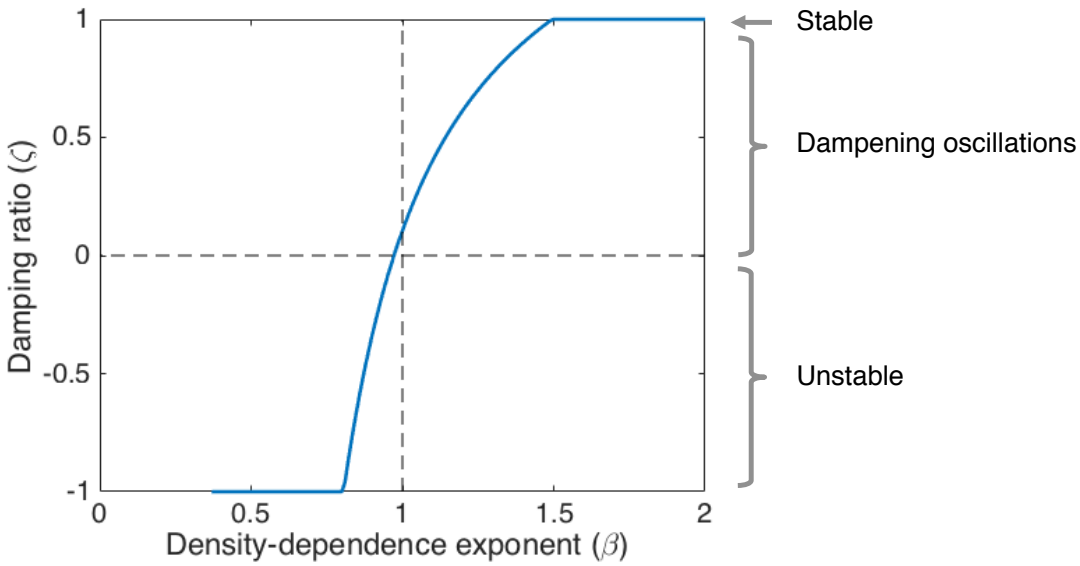

Supplementary Figure 1: Stability of the 2-pool microbial model for a range of density-dependent microbial turnover exponents.
The damping ratio (ζ; defined in equation (21)) illustrates the degree of oscillatory behavior that the system will display following a perturbation. The system is increasingly stable with a larger density-dependent microbial turnover exponent (β), where for $\beta \geq 1.5$, a stable node ($\zeta = 1$) is achieved.

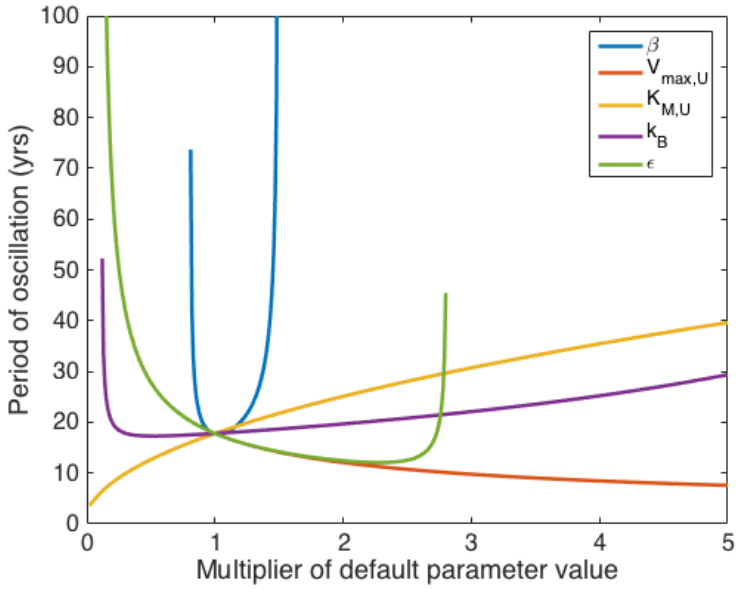

Supplementary Figure 2: Period of oscillation of the 2-pool microbial model as a function of the model parameters.
This depicts the degree of oscillatory behavior of the linearized system near its steady-state following a perturbation. The period of oscillation ($2\pi/\gamma$, where $\gamma = \mathrm{Im}(\lambda)$ for eigenvalue λ) depends on the model parameters. Parameters are defined in Supplementary Table 1.

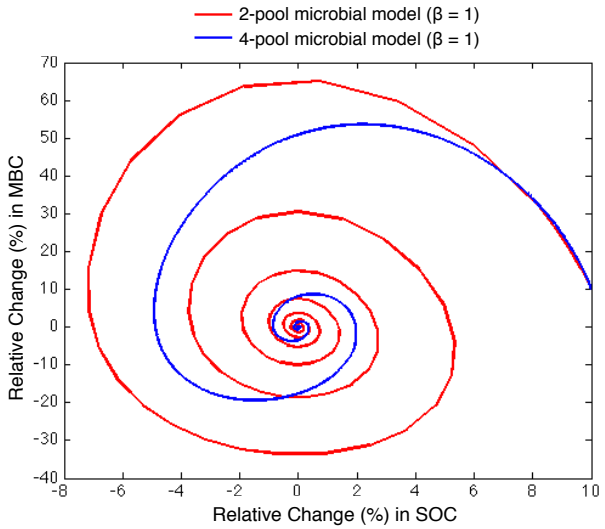

Supplementary Figure 3: Stability and periodicity of the 2- and 4-pool microbial models without density-dependent microbial turnover.
Phase portrait of the relative change of soil organic carbon (SOC) and microbial biomass carbon (MBC) in response to a 10% change in initial conditions. For parameter sets commonly used in the literature (Supplementary Table 1), the 2-pool microbial model has a pair of complex eigenvalues ($\lambda_j = \alpha_j \pm \gamma_j i$) with $\alpha_j < 0$, $\gamma_j \neq 0$ and the 4-pool microbial model has a complex pair of λ and 2 negative real λ with $\alpha_j < 0$, $\gamma_j \neq 0$. Thus, both models exhibit damped oscillations. Similarly the 5-pool microbial model has a complex pair of λ and 3 negative real λ with $\alpha_j < 0$, $\gamma_j \neq 0$, again exhibiting damped oscillations. In contrast, the 3-pool linear model has all 3 negative, real λ with $\alpha_j < 0$, $\gamma_j = 0$, which signifies a stable node. The 2-pool microbial model is the most oscillatory, as expected, since its damping ratio is closest to zero.

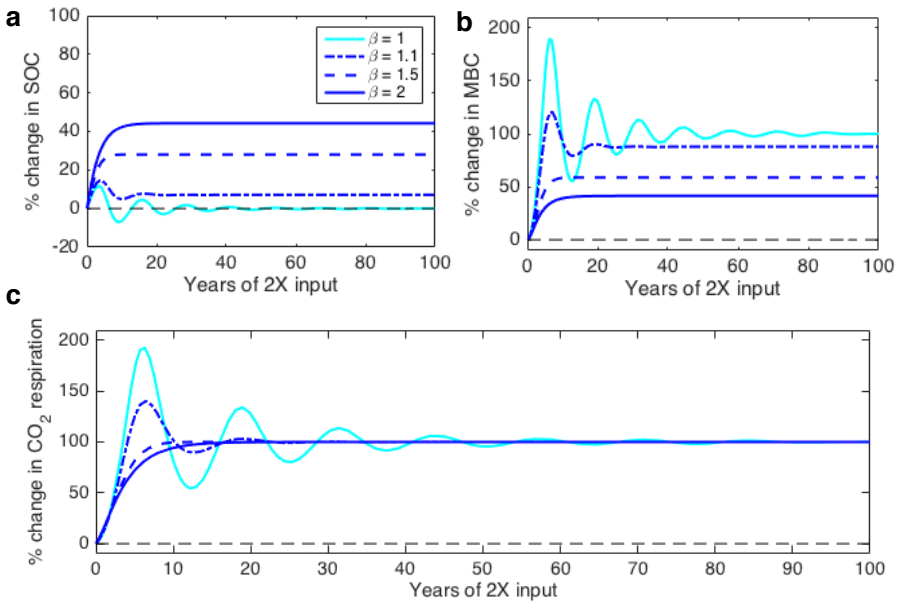

Supplementary Figure 4: Response of the 2-pool microbial model to a step 2X of inputs for a range of β using standard parameter values.
Percent change of modeled (a) SOC, (b) MBC, and (c) CO_2, where $\beta > 1$ corresponds to a microbial model with density-dependent microbial turnover. The standard value of carbon use efficiency (CUE; ε) at 20°C is 0.31, as in Supplementary Table 1.

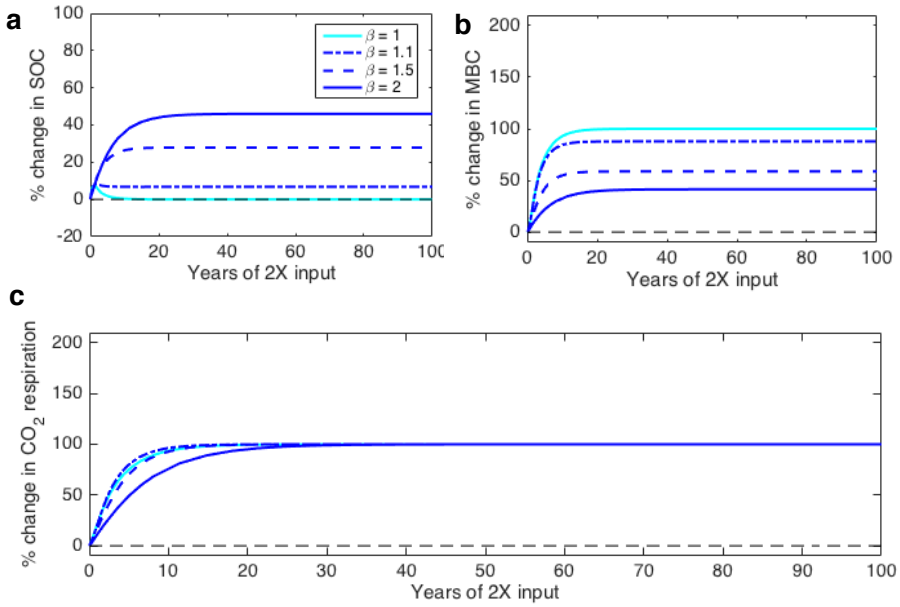

Supplementary Figure 5: Response of the 2-pool microbial model to a step 2X of inputs for a range of β using a larger carbon use efficiency than the standard value.
Percent change of modeled (a) SOC, (b) MBC, and (c) CO_2, where $\beta > 1$ corresponds to a microbial model with density-dependent microbial turnover. Here a carbon use efficiency (CUE; ε) at 20°C of 0.90 was used. Although this CUE may be unrealistically high under most soil conditions, this illustrates how the transient dynamics are dependent on the parameter values, while the steady-state behavior is largely a consequence of the model structure. Here oscillations are diminished with larger CUE (as compared to Supplementary Fig. 4). Varying the parameter K_m (not shown) results in a response curve that is less steep at early times, especially for larger β exponents.

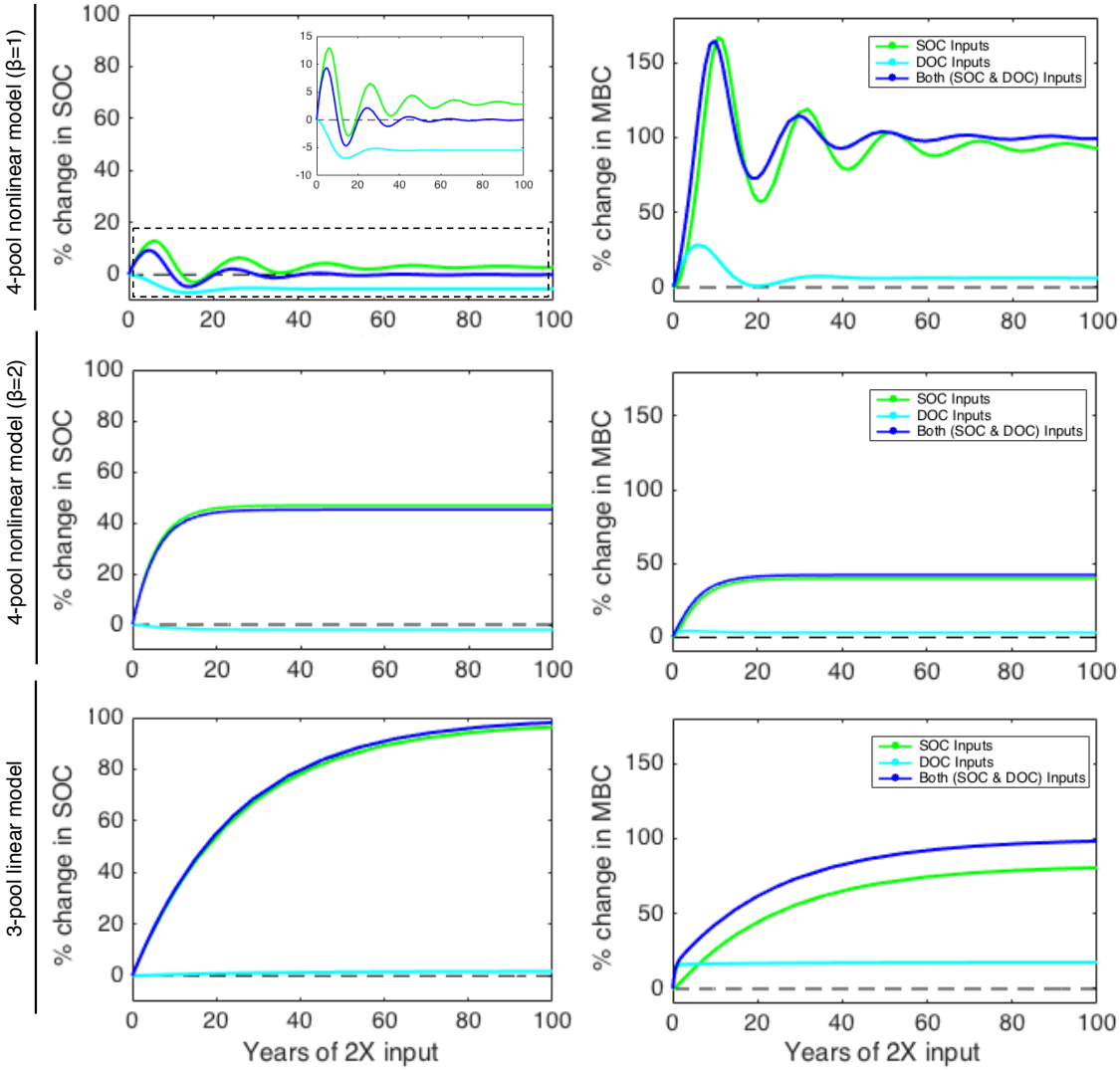

Supplementary Figure 6: Response of the 4-pool microbial model with and without density-dependence and the linear 3-pool model to a doubling of inputs.
SOC, DOC, or both inputs are individually doubled (2X) in each model. Left panels: Percent change in SOC with time. For the 4-pool microbial model, the SOC steady-state increases with 2X SOC, decreases with 2X DOC, and is insensitive to 2X SOC + 2X DOC. The inset plot zooms into the dashed box. Right panels: Percent change in microbial biomass carbon (MBC) with time.

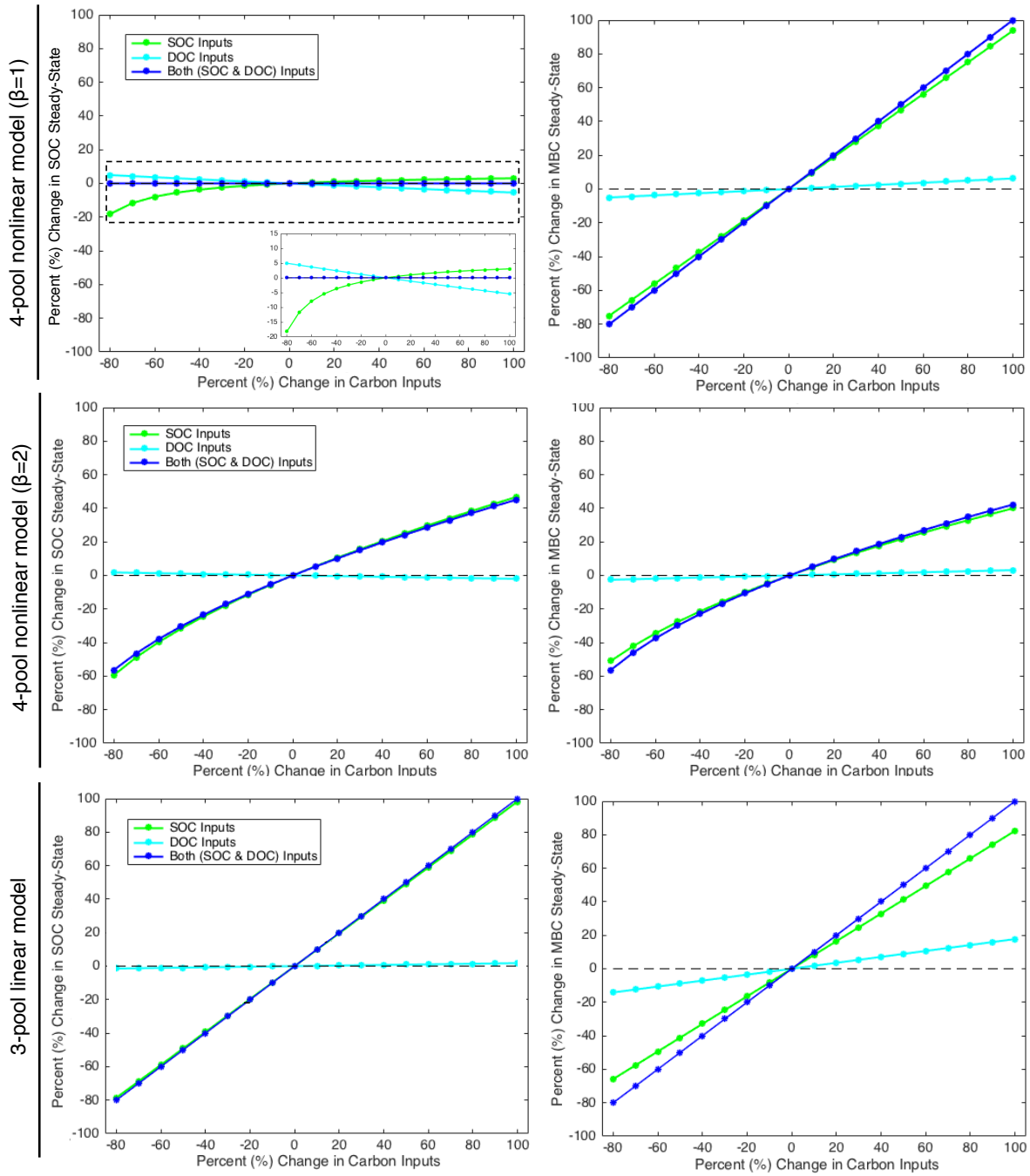

Supplementary Figure 7: Response of the 4-pool microbial model with and without density-dependence and the linear 3-pool model to perturbations in inputs.
SOC, DOC, or both inputs are individually perturbed in each model. Left panels: Percent change in the SOC steady-state as a function of the percent change in C inputs, where the inset plot zooms into the dashed box. Right panels: Percent change in the MBC steady-state as a function of the percent change in C inputs.

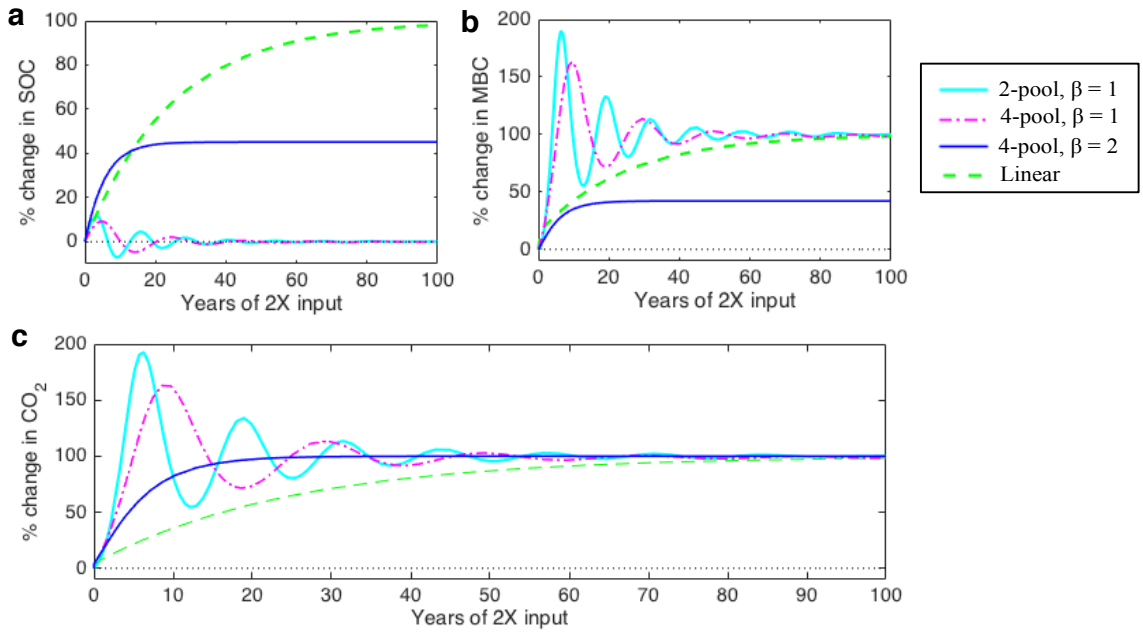

Supplementary Figure 8: Response of soil to doubling of plant C inputs in models.
Percent change of modeled **(a)** SOC, **(b)** MBC, and **(c)** CO_2 following a doubled (2X) step increase in inputs. A value of $\beta > 1$ corresponds to a microbial model with density-dependent microbial turnover.

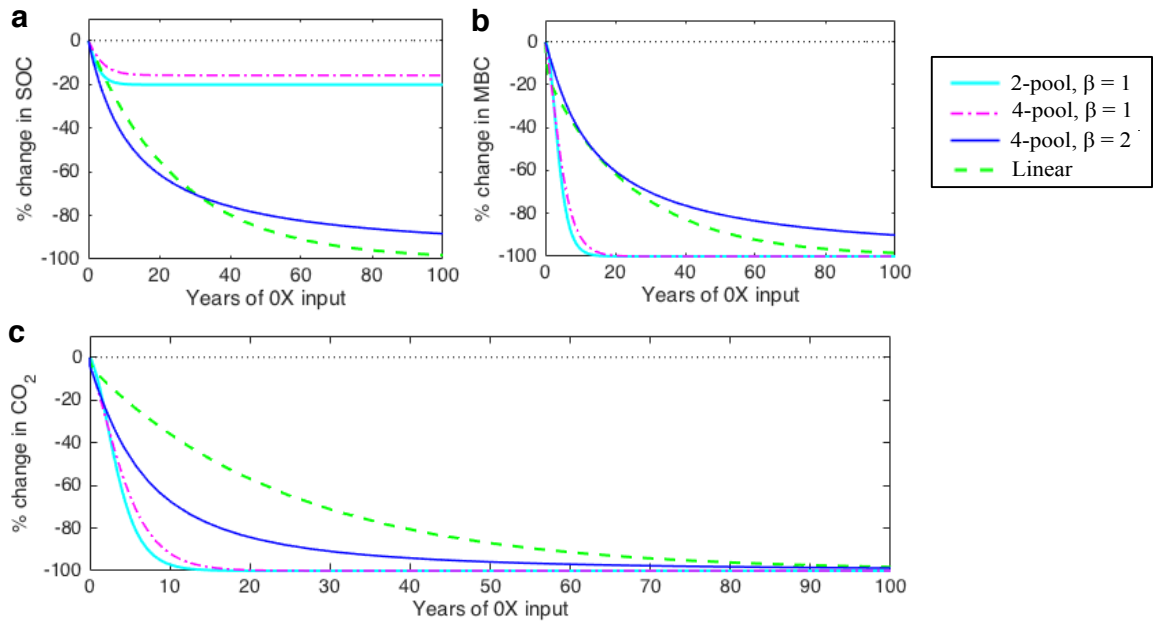

Supplementary Figure 9: Response of soil to complete removal of plant C inputs in models.
Percent change of modeled (a) SOC, (b) MBC, and (c) CO_2 following sustained 0X inputs. A value of $\beta > 1$ corresponds to a microbial model with density-dependent microbial turnover.

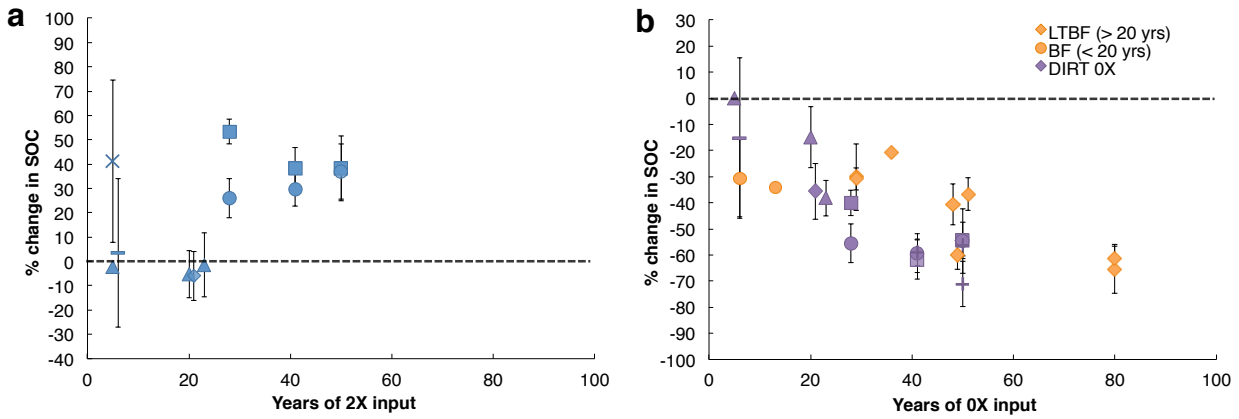

Supplementary Figure 10: Response of SOC to doubling and removal of plant C inputs from experiments labeled by site.
(a) Percent change in SOC at Detritus Input and Removal Treatment (DIRT) experiments after a sustained 2X step increase in inputs. **(b)** Percent change in SOC at DIRT, Bare Fallow (BF) and Long-Term Bare Fallow (LTBF) experiments after sustained 0X inputs. Points indicate means and bars the standard error of the mean. Data sources are reported in Supplementary Tables 2-3. For the DIRT 2X and 0X experiments, the sites are depicted by the following marker styles in blue and purple, respectively: squares = Noe woods, circles = Wingra woods, + = Curtis prairie, triangles = Harvard, diamond = Bousson, dash = Sikfokut, x = HJ Andrews.

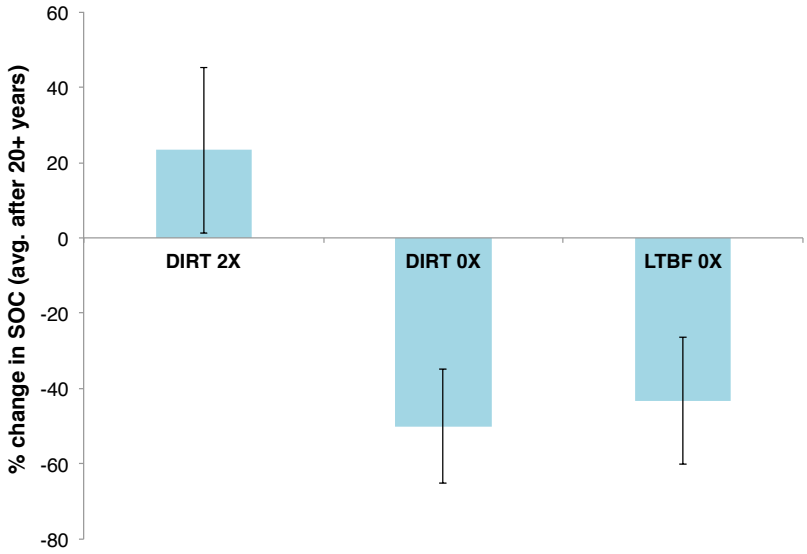

Supplementary Figure 11: Response of SOC to doubling and removal of plant C inputs from experiments. Average percent change in SOC after 20+ years of litter manipulation across all Detritus Input and Removal Treatment (DIRT) and Long-term Bare Fallow (LTBF) sites, which consistently doubled (2X) and removed (0X) inputs to the soil over time. Points indicate means and bars the standard error of the mean. Data sources are reported in Supplementary Tables 2-3.

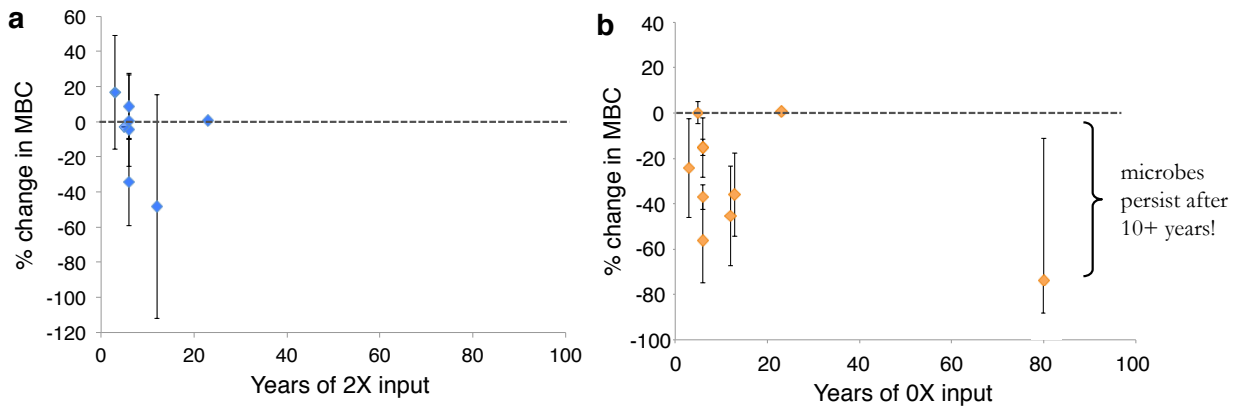

Supplementary Figure 12: Response of microbial biomass carbon to doubling and removal of plant C inputs from experiments.
(a) Percent change of microbial biomass carbon (MBC) at DIRT experiments after a sustained doubling (2X) in inputs. **(b)** Percent change of MBC at DIRT, BF and LTBF experiments after sustained removal (0X) of inputs. Points indicate means and bars the standard error of the mean. Data sources are reported in Supplementary Tables 2-3. Substantial seasonal variability was observed in ref [3]. MBC does not double in response to 2X inputs and does not disappear within 10 years of 0X, as predicted by common microbial model formulations.

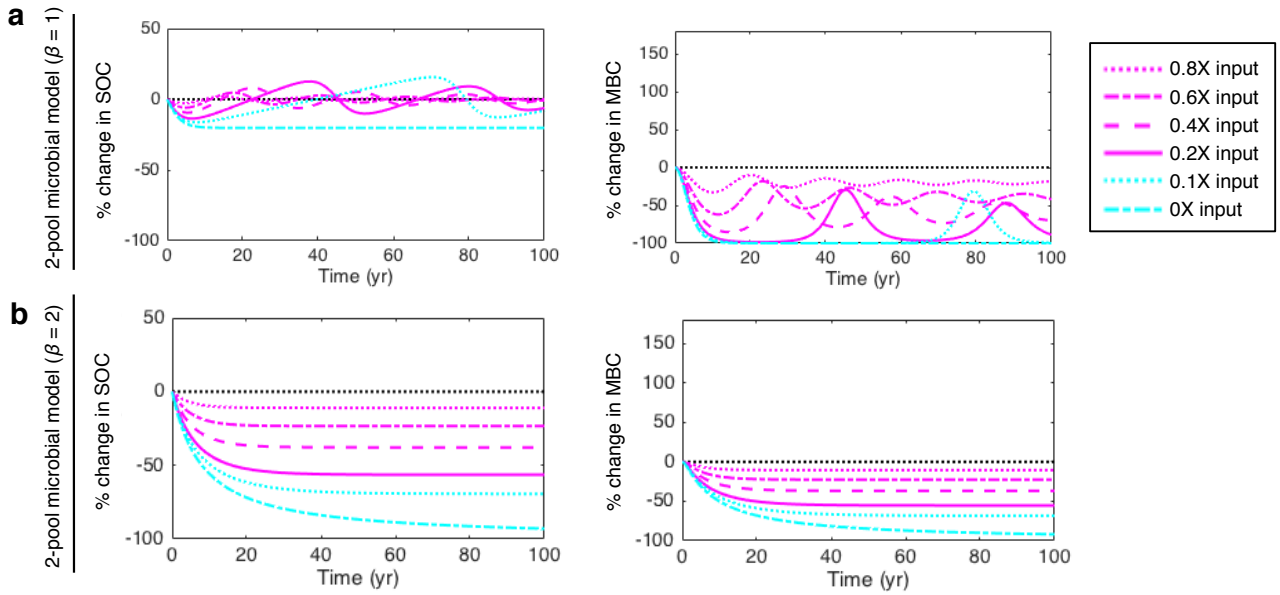

Supplementary Figure 13: Stability and sensitivity of the 2-pool microbial model with and without density-dependence to a decrease and complete removal of plant C inputs.
(a) Percent change of modeled SOC and MBC in the 2-pool microbial model without density dependence (β = 1) following a step decrease (< 1X) and complete removal (0X) in C inputs. **(b)** Percent change of modeled SOC and MBC in the 2-pool microbial model with density-dependence (β = 2) following a step decrease (< 1X) and complete removal (0X) in C inputs.

Supplementary Table 1: Parameter values for each SOC model. Parameter values are given at a reference temperature of 20°C.

Parameter	Description	Unit	Value	Reference
2-pool microbial model (C_S, C_B)				
I	Plant carbon input rate	mg C g^{-1} soil hr^{-1}	0.00016	ref. [4]
$V_{max,U}$	Maximum assimilation rate	mg C mg^{-1} MBC hr^{-1}	0.01	"
$K_{M,U}$	Half-saturation for assimilation	mg C g^{-1} soil	250	"
k_B	Mortality rate	mg C mg^{-1} C hr^{-1}	0.00028	"
ε	Carbon use efficiency	-	0.31	ref. [4,5]
β	Density-dependent exponent	-	[1 to 2]	This study
4-pool microbial model (C_S, C_D, C_B, C_E) *				
V_{max}	Maximum decomposition rate	mg C mg^{-1} C hr^{-1}	1	ref. [4]
K_M	Half-saturation for decomposition	mg C g^{-1} soil	250	"
$V_{max,U}$	Maximum assimilation rate	mg C mg^{-1} MBC hr^{-1}	0.01	"
$K_{M,U}$	Half-saturation for assimilation	mg C g^{-1} soil	0.26	"
f	Fraction of inputs into C_S	-	0.94	"
a_{BS}	Fraction of microbial turnover into C_S	-	0.5	"
r_E	Enzyme turnover rate	mg C mg^{-1} C hr^{-1}	0.001	"
r_p	Enzyme production rate	mg C mg^{-1} MBC hr^{-1}	5.6×10^{-6}	"
β	Density-dependent exponent	-	[1 to 2]	This study
5-pool microbial model (C_S, C_D, C_B, C_E, C_q) *				
k_{ads}	Adsorption rate constant	mg C mg^{-1} C hr^{-1}	0.01	This study; ref [6]
k_{des}	Desorption rate constant	mg C mg^{-1} C hr^{-1}	0.001	This study; ref [6]
Q_{max}	Maximum DOC adsorption capacity	mg C g^{-1} soil	1.7	ref. [7]
3-pool linear model (C_S, C_D, C_B)				
k_S	Decomposition rate constant of SOC	mg C mg^{-1} C hr^{-1}	5.6×10^{-6}	ref. [4]
k_D	Decomposition rate constant of DOC	mg C mg^{-1} C hr^{-1}	0.001	"
k_B	Turnover rate constant of MBC	mg C mg^{-1} C hr^{-1}	0.00028	"
k_{uptake}	Uptake rate constant of DOC	mg C g^{-1} DOC hr^{-1}	0.0005	"
f_S	Fraction of SOC entering DOC	-	0.31	"
f_D	Fraction of DOC entering SOC	-	0.31	"
f_B	Fraction of MBC turnover recycled	-	0.31	"
$f_{B\rightarrow S}$	Fraction of recycled MBC into SOC	-	0.5	"

* Unless otherwise noted, as complexity is added in subsequent microbial models, all parameters that have an analogous value in a simpler model conserve their value in the more complex models.

Supplementary Table 2: Summary of Detritus Input and Removal Treatment experiments synthesized in our study.

Data sources and details for the synthesized Detritus Input and Removal Treatment (DIRT) experiments are listed.

Source	Location	Type	Duration (yrs)	SOC	MBC
DIRT (>20 years)					
Lajtha et al. 2014 (ref. [8])	Noe	2X	50	y	-
	Noe	2X	41	y	-
	Noe	2X	28	y	-
	Wingra	2X	50	y	-
	Wingra	2X	41	y	-
	Wingra	2X	28	y	-
	Noe	0X	50	y	-
	Noe	0X	41	y	-
	Noe	0X	28	y	-
	Wingra	0X	50	y	-
	Wingra	0X	41	y	-
	Wingra	0X	28	y	-
	Curtis 1	0X	50	y	-
	Curtis 1	0X	41	y	-
	Curtis 3	0X	50	y	-
Rousk & Frey 2015 (ref. [9])	Harvard	2X	23	y	y
	Harvard	0X	23	y	y
Lajtha et al. 2014 (ref. [10])	Harvard	2X	20	y	-
	Harvard	0X	20	y	-
Bowden et al. 2014 (ref. [11])	Bousson	2X	21	y	-
	Bousson	0X	21	y	-
DIRT (<20 years)					
Crow et al. 2009 (ref. [12])	HJ Andrews	2X	5	y	-
Brant et al. 2006 (ref. [13])	HJ Andrews	2X	6	-	y
	HJ Andrews	0X	6	-	y
Brant et al. 2006 (ref. [3])	Bousson	2X	12	-	y
	Bousson	0X	12	-	y
	HJ Andrews	2X	6	-	y
	HJ Andrews	0X	6	-	y
	HJ Andrews	2X	6	-	y
	HJ Andrews	0X	6	-	y
	HJ Andrews	2X	6	-	y
	HJ Andrews	0X	6	-	y
	Sikfokut	2X	3	-	y
	Sikfokut	0X	3	-	y
Nadelhoffer et al. 2004 (ref. [14])	Harvard	2X	5	y	y
	Harvard	0X	5	y	y
Fekete et al. 2011 (ref. [15,16])	Sikfokut	2X	6	y	-
	Sikfokut	0X	6	y	-

Supplementary Table 3: Summary of Long-term Bare Fallow and Bare Fallow experiments synthesized in our study.

Data sources and details for the synthesized Long-term Bare Fallow (LTBF) and Bare Fallow (BF) experiments are listed.

Source	Location	Type	Duration (yrs)	SOC	MBC
LTBF (>20 years)					
Barre et al. 2010 (ref. [17])	Kursk	0X	36	y	-
	Ultuna	0X	51	y	-
	Askov B3	0X	29	y	-
	Askov B4	0X	29	y	-
	Grignon	0X	48	y	-
	Versailles	0X	80	y	-
	Rothamsted	0X	49	y	-
Guenet et al. 2011 (ref. [18])	Versailles	0X	80	y	y
BF (<20 years)					
Pothoff et al. 2006 (ref. [19])	UC Hastings	0X	6	y	y
Wang et al. 2007 (ref. [20])	China	0X	13	y	y

Supplementary References

1. Xu, X., Thornton, P. E. & Post, W. M. A global analysis of soil microbial biomass carbon, nitrogen and phosphorus in terrestrial ecosystems. Glob. Ecol. Biogeogr. 22, 737–749 (2013).
2. Serna-Chavez, H. M., Fierer, N. & Van Bodegom, P. M. Global drivers and patterns of microbial abundance in soil. Glob. Ecol. Biogeogr. 22, 1162–1172 (2013).
3. Brant, J. B., Sulzman, E. W. & Myrold, D. D. Microbial community utilization of added carbon substrates in response to long-term carbon input manipulation. Soil Biol. Biochem. 38, 2219–2232 (2006).
4. Li, J., Wang, G., Allison, S. D., Mayes, M. A. & Luo, Y. Soil carbon sensitivity to temperature and carbon use efficiency compared across microbial-ecosystem models of varying complexity. Biogeochemistry 119, 67–84 (2014).
5. Sinsabaugh, R. L. et al. Stoichiometry of microbial carbon use efficiency in soils. Ecol. Monogr. 86, 172–189 (2016).
6. Ahrens, B., Braakhekke, M. C., Guggenberger, G., Schrumpf, M. & Reichstein, M. Contribution of sorption, DOC transport and microbial interactions to the ^{14}C age of a soil organic carbon profile: Insights from a calibrated process model. Soil Biol. Biochem. 88, 390–402 (2015).
7. Mayes, M. A., Heal, K. R., Brandt, C. C., Phillips, J. R. & Jardine, P. M. Relation between Soil Order and Sorption of Dissolved Organic Carbon in Temperate Subsoils. Soil Sci. Soc. Am. J. 76, 1027–1037 (2012).
8. Lajtha, K. et al. Changes to particulate versus mineral-associated soil carbon after 50 years of litter manipulation in forest and prairie experimental ecosystems. Biogeochemistry 119, 341–360 (2014).
9. Rousk, J. & Frey, S. D. Revisiting the hypothesis that fungal-to-bacterial dominance characterises turnover of soil organic matter and nutrients. Ecology 85, 457–472 (2015).
10. Lajtha, K., Bowden, R. D. & Nadelhoffer, K. Litter and Root Manipulations Provide Insights into Soil Organic Matter Dynamics and Stability. Soil Sci. Soc. Am. J. 78, S261 (2014).
11. Bowden, R. D. et al. Litter Input Controls on Soil Carbon in a Temperate Deciduous Forest. North Am. For. Soils S66–S75 (2014). doi:10.2136/sssaj2013.09.0413nafsc
12. Crow, S. E. et al. Increased coniferous needle inputs accelerate decomposition of soil carbon in an old-growth forest. For. Ecol. Manage. 258, 2224–2232 (2009).
13. Brant, J. B., Myrold, D. D. & Sulzman, E. W. Root controls on soil microbial community structure in forest soils. Oecologia 148, 650–659 (2006).
14. Nadelhoffer, K. J. et al. The DIRT Experiment: Litter and Root Influences on Forest Soil Organic Matter Stocks and Function. For. time Environ. consequences 1000 years Chang. New Engl. 300–315 (2004).
15. Fekete, I., Varga, C., Kotroczó, Z., Tóth, J. A. & Várbiró, G. The relation between various detritus inputs and soil enzyme activities in a Central European deciduous forest. Geoderma 167–168, 15–21 (2011).
16. Fekete, I., Kotroczó, Z., Varga, C., Veres, Z. & Tóth, J. A. The effects of detritus input on soil organic matter content and carbon dioxide emission in a central European deciduous forest. Acta Silv. Lignaria Hungarica 7, 87–96 (2011).
17. Barré, P. et al. Quantifying and isolating stable soil organic carbon using long-term bare fallow experiments. Biogeosciences 7, 3839–3850 (2010).

18. Guenet, B. et al. Metabolic capacities of microorganisms from a long-term bare fallow. Appl. Soil Ecol. 51, 87–93 (2011).
19. Potthoff, M. et al. Soil microbial community composition as affected by restoration practices in California grassland. Soil Biol. Biochem. 38, 1851–1860 (2006).
20. Wang, G. H. et al. Biomass and catabolic diversity of microbial communities with long-term restoration, bare fallow and cropping history in Chinese Mollisols. Plant, Soil Environ. 53, 177–185 (2007).

CHAPTER 5: The role of mineral-organic associations on the capacity of soils to store carbon: insights from data and models

CHAPTER 5: The role of mineral-organic associations on the capacity of soils to store carbon: insights from data and models

This chapter contains material being prepared for submission as the original journal articles:

Georgiou, K., et al. Representing mineral-organic associations in soil carbon models: insights and ways forward

Georgiou, K., et al. The global mineralogical capacity of soils to store carbon.

Abstract

Mineral-organic associations (MOAs) play a key role in governing soil carbon (C) stabilization and long-term storage, and thus, improving their representation for inclusion in Earth system models is crucial for understanding and predicting feedbacks under global change. Despite the important role of MOAs in soil organic carbon (SOC) preservation, decidedly little attention has been afforded to their explicit representation in soil C models. Here we explore mathematical representations of MOAs, drawing insights from theory and experiments to recommend model structures and propose targeted data syntheses to constrain key parameters. We compare a range of model formulations, motivated by the myriad of underlying MOAs, and leverage laboratory incubations and field experiments to inform model parameters. Specifically, we describe linear, Langmuir, Freundlich, and Sips adsorption models, where the latter emerges from heterogeneous compositions of substrate and surface components. We show predicted trends of mineral-associated organic carbon (MOC) as a function of mineralogy, and discuss the role of soil carbon saturation on emergent patterns. Specifically, our results highlight that the response of MOC to changes in plant C inputs depends greatly on the level of C saturation and thus, the representation of MOAs in models can lead to nonlinear steady-state responses in MOC. We also find that, consistent with field experiments, the trend in MOC with mineralogy can be linear, but, interestingly, the slope depends on the degree of C saturation. We contend that this latter finding is an important consideration for explaining field studies that did not find a universal slope and interpreted this as an inability of mineralogy to explain observed patterns. Using a synthesis of field observations, we infer a MOC saturation capacity for different soil types, which is essential for parameterizing process-based SOC models globally.

Introduction

Mineral-associated organic carbon (MOC) constitutes a large portion (30-90%) of total soil organic carbon (SOC) stocks (Kleber *et al.*, 2015) (Supplementary Figure 1). Such associations can protect MOC from microbial attack and, as a result, MOC turnover times can be up to 100 times larger than free (particulate) organic carbon (Kleber *et al.*, 2015). Despite the major role of mineral-organic associations (MOAs) in SOC preservation, little attention has been afforded to their explicit representation in mechanistic soil carbon (C) models thus far. Given potential MOC vulnerability to novel conditions (e.g., warming), it is critical to explicitly model MOAs and explore emergent mineral-microbial feedbacks.

MOAs in soils are chemically complex, where many types of minerals and substrates interact through a plethora of bonding mechanisms to drive emergent bulk-pool responses (Figure 1).

While it is unclear how this underlying complexity integrates to larger scales, data limitations and computational costs necessitate effective model representations that aggregate biochemical heterogeneity and spatiotemporal variability into homogenous bulk pools. This motivates the questions: (1) how should micro-scale MOAs be represented in macro-scale models, and (2) what data are necessary for parameterizing macro-scale models globally? We describe scaling considerations and model insights below, and perform an observational synthesis to constrain model formulations and parameterizations.

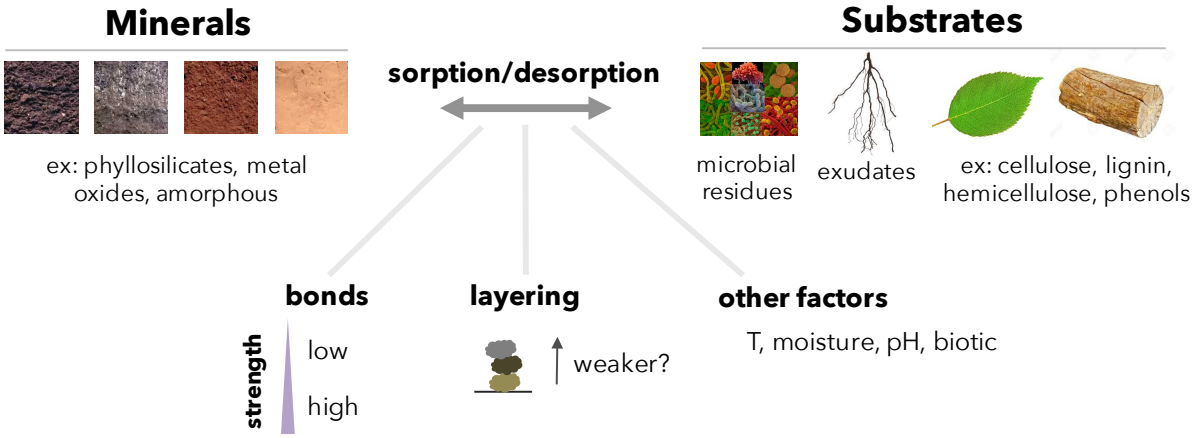

Figure 1: Diverse minerals and substrates interact to form MOAs that protect MOC from microbial decomposition.
However, data and computational costs necessitate simplified models that aggregate biochemical and spatial heterogeneity.

Modeling MOAs: Adsorption kinetics and theory

Currently, most soil C models represent MOAs implicitly by using soil texture (% clay + silt) as a proxy to partition C between first-order pools (Parton, Stewart and Cole, 1988). In contrast, mechanistic models explicitly represent mineral-associated and free (unbound) substrate pools, which undergo a constant and dynamic exchange driven by substrate concentrations and environmental conditions. Such models that explicitly represent MOAs allow for emergent behavior (e.g., mineral-microbe feedbacks and carbon saturation) that can be diagnosed and attributed to underlying mechanisms. Furthermore, measurements of MOC afford an additional constraint for validating explicit models.

Recent mechanistic models have implemented explicit representations that include: linear (Sulman *et al.*, 2014; Wieder *et al.*, 2015), Freundlich (Grant, Juma and Mcgill, 1993), and Langmuir (Wang, Post and Mayes, 2013; Tang and Riley, 2015) formulations. In their respective derivations, these formulations carry assumptions that are often not met in reality given scaling considerations (Table 1) and, as such, they are generally used empirically. Here we detail four relevant explicit formulations and their key characteristics and limitations (Table 1). The classic description of these representations is their equilibrium isotherm (Figure 2), but each formulation can also be expressed dynamically (Table 1).

One key property for any evaluation of explicit formulations is the potential for carbon saturation (Figure 2). It is widely observed that mineral surfaces can experience MOC saturation in laboratory incubations and field experiments (Mayes *et al.*, 2012; Feng *et al.*, 2014; Jagadamma *et al.*, 2014), suggesting that a Langmuir- or Hill-type formulation may be warranted. While the Freundlich isotherm also displays saturating behavior, it does not include a strict saturation limit and its empirical nature makes it difficult to extrapolate parameters across different soil types. We thus focus our comparison on the Langmuir and Hill formulations, due to their strong theoretical basis, which allows for intuition on dynamics and an understanding of the origin and significance of the parameters.

While the Langmuir and Hill formulations are, in fact, related, they can differ greatly in their predictions and implications. The strength and sign of the exponent (α) in the Hill equation (Table 1) dictates the "cooperativity" of binding interactions. For $\alpha > 1$, the binding of molecules increases the affinity for subsequent molecules, while for $\alpha < 1$, binding decreases affinity for others. For $\alpha = 1$ (i.e., Langmuir), the affinity of a molecule is completely independent of whether other molecules are bound. Interestingly, it can be shown mathematically that for a heterogeneous mixture of MOAs, each exhibiting a Langmuir isotherm with distinct affinity coefficients, the emergent bulk behavior approaches a Hill isotherm (Sposito, 1980), and at low concentrations, a Freundlich isotherm. This suggests that scaling spatial and chemical heterogeneity of underlying constituents to homogenous bulk pools may warrant an effective representation that resembles a Hill isotherm. While these formulations can be used empirically, understanding the theoretical origin and limitations of effective representations is critical for diagnosing interactions and emergent feedbacks.

Table 1: Types of representations for MOAs: equations, assumptions, and limitations.
Formulations used to represent MOAs in SOC models are detailed here. We note that other formulations include Toth, multi-surface Langmuir (with and without interactions), and BET isotherms; however, these are not considered here, since the current data are not sufficient to constrain the additional complexity of these representations globally.

	At steady-state	Dynamics	Characteristics & Limitations
Implicit Parton et al. 1988	(pool partitioning)	(pool partitioning)	Empirical
Linear Sulman et al. 2014; Wieder et al. 2015.	$x = K \cdot c$	$\frac{dx}{dt} = kc - mx$	First-order; limited concentrations; largely empirical
Freundlich Grant et al. 1993.	$x = K \cdot c^{\alpha}$	$\frac{dx}{dt} = kc^{\alpha} - mx$	Allows for surface heterogeneity; largely empirical
Langmuir Wang et al. 2013; Tang & Riley 2015; Ahrens et al. 2015.	$x = \frac{Q_{max} \cdot K \cdot c}{1 + K \cdot c}$	$\frac{dx}{dt} = kc(Q_{max} - x) - mx$	Finite, uniform sites; **no lateral interactions**; single adsorbent & adsorbate; **monolayer**
Hill/Sips	$x = \frac{Q_{max} \cdot K \cdot c^{\alpha}}{1 + K \cdot c^{\alpha}}$	$\frac{dx}{dt} = kc^{\alpha}(Q_{max} - x) - mx$	Finite sites; allows for **cooperative binding** & **heterogeneous systems** Sposito 1980.

where x = **MOC** and c = **substrate** (Q_{max} = **max**, $\frac{k}{m} = K$ = **affinity**, α = **cooperativity**)

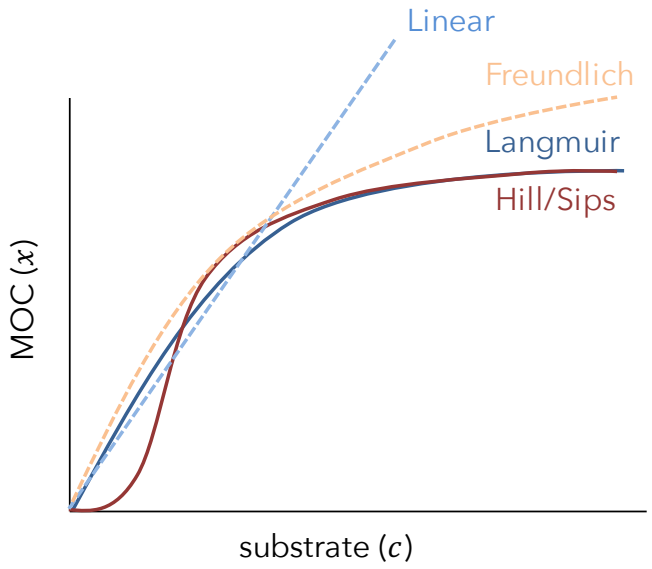

Figure 2: Adsorption isotherm (amount adsorbed as a function of free substrate in solution) formulations diverge in distinct regimes.
Amount adsorbed – i.e., MOC or x – as a function of free substrate – i.e., c – in solution (see equations in Table 1). Notable regime differences: (i) Hill diverges at low substrate concentrations and (ii) linear and Freundlich diverge at high substrate concentrations.

MOC vs. mineralogy: Model insights and predictions

Many empirical studies have explored the relationship between MOC and soil mineralogy using texture, i.e., % clay + silt content, as a proxy in different soils. While some have argued for a linear trend between MOC stocks and % clay + silt content (Hassink, 1997; Angers *et al.*, 2011), this relationship can appear unconvincing (Angers *et al.*, 2011; Beare *et al.*, 2014). Furthermore, other studies have explored the dependence of total SOC on mineralogy, despite the fact that SOC includes both MOC and particulate organic matter, where the latter may not have a direct link to mineral content. Such studies have found poor linear correlations between SOC and clay + silt content, as a proxy for mineralogy, and have simply concluded that % clay + silt is not a good predictor (Rasmussen *et al.*, 2018). However, we contend that these observations are, in fact, expected from theory, and that such studies may have overlooked the co-varying explanatory variables that drive the emergent relationship.

Indeed, we hypothesize that there is not a universal slope between MOC and mineralogy, but, rather, the level of MOC saturation dictates the emergent relationship (Figure 3). Near saturation, all observations collapse along the same "saturated" line; however, below saturation, other variables (e.g., C inputs, temperature, moisture, and pH) can affect the observed trend. Take, for example, surface and deep soils with similar mineralogy and Q_{max}. The available (unbound) substrate concentration is generally higher in surface soils (due to higher C inputs) and, consequently, more adsorption and total MOC storage results. Our findings suggest that MOC is far from saturation in most soils, and covariates can play an important role in the observed relationship between MOC and mineralogy. Yet, while other variables can affect the departure from saturation, we maintain that the maximum MOC capacity (denoted Q_{max}) is an intrinsic property of the soil minerals.

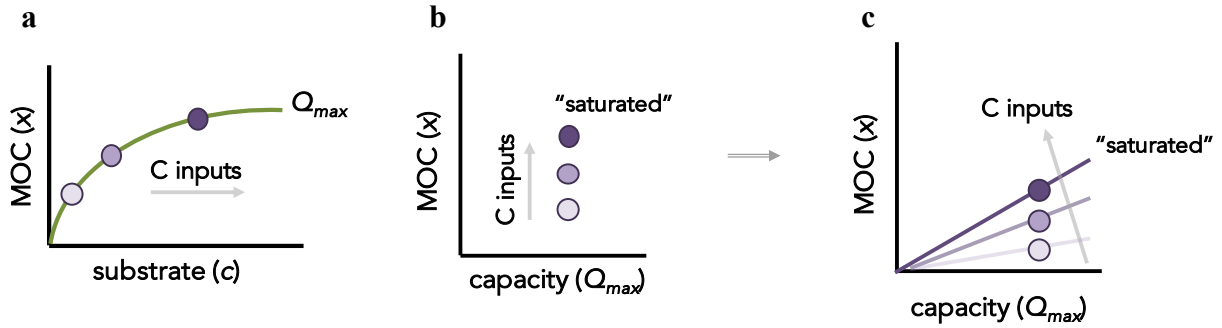

Figure 3: MOC at various levels of C saturation.
Predicted trend of (a) MOC versus free (unbound) substrate at equilibrium and (b) corresponding MOC for a particular maximum C capacity (Q_{max}) given a range of C input (unbound substrate) concentrations. (c) MOC across soils with different Q_{max} and a range of C input (unbound substrate) concentrations.

We explore predictions from mechanistic models and show that, with insights from theory and sufficient observations across soil types and biomes, we can understand why conflicting conclusions are reached across studies. While we focus on saturating adsorption representations (i.e., Langmuir and Hill) herein, the intuition gained can easily be extended to other formulations. We find that, indeed, a single linear relationship cannot be expected (Figure 4a). Mineral soils (i.e., excluding permafrost soils, peat, and wetlands) in regions with greater substrate concentrations (higher productivity) and lower temperatures (given proportionally more adsorption at lower temperatures, i.e., higher $K = k_{ads}/k_{des}$) are expected to have larger slopes. Additionally, the response of MOC to changes in substrate concentration (e.g., via changes in C inputs) can depend on the level of MOC saturation (Figure 4b). While we have presented semi-qualitative model insights – with a single set of parameters – thus far, we follow with a more rigorous analysis to extend our results across soil types and input rates.

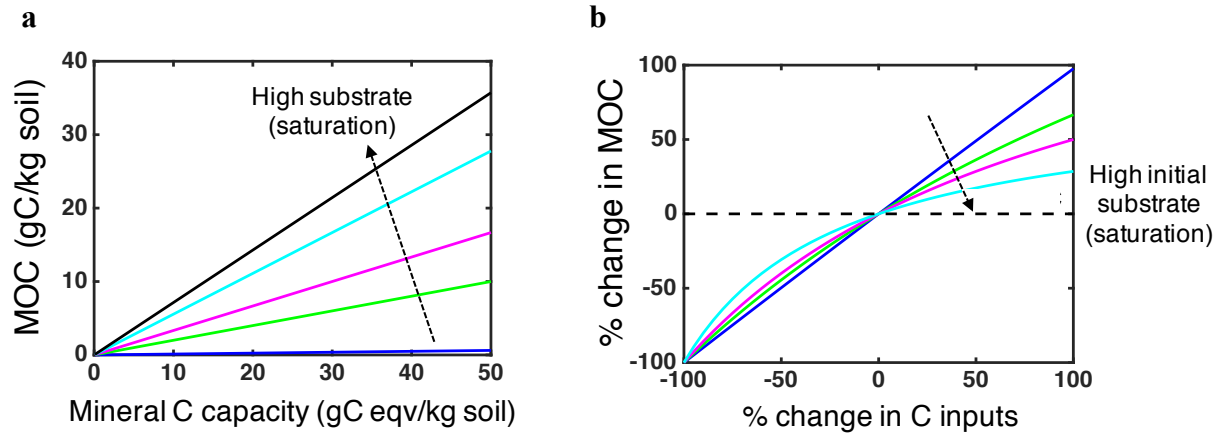

Figure 4: Controls on MOC storage: exploring mineralogy and C inputs.
(a) MOC across soils with different Q_{max} for a range of substrate (dissolved organic carbon; DOC) concentrations spanning several orders of magnitude. (b) Response of MOC to an increase in substrate concentrations with a range of initial substrate concentrations.

Comparing models: Approaching saturation

To allow for inter-site variability in parameter values and input rates, we perform a Monte Carlo simulation in which we sample values from observationally constrained ranges. Specifically, we explore explicit Langmuir (α = 1) and Hill (α > 1) representations (Table 1), for which necessary model inputs include substrate concentrations (c; namely, dissolved organic carbon, DOC) and affinity coefficients (association; $K = k_{ads}/k_{des}$). DOC can vary spatiotemporally over an order of magnitude, and concentrations are generally lower with depth (Sanderman and Amundson, 2009). We examine modeled MOC at equilibrium, but note that temporal variability in DOC can contribute minor nonlinearities when using the Hill formulation, but not the Langmuir; the dynamic representation of the latter is linearly proportional to concentration (Table 1). The coefficient K can vary across different mineral types, and, thus, we sample from a range observed in experiments (Jagadamma, Mayes and Phillips, 2012; Mayes *et al.*, 2012). Specifically, we sample K uniformly between 10^1 and 10^3 kg soil/g C (Mayes *et al.*, 2012). For *surface soils*, we sample DOC uniformly between 0.05 - 0.1 g C/kg soil, whereas for *deep soils*, we sample between 0.01 - 0.05 g C/kg soil (Sanderman, Baldock and Amundson, 2008). To estimate SOC from MOC, we sample MOC/SOC uniformly between 30 – 99% given the range observed in our observational synthesis (Supplementary Figure 1).

We show the predicted MOC, and by extension SOC, as functions of soil mineralogy (Figure 5; Supplementary Figure 2). The independent variable, Q_{max} (g C eqv/kg soil), corresponds to the maximum amount of MOC that can be stored in a particular soil. Here we base this value on the general range of MOC measured by size- and density- fractionation in soils globally. For broader applications of these explicit formulations, a pedo-transfer function can be used to relate Q_{max} to readily measured mineral content (% clay + silt) and properties.

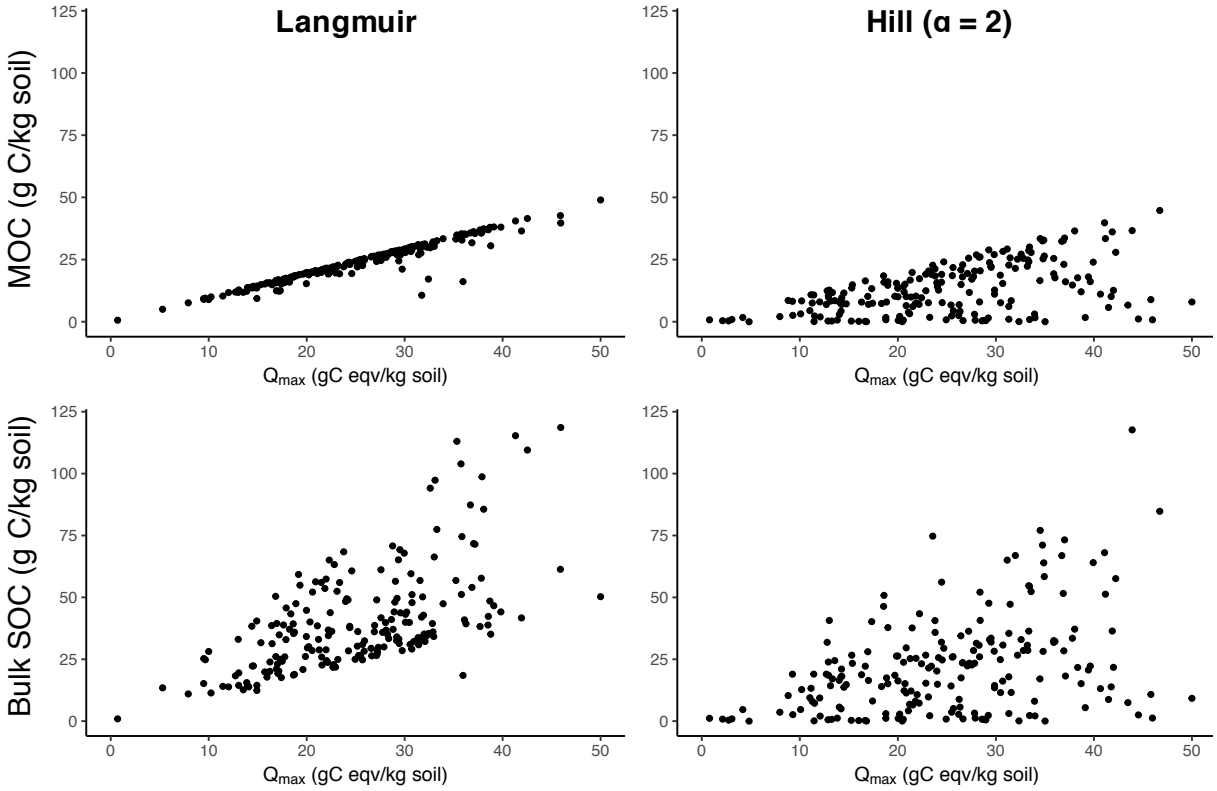

Figure 5: MOC and bulk SOC in all (surface and deep) soil as a function of soil mineralogy (Q_{max}; gC eqv/kg soil) with explicit Langmuir and Hill formulations.

We find that the mineral surfaces are largely saturated with the Langmuir representation, while the low DOC values carry more weight in the Hill representation and allow a departure from saturation (Figure 5). This is particularly evident when comparing surface and deep soils (Supplementary Figure 2), where the latter are further from saturation with the Hill formulation. This modeling experiment, using literature-based ranges of parameter values, suggests that the Hill formulation may allow a more flexible response that can better match observations (Figure 8; Supplementary Figure 3).

In estimating SOC from MOC, we sampled from an empirically constrained distribution of the MOC/SOC ratio (Supplementary Figure 1) (Kleber *et al.*, 2015). We find that low MOC/SOC values (e.g., 30% vs. a high 90%) play a key role in the predicted trend between SOC and mineral content, particularly when inferring a SOC storage capacity from the boundary line (maximum) slope (Figure 5). We note that studies that simply assume a constant MOC/ SOC ~ 85% (Angers *et al.*, 2011; Beare *et al.*, 2014), based on an average value, may greatly overestimate the capacity of soils to store SOC.

Observational synthesis: Towards a pedo-transfer function

To inform and better constrain explicit model formulations of MOAs, MOC observations across a range of mineral soils are needed. We conduct a synthesis of MOC and corresponding mineral content (% clay + silt) and composition (clay type) to compare to model results. We observe that

most soils fall below an upper saturation limit and that, below this limit, many covariates can govern emergent patterns (Figure 6). For example, we find that temperature decreases MOC and that C inputs increase MOC, when all other variables are held constant for each relationship. Furthermore, we observe that surface soils contain higher MOC, where a shift in the MOC distribution is clearly visible with increasing depth (Supplementary Figure 3). These findings corroborate our model predictions and insights, and imply that a saturating isotherm may best describe MOAs in models; specifically, our results suggest that the Hill formulation may be preferable.

These data are not only important for constraining formulations and exploring underlying relationships, but, also, the presence of a boundary line (maximum) slope is essential for parameterizing Q_{max} in models. Indeed, the derived slope (0.10 ± 0.01 gC/g mineral for *high-activity* clay soils and 0.05 ± 0.01 gC/g mineral for *low-activity* clay soils) provides a pedo-transfer function to convert from readily measured soil texture (% clay + silt, i.e., g mineral/100g soil) to the maximum mineralogical capacity (Q_{max}) needed in models (Figure 6). This slope can be conceptually broken into two parts; namely, C loading (g C/m^2 surface area) multiplied by specific surface area (SSA; m^2 surface area/g mineral). The intuitive components of this value, and its role in the theory-based model formulations, give both Langmuir and Hill an advantage for extrapolation across soils and increased physical understanding. Indeed, this empirically derived saturation relationship (Figure 6), gives us the opportunity to extrapolate Q_{max} globally for application in Earth system models.

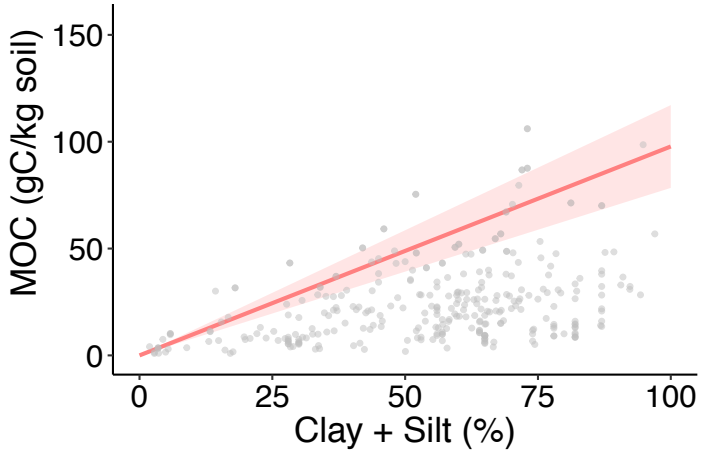

Figure 6: The role of soil texture (% clay + silt) on the capacity of high-activity soils to store mineral-associated organic carbon in natural ecosystems.
MOC as a function of clay and silt (< 60 μm) content in high-activity mineral soils (i.e., 2:1 clays and amorphous minerals) across diverse biomes and climates. The regression illustrates the boundary line with uncertainty, fit to a subset (top 5%) of points. The slope of this regression (0.10 ± 0.01 gC/g mineral; divided by 10 to convert units to g C/g mineral) signifies the maximum capacity (i.e., saturation) of *high-activity* mineral soils to store carbon. The boundary line relationship for *low-activity* mineral soils (1:1 clays; not shown here) has a slope of 0.05 ± 0.01 gC/g mineral. These relationship can be used to constrain Q_{max} in models globally.

Conclusions and ways forward

Given the potential for emergent, mineral-microbial feedbacks under novel environmental conditions, it is critically important to better understand and explicitly represent MOAs in soil C models. The chemically and spatiotemporally heterogeneous nature of MOC at the micro-scale introduces challenges in selecting effective model representations to be applied at macro-scales. Here we described potential mathematical representations, with interest in scaling considerations, and explored their respective characteristics and limitations. We discussed model insights, in conjunction with an observational synthesis, to make recommendations on ways forward. Specifically, we found that the level of C saturation can influence the observed relationship between MOC and mineral content, at times masking a direct linear correlation between the two. Consequently, we used the boundary line (maximum slope) of MOC versus clay + silt content to infer the maximum capacity of different soil types (dominated by either *high- or low-activity minerals*; Figure 6) to store C, which constitutes a key parameter (Q_{max}) in both Langmuir and Sips/Hill formulations, and is necessary for extrapolation to Earth system models. Finally, we highlight the need for measurements of auxiliary data – in particular, net primary productivity (NPP), DOC, vegetation type, climate, and additional mineralogical properties, e.g., specific surface area (SSA), cation exchange capacity (CEC), and clay type – to allow a more rigorous exploration of the role of underlying covariates.

References

Angers, D. A., Arrouays, D., Saby, N. P. A. and Walter, C. (2011) 'Estimating and mapping the carbon saturation deficit of French agricultural topsoils', *Soil Use and Management*, 27(4), pp. 448–452. doi: 10.1111/j.1475-2743.2011.00366.x.

Beare, M. H., Mcneill, S. J., Curtin, D., Parfitt, R. L., Jones, H. S., Dodd, M. B. and Sharp, J. (2014) 'Estimating the organic carbon stabilisation capacity and saturation deficit of soils: a New Zealand case study', *Biogeochemistry*, 120, pp. 71–87. doi: 10.1007/s10533-014-9982-1.

Feng, W., Plante, A. F., Aufdenkampe, A. K. and Six, J. (2014) 'Soil organic matter stability in organo-mineral complexes as a function of increasing C loading', *Soil Biology and Biochemistry*. Elsevier Ltd, 69, pp. 398–0405. doi: 10.1016/j.soilbio.2013.11.024.

Feng, W., Plante, A. F. and Six, J. (2013) 'Improving estimates of maximal organic carbon stabilization by fine soil particles', *Biogeochemistry*, 112(1–3), pp. 81–93. doi: 10.1007/s10533-011-9679-7.

Grant, R. F., Juma, N. G. and Mcgill, W. B. (1993) 'Simulation of carbon and nitrogen transformations in soil: mineralization', *Soil Biology & Biochemistry*, 25, pp. 1317–1329.

Hassink, J. (1997) 'The capacity of soils to preserve organic C and N by their association with clay and silt particles', *Plant and Soil*, 191(1), pp. 77–87. doi: 10.1023/A:1004213929699.

Jagadamma, S., Mayes, M. A. and Phillips, J. R. (2012) 'Selective Sorption of Dissolved Organic Carbon Compounds by Temperate Soils', *PLoS ONE*, 7(11). doi: 10.1371/journal.pone.0050434.

Jagadamma, S., Mayes, M. A., Zinn, Y. L., Gísladóttir, G. and Russell, A. E. (2014) 'Sorption of organic carbon compounds to the fine fraction of surface and subsurface soils', *Geoderma*. Elsevier B.V., 213, pp. 79–86. doi: 10.1016/j.geoderma.2013.07.030.

Kleber, M., Eusterhues, K., Keiluweit, M., Mikutta, C., Mikutta, R. and Nico, P. S. (2015) *Mineral – Organic Associations : Formation , Properties , and Relevance in Soil Environments*, *Advances in Agronomy*. Elsevier Ltd. doi: 10.1016/bs.agron.2014.10.005.

Mayes, M. A., Heal, K. R., Brandt, C. C., Phillips, J. R. and Jardine, P. M. (2012) 'Relation between Soil Order and Sorption of Dissolved Organic Carbon in Temperate Subsoils', *Soil Science Society of America Journal*, 76, pp. 1027–1037. doi: 10.2136/sssaj.

Parton, W. J., Stewart, J. W. B. and Cole, C. V (1988) 'Dynamics of C , N , P and S in grassland soils: a model', *Biogeochemistry*, 131, pp. 109–131.

Rasmussen, C., Heckman, K., Wieder, W. R., Keiluweit, M., Lawrence, C. R., Asefaw, A., Blankinship, J. C., Crow, S. E., Druhan, J. L., Hicks, C. E., Schimel, J. P., Alain, E. M. and Christina, F. P. (2018) 'Beyond clay : towards an improved set of variables for predicting soil organic matter content', *Biogeochemistry*, 137, pp. 297–306. doi: 10.1007/s10533-018-0424-3.

Sanderman, J. and Amundson, R. (2009) 'A comparative study of dissolved organic carbon transport and stabilization in California forest and grassland soils', *Biogeochemistry*, 92, pp. 41–59. doi: 10.1007/s10533-008-9249-9.

Sanderman, J., Baldock, J. A. and Amundson, R. (2008) 'Dissolved organic carbon chemistry and dynamics in contrasting forest and grassland soils Cation exchange capacity', *Biogeochemistry*, 89, pp. 181–198. doi: 10.1007/s10533-008-9211-x.

Sposito, G. (1980) 'Derivation of the Freundlich equation for ion exchange reactions in soils', *Soil Science Society of America Journal*, 44, pp. 652–654.

Sulman, B. N., Phillips, R. P., Oishi, a. C., Shevliakova, E. and Pacala, S. W. (2014) 'Microbe-driven turnover offsets mineral-mediated storage of soil carbon under elevated CO2', *Nature*

Climate Change, 4(December), pp. 1099–1102. doi: 10.1038/nclimate2436.
Tang, J. and Riley, W. J. (2015) 'Weaker soil carbon-climate feedbacks resulting from microbial and abiotic interactions', *Nature Clim. Change*, 5, pp. 56–60. doi: 10.1038/nclimate2438.
Wang, G., Post, W. M. and Mayes, M. a. (2013) 'Development of microbial-enzyme-mediated decomposition model parameters through steady-state and dynamic analyses', *Ecological Applications*, 23(1), pp. 255–272. doi: 10.1890/12-0681.1.
Wieder, W. R., Grandy, a. S., Kallenbach, C. M., Taylor, P. G. and Bonan, G. B. (2015) 'Representing life in the Earth system with soil microbial functional traits in the MIMICS model', *Geoscientific Model Development*, 8(6), pp. 1789–1808. doi: 10.5194/gmd-8-1789-2015.

Supplementary Figures & Tables

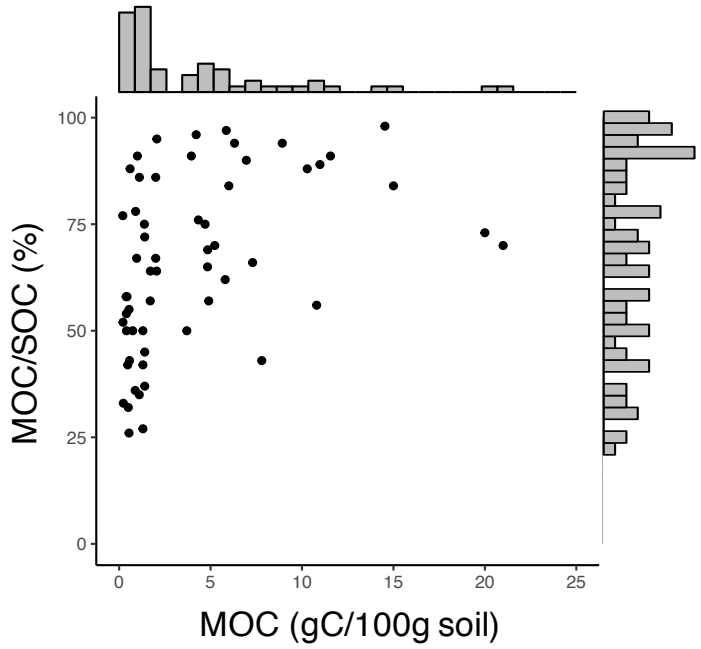

Supplementary Figure 1: MOC/SOC ratio (%) across different soil types and biomes.
Percent of total SOC in mineral-organic associations (MOC/SOC) as a function of mineral-organic associated carbon (MOC in weight %). At most sites, the majority (>50%) of SOC is contained within MOAs.

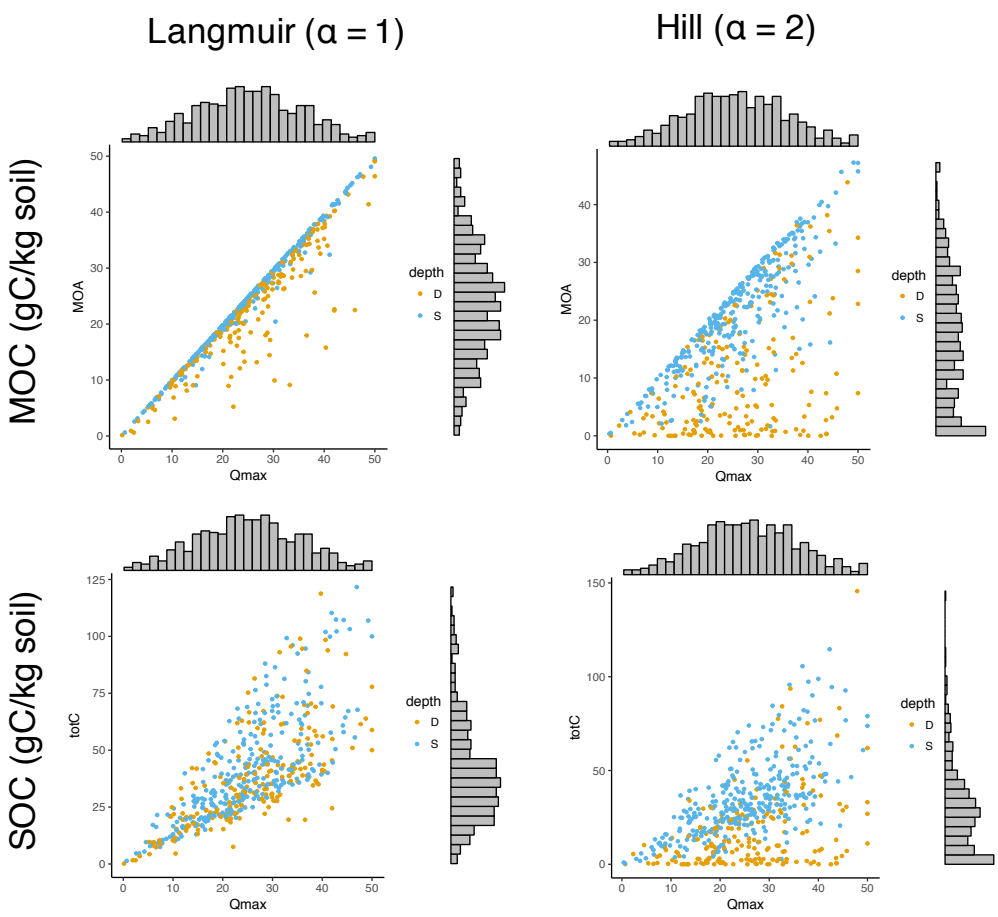

Supplementary Figure 2: Monte Carlo simulations for Langmuir and Hill/Sips with depth.
Predicted MOC and SOC as functions of maximum C capacity (Q_{max}) with Langmuir and Hill model formulations for deep (shown in orange) and surface (shown in blue) soils.

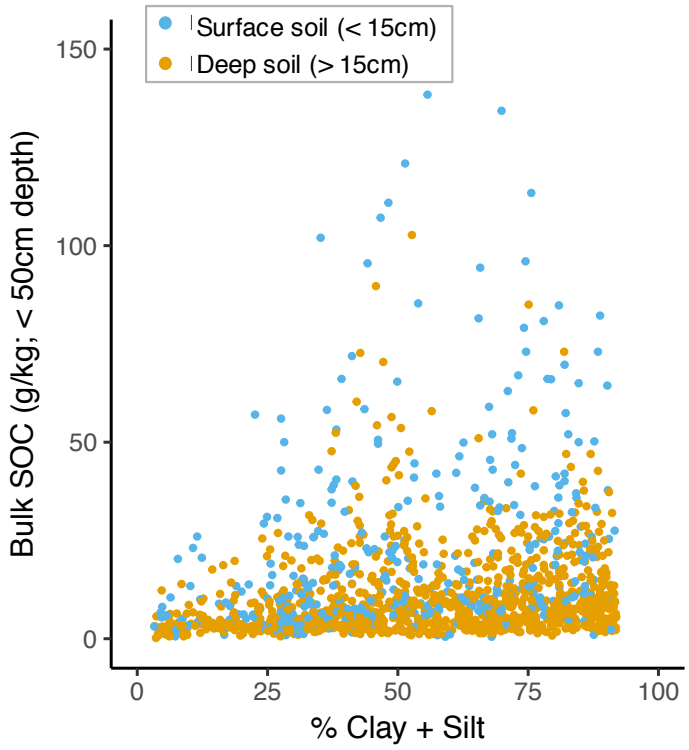

Supplementary Figure 3: Global SOC data with depth.
SOC as a function of soil texture (% clay + silt) with depth for n=5000 profiles from the World Soil Information Service (WoSIS) Soil Profile Database.

CHAPTER 6: A method of alternating characteristics with application to advection-dominated environmental systems

CHAPTER 6: A method of alternating characteristics with application to advection-dominated environmental systems

This chapter is reprinted, with permission, from the original journal article:

Georgiou, K., J. Harte, A. Mesbah, W.J. Riley. A method of alternating characteristics with application to advection-dominated environmental systems. *Computational Geosciences*, (2018).

Abstract

We present a numerical method for solving a class of systems of partial differential equations (PDEs) that arise in modeling environmental processes undergoing advection and biogeochemical reactions. The salient feature of these PDEs is that all partial derivatives appear in linear expressions. As a result, the system can be viewed as a set of ordinary differential equations (ODEs), albeit, each one along a different characteristic. The method then consists of alternating between equations and integrating each one step-wise along its own characteristic, thus creating a customized grid on which solutions are computed. Since the solutions of such PDEs are generally smoother along their characteristics, the method offers the potential of using larger time steps while maintaining accuracy and reducing numerical dispersion. The advantages in efficiency and accuracy of the proposed method are demonstrated in two illustrative examples that simulate depth-resolved reactive transport and soil carbon cycling.

Introduction

Typically, models of environmental processes must be solved over long time horizons and over many spatial grid points to make projections that establish how external stimuli might affect the state of a system [1-2, 5, 14, 36, 41-42, 46, 48]. In addition, multi-model ensembles are often used due to uncertainty in model structure and parameter values to obtain not only one projection but also a range depicting its uncertainty [17, 23, 46, 48]. Such simulations require considerable computational resources, especially since the solutions must be obtained over sufficiently small time steps to maintain accuracy and avoid errors due to numerical dispersion. There is thus an ongoing need for improving the numerical tools used to solve spatially- and temporally- resolved reactive-transport models over large space- and time- horizons.

The type of equations we are concerned with here are typical of those arising in environmental systems in which one or more components undergo advective transport in addition to chemical or biological reactions. Such equations occur, for example, in modeling of pollutant transport through a porous, reactive medium or in modeling of soil carbon cycling where leaching processes transport dissolved organic carbon vertically through the soil profile [1, 16, 22-23, 36, 41-42, 45]. These types of systems give rise to equations of the form:

$$\frac{\partial u_i}{\partial t} = f_i(t, x, u_i, \dots, u_n) - c_i(t, x)\frac{\partial u_i}{\partial x} \ , \qquad \text{for } \ i = 1, \dots, n \ , \tag{1}$$

where u_i is the concentration of the i^{th} component of the system, $f_i(t, u_i, \dots, u_n)$ is a non-linear function that encodes the reactions governing u_i, and $c_i(t, x)$ is the advective velocity (e.g., of

water through the soil profile). We then have equations in which the partial derivatives with respect to space and time appear linearly for each i^{th} component, modified only by coefficients. We note that the advective velocity (c_i) may in fact be spatially varying, so we present an extension of our method to accommodate this dependence. These equations comprise a system of coupled, hyperbolic PDEs and, although they can be solved numerically via standard methods [11-12, 20, 26, 33, 35, 43], the specific form that arises in environmental processes is often amenable to a natural and simpler numerical solution as a set of ODEs along a customized grid by a suitable adaptation of the method of characteristics [12, 33].

In essence, the proposed method transforms the above coupled PDEs into coupled ODEs, each one propagating along its own characteristic, and alternates in solving each equation by step-wise numerical integration along its corresponding characteristic. The method takes advantage of the fact that the solutions of advection-dominated PDEs are generally much smoother along their characteristics than they are in the time direction [12, 49]. This allows for larger time steps in a simulation without loss of accuracy, and reduces the numerical dispersion present in many Eulerian methods [12, 43]. Additionally, since the grid is uniquely defined by the physics (via the characteristics) of the system, the proposed method is not susceptible to grid orientation effects, in contrast to finite-difference methods. We implement a numerical integration using the implicit Euler method to achieve better accuracy and stability compared to the explicit Euler scheme [24, 33]. For specific forms of the governing equations, the method can be generalized to more than one spatial dimension.

In the next section, the proposed method, termed the *Method of Alternating Characteristics* (MAC), is described for a system of two, three, or more characteristic directions, and extended to spatially-variable characteristic directions and more than one spatial dimension, as well as to systems where both advection and diffusion are present. We then present two example applications that arise in modeling reactive transport and depth-resolved soil carbon cycling. We solve each system of equations using the Method of Alternating Characteristics and standard methods for approximating PDEs (e.g., finite differences). We compare the solutions in terms of accuracy, speed, and robustness and explore advantages of the proposed method. While optimized integration schemes may outperform our chosen standard, we emphasize that the goal here is to illustrate that the physics of advection-dominated environmental systems is uniquely-suited for the proposed method and that further optimization may be necessary.

Method of Alternating Characteristics

In general, for a given component i, the partial differential equation

$$\frac{\partial u_i}{\partial t} = f_i(t, x, u_i, \dots, u_n) - c_i(t, x)\frac{\partial u_i}{\partial x} \ ,$$

that is linear in the spatial partial derivative, can be turned into the equivalent ordinary differential equation

$$\frac{\mathrm{d}u_i}{\mathrm{d}t} = \frac{\partial u_i}{\partial t} + \frac{\partial u_i}{\partial x}\frac{\mathrm{d}x}{\mathrm{d}t} = f_i(t, x, u_i, \dots, u_n)$$

along the characteristic $x(t)$ defined by $\frac{\mathrm{d}x(t)}{\mathrm{d}t} = c_i(t,x)$ [12, 33].

For a system with two or more PDEs as above, the basic idea of the MAC is to alternate between (ordinary) integration along characteristics, each time integrating step-wise the corresponding ODE equation along its respective characteristic. We first focus on the case where c_i is constant, in which case the characteristic is

$$x(t) = x_0 + c_i t$$

and will be referred to as a "constant characteristic direction". The method is described in detail, first for a system with two constant characteristic directions, followed by a discussion for extending this method to systems with more general (e.g., spatially-varying) characteristic directions as well as systems with more than two characteristics. Our interest is mainly in one spatial dimension; however, we also remark and discuss special cases where the method can be extended to more than one spatial dimension.

In the developments that follow we adopt the commonly used compact notation of denoting partial derivatives $\frac{\partial u}{\partial x}$ by u_x and $\frac{\partial u}{\partial t}$ by u_t.

System of two constant characteristic directions

Consider a system of two PDEs as in equation (1), with constant advective velocities c_i where $i \in \{1, 2\}$. Without loss of generality, we can assume that one of the two is equal to zero and the other normalized to 1. Thus, simplifying the notation for illustration, we consider two scalar functions $u(t,x)$ and $v(t,x)$ satisfying

$$u_t = f(t,x,u,v) - u_x \quad (2a)$$
$$v_t = g(t,x,u,v)\,. \quad (2b)$$

Along the characteristic of v (i.e., $x^v(t) = x_0$ since $\dot{x}^v(t) = \frac{\mathrm{d}x^v(t)}{\mathrm{d}t} = 0$, where the superscript denotes the dependent variable to which the characteristic belongs), equation (2b) becomes the ODE

$$\frac{\mathrm{d}v}{\mathrm{d}t} = g(t, x_0, u, v)$$

where the function g depends on $u(t, x_0)$. However, $u(t, x_0)$ is not known ahead of time and depends on values of $u(t,x)$ at nearby points in the spatial direction, via equation (2a). In turn, equation (2a) can be written as an ODE when solved along its corresponding characteristic,

$$\begin{aligned}\frac{\mathrm{d}u}{\mathrm{d}t} &= u_t + u_x\,\dot{x}^u \\ &= f(t, x_0 + t, u, v)\end{aligned}$$

along the line $\dot{x}^u(t) = 1$, or, equivalently, along $x^u(t) = x_0 + t$. This is so because equation (2a) has the character of a wave equation [33]. Here the function f depends on $v(t, x_0 + t)$ which evolves in time and space via equation (2b).

We summarize that equation (2b) can be solved as an ODE along the characteristic $\dot{x}^v = 0$, while equation (2a) can be solved as an ODE along $\dot{x}^u = 1$. We briefly note that along the line $\dot{x}^v = 1$, equation (2b) is no longer an ODE, but rather, it becomes

$$\begin{aligned} \frac{\mathrm{d}v}{\mathrm{d}t} &= v_t + v_x \, \dot{x}^v \\ &= g(t, x_0 + t, u, v) + v_x \, . \end{aligned}$$

Thus, the wave nature of one of the two equations complicates matters and we cannot reduce the system to a corresponding system of ODEs unless we alternate between the directions of the two characteristics: $\dot{x}^u = 1$ to solve for u and $\dot{x}^v = 0$ for v. By developing a customized grid, we can alternate between these characteristic directions and solve the system as two ODEs, rather than as numerically-approximated PDEs.

For the particular example above, with characteristics $\dot{x}^v = 0$ and $\dot{x}^u = 1$, the corresponding grid is shown in Fig. 1a, where we can solve the ODE for u diagonally and for v horizontally. We can only solve each over the time step Δt since we must update the value of both u and v at the nodes of the grid for successive points in time.

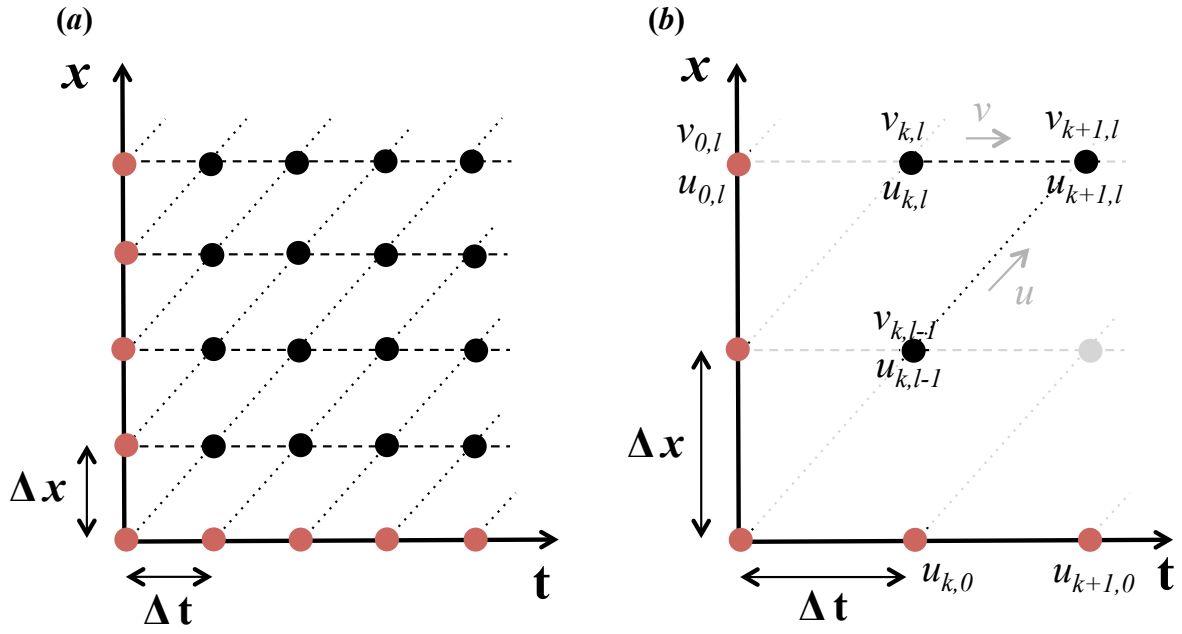

Figure 1: Schematic of a customized grid for propagating the integration along two constant characteristics. **(*a*)** Characteristic directions $x^v(t) = x_0$ (dashed horizontal lines; $\dot{x}^v = 0$) and $x^u(t) = t + x_0$ (dotted diagonal lines; $\dot{x}^u = 1$) for solving the system of PDEs in equation (2). Boundary and initial conditions are depicted in red. **(*b*)** Propagating the integration along two characteristics using the explicit or implicit Euler methods (as in equations (3) or (4), respectively) to obtain $u_{k+1,l}$ and $v_{k+1,l}$, where initial ($u_{0,l}$, $v_{0,l}$) and boundary ($u_{k,0}$) conditions are shown in red.

Thus, the *numerical scheme* amounts to updating the value of u and v at the node points, as follows:

Fix Δt and consider successively the points in time $t \in \{0, \Delta t, 2\Delta t, \dots, k\Delta t, \dots\}$ and the corresponding values of

$$u_{k,l} = u(k\Delta t, l\Delta x) \quad \text{and} \quad v_{k,l} = v(k\Delta t, l\Delta x)\,.$$

In the case of equation (2), $\Delta x = \Delta t$ since the one characteristic is $x^u(t) = \text{constant} + t$ at the corresponding spatial coordinates. Starting from given boundary values

$$\{u_{0,l}, v_{0,l} \mid l = 0, 1, 2, \dots\} \quad \text{and} \quad \{u_{k,0} \mid k = 1,2, \dots\}\,,$$

compute recursively for increasing values of $k \geq 0$,

$$u_{k+1,l} = u_{k,l-1} + f\big(u_{k,l-1},\, v_{k,l-1}\big)\,\Delta t, \quad \text{for} \quad l = 1, 2, \dots \tag{3a}$$

$$v_{k+1,l} = v_{k,l} + g\big(u_{k,l},\, v_{k,l}\big)\,\Delta t, \quad \text{for} \quad l = 0, 1, 2, \dots \tag{3b}$$

This constitutes the *explicit* (forward) Euler method and is shown schematically for $u_{k+1,l}$ and $v_{k+1,l}$ in Fig. 1B.

A small modification of the approach allows usage of the *implicit* (backward) Euler method for solving the differential equations along the characteristics. More specifically replace equation (3) by the implicit equations:

$$u_{k+1,l} = u_{k,l-1} + f\big(u_{k+1,l},\, v_{k+1,l}\big)\,\Delta t, \quad \text{for} \quad l = 1, 2, \dots \tag{4a}$$

$$v_{k+1,l} = v_{k,l} + g\big(u_{k+1,l},\, v_{k+1,l}\big)\,\Delta t, \quad \text{for} \quad l = 0, 1, 2, \dots \tag{4b}$$

These can then be solved by a fixed-point iteration

$$u_{k+1,l}^{(i+1)} = u_{k,l-1} + f\Big(u_{k+1,l}^{(i)},\, v_{k+1,l}^{(i)}\Big)\,\Delta t, \quad \text{for} \quad l = 1, 2, \dots \tag{5a}$$

$$v_{k+1,l}^{(i+1)} = v_{k,l} + g\Big(u_{k+1,l}^{(i)},\, v_{k+1,l}^{(i)}\Big)\,\Delta t, \quad \text{for} \quad l = 0, 1, 2, \dots \tag{5b}$$

starting from

$$u_{k+1,l}^{(0)} = u_{k,l-1} \quad \text{and} \quad v_{k+1,l}^{(0)} = v_{k,l}\,.$$

The above system of equations is a vectorial equation of the form

$$\begin{bmatrix} u_{k+1,l}^{(i+1)} \\ v_{k+1,l}^{(i+1)} \end{bmatrix} = F\left(\begin{bmatrix} u_{k+1,l}^{(i)} \\ u_{k+1,l}^{(i)} \end{bmatrix}\right),$$

where the map

$$F\left(\begin{bmatrix} \boldsymbol{u} \\ \boldsymbol{v} \end{bmatrix}\right) = \begin{bmatrix} u_{k,l-1} + f(\boldsymbol{u}, \boldsymbol{v})\,\Delta t \\ v_{k,l} + g(\boldsymbol{u}, \boldsymbol{v})\,\Delta t \end{bmatrix}.$$

It is clear that for sufficiently small Δt, F is Lipschitz continuous with Lipschitz constant $L < 1$, since

$$\left\| F\left(\begin{bmatrix} \boldsymbol{u_1} \\ \boldsymbol{v_1} \end{bmatrix}\right) - F\left(\begin{bmatrix} \boldsymbol{u_0} \\ \boldsymbol{v_0} \end{bmatrix}\right) \right\| = \left\| \Delta t \begin{bmatrix} f(\boldsymbol{u_1}, \boldsymbol{v_1}) - f(\boldsymbol{u_0}, \boldsymbol{v_0}) \\ g(\boldsymbol{u_1}, \boldsymbol{v_1}) - g(\boldsymbol{u_0}, \boldsymbol{v_0}) \end{bmatrix} \right\| < \left\| \begin{bmatrix} \boldsymbol{u_1} \\ \boldsymbol{v_1} \end{bmatrix} - \begin{bmatrix} \boldsymbol{u_0} \\ \boldsymbol{v_0} \end{bmatrix} \right\|.$$

Therefore, the fixed-point iteration in equation (5) converges. In the simulations, a fixed number of steps for the iteration are deemed sufficient, and it is observed that they give an improvement over the standard explicit Euler method.

The proposed method can be applied to a system of more than two equations without any modification provided they share the same two characteristics. In fact, this is not unusual in many natural systems. For example, in soil, some chemical components may experience advection (i.e., leaching) with a particular gravity- or pressure-driven water velocity, while other components experience no leaching [1, 36]. In that case, a subset of equations can be solved along the characteristic dictated by the magnitude of the water advective velocity (i.e., $\dot{x}(t) = c$ for some value c), while the remaining equations can be solved along constant values of x (i.e., $\dot{x}(t) = 0$).

If, however, there are more than two characteristics, e.g., for three dependent variables u, v and w, then we need to adjust the grid appropriately and possibly interpolate values of some of the dependent variables. This scenario will be discussed below, along with the case where the velocities (and therefore the characteristics) vary spatially.

System of three or more characteristic directions

Consider the case of three coupled PDEs

$$u_t = f(u, v, w) - u_x \tag{6a}$$

$$v_t = g(u, v, w) \tag{6b}$$

$$w_t = h(u, v, w) - cw_x\,. \tag{6c}$$

Once again, and without loss of generality, one velocity is normalized to 1, another to 0, and the remaining advective velocity is c.

We may form a grid as before on which to alternate directions and integrate equations (6a) and (6b). However, in order to update the values of w, we need to integrate equation (6c) along a different characteristic. If the advective velocity of w (c; denoted $\dot{x}^w$) is an integer (i.e., integer multiple of $\dot{x}^u$), then the grid points dictated by the advective velocities of u and v are sufficient; namely, the (uv)-grid as defined in the previous section. Then all dependent variables can be consistently determined on these points. If, however, c is not an integer multiple of the advective velocity of u, then the value of w needs to be interpolated accordingly. More specifically, the value of w can be computed by integrating equation (6c) at points that fall outside the grid and those values can then be used to approximate w on the (uv)-grid (see Fig. 2). For instance, the values of w at points $(\Delta t, x_1)$ and $(\Delta t, x_2)$ can be used to linearly interpolate the value of w at $(\Delta t, \Delta x)$, as shown in Fig. 2. We note that, in principle, the interpolation should be of at least the same order as the integration scheme, which is here of first order.

In this way, following the rationale in the MAC, we can again use ordinary integration along characteristics as specified by the physics of the system. The choice of which equations to normalize and, thereby, determine the grid on which to evaluate the parameters, may have an impact on the numerical accuracy. Further analysis is needed to assess the optimal choice.

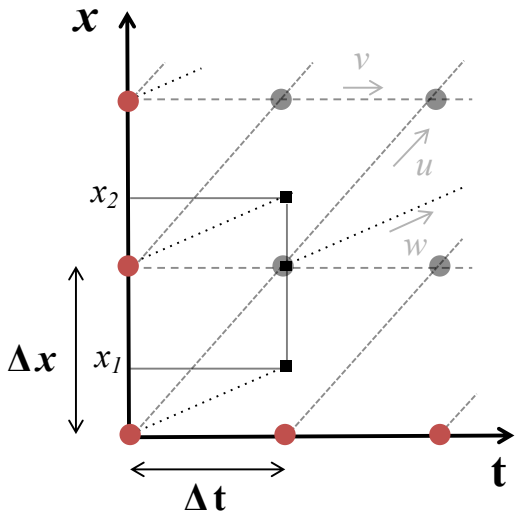

Figure 2: Schematic of a customized grid for propagating the integration along three characteristic directions.
Customized grid for three characteristic directions – $\dot{x}^u = 1$, $\dot{x}^v = 0$, and $\dot{x}^w = c$, as in equation (6) – with interpolation of integrated values of $\dot{x}^w = c$ from spatial locations $(\Delta t, x_1)$ and $(\Delta t, x_2)$ in-between existing grid points (shown as black squares). The order of interpolation should be of at least the same order as the integration scheme. The integration then proceeds as before, alternating ordinary integration of each equation, along the customized grid. Boundary conditions are shown in red.

System with spatially-varying characteristic directions

On account of the underlying physics, the advective velocity may vary in space and time, i.e, as $c(t, x)$ [16, 23, 41-42]. For example, the number and size of pore spaces in soil (and

consequently, the bulk density) through which water flows may vary with depth [1, 29, 36, 47]. Given mass balance considerations and no accumulation, this implies that the velocity changes with depth as the flow path changes. Additionally, leaching may vary according to the amount of water entering the soil (e.g., due to changes in precipitation) at a particular point in time [15, 29, 36, 47]. Thus, we can see that the method presented above often needs to be extended to the case of variable characteristic directions.

For illustration purposes, we consider the case where the advective velocity is only spatially variable, i.e., it is $c(x)$. Fig. 3 displays a suitable grid for the numerical scheme to solve an example with depth-varying advective velocity. Of particular interest, conferring advantages to the MAC, may be the case where the depth-varying velocity changes abruptly between layers (rough coefficients in the PDEs) as dictated by the underlying physics. An example of such a case will be simulated and discussed.

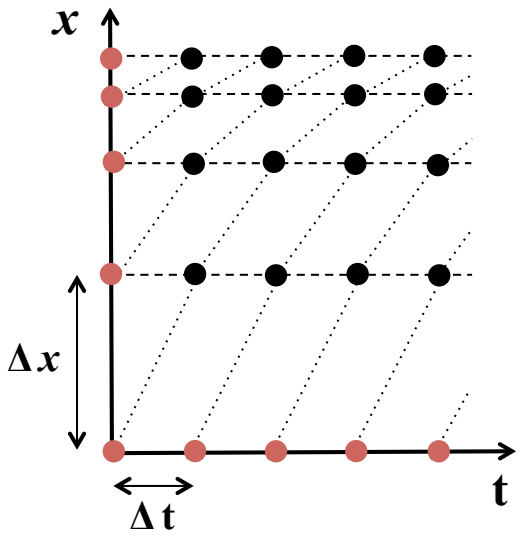

Figure 3. Schematic of a customized grid for propagating the integration along two varying characteristics, such as those arising in systems with spatially-variable advective velocity.
In this example, $\dot{x}^v = 0$ (dashed horizontal lines) and $\dot{x}^u = c(x)$ (dotted diagonal lines). The step Δx varies with x and is dictated by $c(x)\,\Delta t$. Boundary conditions are shown in red.

In principle, it is also possible to include temporal variation, either as $c(t)$ or $c(t,x)$ depending on the system. However, in such a case, the suitable grid may be complicated or may require additional interpolation. Since MAC is a first-order method, in principle, any approximation should be at least of first order. In practice, however, simplifications are often employed that ignore this time dependence. In the case of soil carbon modeling, a temporally-averaged water flux is often used, calculated based on monthly- or annually-averaged precipitation [1, 29]. Hence, the velocity is taken as a constant in time and the use of a temporally-varying velocity may depend on the timescale of interest.

Characteristics in more than one spatial dimension

The basic property that allows adapting the method of characteristics to a hyperbolic system of PDEs is the ability to generate a customized lattice (grid) where the spatial and temporal derivatives can be numerically approximated, consistently and simultaneously, for each of the equations of the hyperbolic system. For this to be the case, it is important that the characteristics display a suitable spatial invariance. The type of equations that arise in environmental models (e.g., of biogeochemical processes) are often simple enough to justify such a property.

Once again, we consider two dependent variables, u and v. We consider two spatial dimensions with coordinates designated as x and y, and PDEs of the form

$$u_t = f(t, x, y, u, v) - c_1(x)\, u_x - \, c_2\, u_y \,, \tag{7a}$$

$$v_t = g(t, x, y, u, v) \,. \tag{7b}$$

This set of equations arises naturally in instances were two components (with concentrations, u and v) chemically interact, while one of the two advects (e.g., component u leaches through the soil) and the other is stationary (e.g., v is adsorbed to the soil matrix). The advective velocities in the x and y directions may depend on different physical factors. For example, the velocity in the y (horizontal) direction could be driven by a constant pressure gradient, possibly due to a nearby river or sloped catchment [15, 31, 37, 47]. The gravity-driven velocity in the x (vertical) direction, on the other hand, may be a function of the depth (rather than being constant) due to differing medium properties (e.g., porosity) with depth [1, 36]. In this instance, the characteristics for component u (distinguished by a superscript) are defined by

$$\dot{x}^u = c_1(x) \tag{8a}$$

$$\dot{y}^u = c_2 \,, \tag{8b}$$

and for component v,

$$\dot{x}^v = 0 \tag{9a}$$

$$\dot{y}^v = 0 \,. \tag{9b}$$

As seen in Fig. 4a, a customized lattice, where spacing is regular in the y-direction and adjustable in the x-direction, provides a grid that allows integration of ODEs numerically along corresponding characteristics in a suitable manner. The curves in Fig. 4B represent the projection of the characteristics of u (that may be spatially-variable, as shown) on the (x, y) plane, whereas the dots represent the projection of the characteristics of v. The lattice consists of points

$$(t, x, y) = (k\Delta t, \textstyle\sum_{i=1}^{l} \Delta x_i \,, m\Delta y)$$

and the corresponding variables for the numerical scheme are labeled accordingly as $u_{k,l,m}$ and $v_{k,l,m}$. Along the characteristics in equations (8) and (9), the ordinary difference equations for the explicit Euler scheme take the form

$$u_{k+1,l,m} = u_{k,l-1,m-1} + f(u_{k,l-1,m-1}, v_{k,l-1,m-1})\,\Delta t \tag{10a}$$

$$v_{k+1,l,m} = v_{k,l,m} + g(u_{k,l,m}, v_{k,l-1,m-1})\,\Delta t\,, \tag{10b}$$

respectively, where u and v are computed recursively for increasingly values of $k \geq 0$, starting from given boundary conditions

$$\{u_{0,l,m}, v_{0,l,m} \,|\, l = 0, 1, 2, \ldots, m = 0, 1, 2, \ldots\} \text{ and } \{u_{k,l,0} \,|\, k = 0, 1, 2, \ldots, l = 0, 1, 2, \ldots\}.$$

Similarly, the implicit Euler method, together with a fixed-point iteration scheme, can be employed using f and g evaluated at $(u_{k+1,l,m}, v_{k+1,l,m})$.

In more general situations, when a family of characteristics cannot be found that meets at the nodes of a lattice, advantages may still be drawn from a customized grid in conjunction with approximation schemes to interpolate at in-between points as discussed earlier.

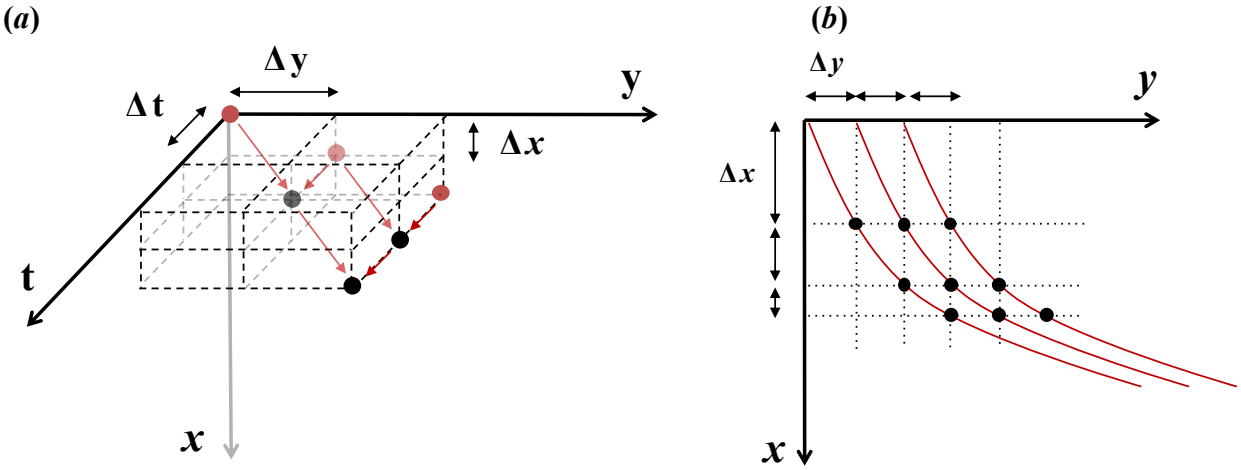

Figure 4: Schematic of a customized lattice for two spatial dimensions.
Customized lattice for two spatial dimensions, where the integration is propagated along distinct characteristics for dependent variables u and v, as arising in equations (7) to (9). **(a)** Characteristic directions $\dot{x}^u = c_1(x)$ and $\dot{y}^u = c_2$ for variable u (red diagonal arrows) and $\dot{x}^v = 0$ and $\dot{y}^v = 0$ for variable v (red arrows perpendicular to x, y-plane) are used to form the customized lattice and propagate ordinary integration of the corresponding coupled ODEs as in equation (10). **(b)** The characteristic curves of u are projected on the x, y-plane (shown in red) and the dots represent the projection of the characteristic curves of v. Here the characteristic $\dot{x}^u = c_1(x)$ is spatially varying, as in equations (7a) and (8a).

System with *diffusion* and advection

For many of the physical processes that we consider, it is expected that a small amount of diffusion will be present; e.g., that dissolved organic carbon will diffuse through the porous soil media. Thus, a more accurate model may be of the form

$$\frac{\partial u_i}{\partial t} = f_i(t, x, u_i, \dots, u_n) - c_i(t, x)\frac{\partial u_i}{\partial x} + \varepsilon_i \frac{\partial^2 u_i}{\partial x^2} .$$

Numerically, we need to introduce $\left(\varepsilon_i \frac{\partial^2 u_i}{\partial x^2}\right)$ as an additional term in equations (3) and (4). A natural choice is to estimate the second partial derivatives with respect to x by either

$$\frac{\partial^2 u}{\partial x^2} \approx \frac{\frac{u_{k,l}-u_{k,l-1}}{\Delta x} - \frac{u_{k,l-1}-u_{k,l-2}}{\Delta x}}{\Delta x} = \frac{u_{k,l}-2u_{k,l-1}+u_{k,l-2}}{\Delta x^2} \qquad (11a)$$

and

$$\frac{\partial^2 v}{\partial x^2} \approx \frac{v_{k,l+1}-2v_{k,l}+v_{k,l-1}}{\Delta x^2}, \qquad (11b)$$

or, alternatively,

$$\frac{\partial^2 u}{\partial x^2} \approx \frac{u_{k+1,l}-2u_{k+1,l-1}+u_{k+1,l-2}}{\Delta x^2} \qquad (12a)$$

and,

$$\frac{\partial^2 v}{\partial x^2} \approx \frac{v_{k+1,l+1}-2v_{k+1,l}+v_{k+1,l-1}}{\Delta x^2}, \qquad (12b)$$

for explicit and implicit difference schemes, respectively. The approximation of the diffusion term can also be accomplished via finite volume methods [21, 26, 35]. If we use equation (11), we need to modify equation (3) as follows

$$u_{k+1,l} = u_{k,l-1} + f\left(u_{k,l-1},\, v_{k,l-1}\right)\Delta t + \varepsilon_u\left(\frac{u_{k,l}-2u_{k,l-1}+u_{k,l-2}}{\Delta x^2}\right)\Delta t, \qquad \text{for } \; l = 1, 2, \dots$$

$$v_{k+1,l} = v_{k,l} + g\left(u_{k,l},\, v_{k,l}\right)\Delta t + \varepsilon_v\left(\frac{v_{k,l+1}-2v_{k,l}+v_{k,l-1}}{\Delta x^2}\right)\Delta t, \qquad \text{for } \; l = 0, 1, 2, \dots$$

If we use equations (4) and (12) instead, the difference equations become implicit as both $u_{k+1,l}$ and $v_{k+1,l}$ appear in the expression for the second partial with respect to x. These equations must be solved by relying on a fixed-point iteration as before. However, since the estimate for the second partial requires Δx^2 in the denominator, the relative sizes of Δt, Δx, and ε's are critical and a Lipschitz constant of less than 1 may not be possible to guarantee. This appears to be the case when the magnitude of $\Delta t \approx \Delta x$ and Δx is small relative to the ε's.

Applications & Results

The *Method of Alternating Characteristics* (MAC) is uniquely suited to solve systems where subsets of the chemical constituents experience different advective velocities. Such instances arise naturally in many depth-resolved reactive transport models with flow through a porous, reactive medium, where only a subset of the constituents experience leaching [1, 16, 22-23, 32, 36, 41-42]. For example, this encompasses many instances of pollutant transport through soil, and extends to models of soil carbon cycling where dissolved organic matter experiences leaching in addition to microbial decomposition and adsorption to mineral surfaces. Earlier method-of-characteristics-based ideas [3, 7, 8, 13, 38] have not been applied to this type of system where multiple characteristics must be reconciled and simultaneously utilized on a customized grid, limiting our ability to compare directly to such methods. The efficiency and accuracy (convergence towards the exact solution) of the MAC is therefore compared to a standard finite-difference scheme. More specifically, the first-order, implicit upwind *finite-difference* scheme (hereafter, FD) is used to allow for a direct comparison with the first-order, implicit Euler method used in the MAC, as detailed in equations (4) and (5). For the system in equations (1) and (2), following the discretization $u_{k,l} = u(k\Delta t, l\Delta x)$ and $v_{k,l} = v(k\Delta t, l\Delta x)$, the upwind scheme employed can be represented in compact notation as follows

$$u_{k+1,l} = u_{k,l} + f\left(u_{k+1,l}, v_{k+1,l}\right)\Delta t - \left[c^{+}\left(\frac{u_{k,l}-u_{k,l-1}}{\Delta x}\right) + c^{-}\left(\frac{u_{k,l+1}-u_{k,l}}{\Delta x}\right)\right]\Delta t \qquad (13)$$

where $c^{+} = \max(c, 0)$ and $c^{-} = \min(c, 0)$, and similarly for $v_{k+1,l}$ with $g\left(u_{k+1,l}, v_{k+1,l}\right)$ [33, 34]. Thus, if $c > 0$, as is the case in the examples below, then $c^{+} = c$ and $c^{-} = 0$. This implicit scheme can be solved by a fixed-point iteration, as described in equations (4) and (5), as opposed to an explicit scheme where f and g are directly evaluated at $\left(u_{k,l}, v_{k,l}\right)$. We note that implicit evaluation of spatial derivatives at t_{k+1} resulted in additional numerical dispersion. We have therefore restricted our attention to the case where only f and g are implicitly evaluated as in equation (13). The upwind finite-difference scheme in equation (13) is first-order in both space and time. While we consider only first-order schemes here, alternative higher-order schemes can be used for both the MAC and FD; e.g., higher-order Runge-Kutta methods to approximate the ODE in the MAC and accordingly for the FD [19, 25]. The performance of the proposed method is highlighted by two examples of typical one-dimensional environmental applications.

Reactive transport through a porous medium

We apply the MAC to simulate depth-resolved, advection-dominated transport in which an unspecified number of substrates (for example, dissolved organic matter or extraneous pollutants) are leached through a porous medium (e.g., soil) while also undergoing reactions with the stationary parent material. Here we imagine that a substrate flows through the soil profile, but can no longer be leached if adsorbed to a mineral surface. In its dissolved and leachable state, the substrate constitutes the *dissolved pool* C_D, while in its adsorbed and stationary state, the substrate-mineral complex makes up the *mineral-associated pool* C_q. The adsorption and desorption reaction rate constants are denoted k_{ads} and k_{des}, respectively, and the advective transport is driven by the water velocity (c) through the medium (see Fig. 5). Assuming that a surplus of mineral binding sites (q_{max}) exist to adsorb the substrate, the temporal and spatial evolution of the two dependent variables is dictated by

$$\frac{\partial C_D(t,x)}{\partial t} = -\underbrace{k_{ads}\, C_D \left(q_{max} - C_q\right)}_{\text{adsorption}} + \underbrace{k_{des}\, C_q}_{\text{desorption}} - \underbrace{c\frac{\partial (C_D)}{\partial x}}_{\text{leaching}} \tag{14a}$$

$$\frac{\partial C_q(t,x)}{\partial t} = \underbrace{k_{ads}\, C_D \left(q_{max} - C_q\right)}_{\text{adsorption}} - \underbrace{k_{des}\, C_q}_{\text{desorption}} \tag{14b}$$

where all functions depend on time t and depth x. This example is easily extended to the case where there are multiple substrates that undergo reactions, multiple mineral surface types, as well as biological activity in which select substrates are consumed. The key is that only a subset of components undergo advection, making the MAC uniquely suited to solve such a system.

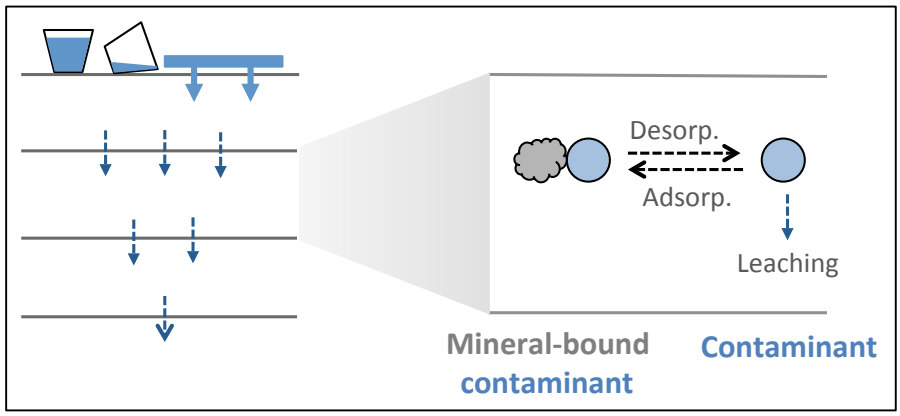

Figure 5: Schematic of depth-resolved reactive transport.
Here a substrate in the soil profile undergoes advective transport (leaching) and reactions (adsorption and desorption) in time (t) and space (x) – see equation (14).

Without loss of generality, the parameters k_{ads}, k_{des}, q_{max}, and c in the above model were assumed to take the values of 1 day^{-1} kg^{-1} m^3, 1 day^{-1}, 1 kg m^{-3}, 0.2 m day^{-1}, respectively, recognizing that in real applications these values are estimated from laboratory experiments; e.g., sorption isotherms for each particular substrate are used to calculate the relevant adsorption and desorption parameters (k_{ads}, k_{des}, q_{max}) [30]. Fig. 6 shows the temporal- and spatial- evolution of the system in equation (14) in response to a step input of pollutant of 1 kg m^{-3} at the surface. The initial condition of both pools is zero pollutant concentration, while the boundary (surface) condition is initially rich in pollutant (imagine a continuous spill) and then free of pollutant (e.g., the spill is contained). Ultimately, the shape of the pollutant profile depends on the initial and boundary conditions, the relative magnitude of the adsorption and desorption rate constants, as well as the advective velocity.

We compared the solutions of equation (14) with time steps Δt ranging from 0.001 to 0.5 days for both the MAC and FD (Fig. 6), where Δx for MAC is predefined by the nature of the method (i.e., $\Delta x = c\, \Delta t$) and thus, the same Δx was adopted for FD to ensure a fair comparison at the same resolution. As aforementioned, we show results from the first-order, implicit upwind finite-difference scheme in equation (13), but also note that the first-order, explicit upwind finite-

difference scheme was more prone to instabilities, as expected [12, 33]. Comparing the solution of FD across a range of time steps in Fig. 6, where the spatial step size is chosen to allow direct comparison to MAC, we can see that there is substantial numerical dispersion at larger time steps. However, comparing the MAC (Fig. 6, top) to the FD (Fig. 6, bottom), we can clearly see that the MAC maintains performance at coarser grid resolution. This pattern is also illustrated in Fig. 7 where the error (defined as the difference between the solution obtained using Δt = 0.5 and Δt = 0.0005) is displayed for both the MAC and FD schemes. The two methods converge at smaller time steps Δt < 0.001 and, thus, Δt = 0.0005 is a good approximation of the true solution [4, 33]. It is observed that the MAC offers a significant advantage, as it allows for faster simulations with larger integration steps that do not sacrifice accuracy.

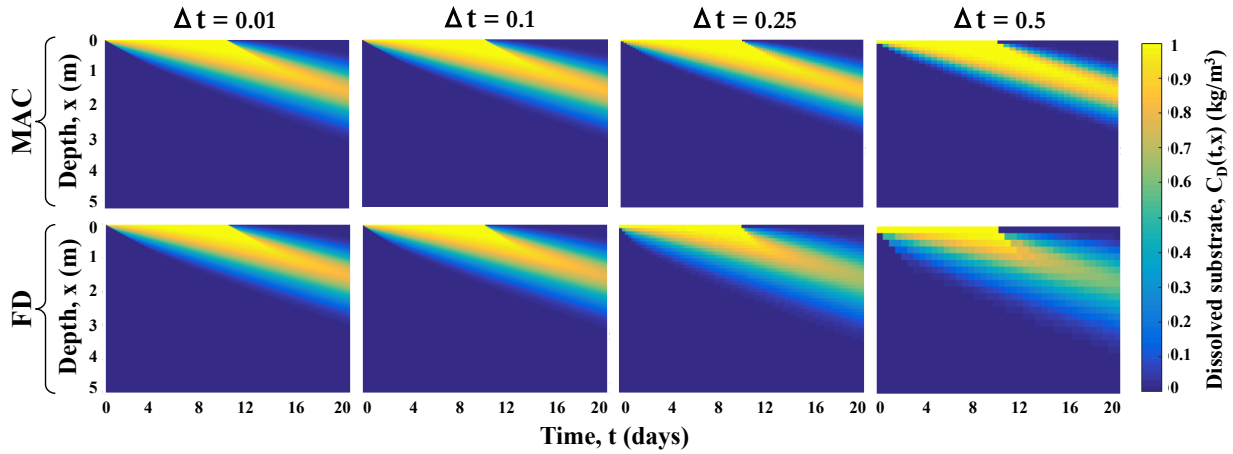

Figure 6: Solving a system undergoing depth-resolved reactive transport using the Method of Alternating Characteristics (MAC) and the method of Finite Differences (FD).
Solving the system in equation (14) using the Method of Alternating Characteristics (MAC) (top panels) and the method of Finite Differences (FD) (bottom panels) with increasing time steps from left to right: Δt = 0.01, 0.1, 0.25, 0.5 days, respectively. More specifically, the ordinary integration in MAC is performed by the first-order, implicit Euler method. For the FD implementation, the standard first-order, implicit upwind scheme in space and time is used to approximate the corresponding PDEs. The step size Δx is predefined for MAC by the nature of the method (i.e., $\Delta x = c\ \Delta t$) and thus, the same Δx was adopted for FD to ensure a fair comparison at the same resolution. The increased numerical dispersion of the FD solution compared to the MAC solution is observed as the step size increases.

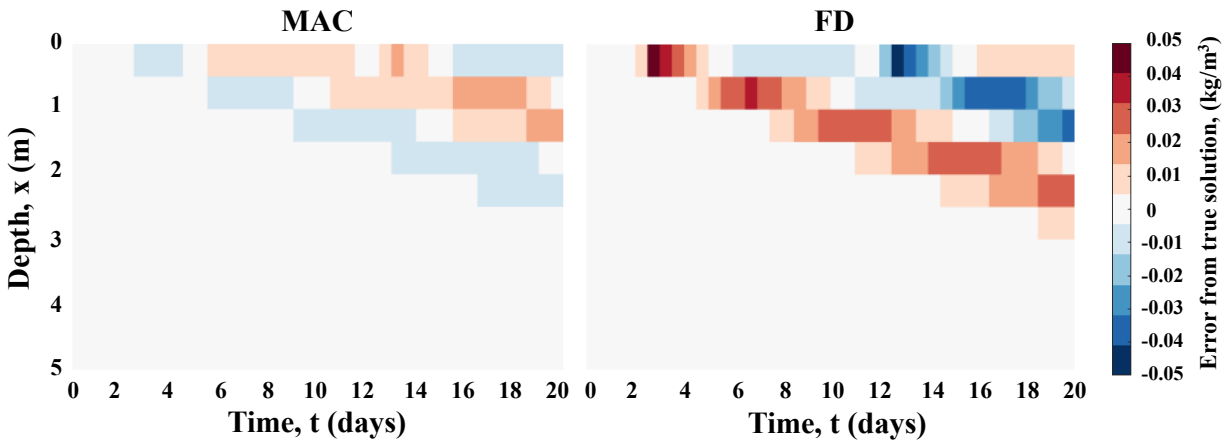

Figure 7: Numerical dispersion arising in the solutions using MAC and FD.
Numerical dispersion, computed as the difference between the solution using Δt = 0.5 and Δt = 0.0005 days for MAC (left) and FD (right), both with first-order, implicit integration schemes of ordinary and partial derivatives, respectively. Since the solutions of the two methods converge for Δt < 0.001, the solution obtained with Δt = 0.0005 days is considered the "true solution" of the system [4, 33]. For consistency, the two methods are compared on a $(\Delta x, \Delta t)$ = (0.5m, 0.5day) grid. MAC shows significantly lower numerical dispersion.

In Fig. 8, we show the simulation runtime and absolute error (defined here as the absolute value of the difference between the solution at each Δt and the true solution at Δt = 0.0005; i.e., |estimated – true| as per [4, 33]) as a function of the time step for each of the two methods. While we show the average absolute error (i.e., the L1 norm, $\sum$ |estimated – true|) over space and time in Fig. 8, we also explored the error at select time points, as well as the average squared error (i.e., the L2 norm, $\sqrt{\sum(\text{estimated} - \text{true})^2}$) since the choice of norm can be important and should reflect the goal of the computation [4, 44]. We can clearly see that, for this system, the MAC has a distinct advantage over FD and especially at larger step sizes. The error is essentially proportional to the step size, as seen in the matching slopes of the MAC and FD lines in Fig. 8B, confirming that we are dealing with first-order numerical methods [33]. By its very nature, the MAC outperforms FD, especially when steep concentration gradients occur. We note that in cases with smoother concentration gradients, the two methods showed similar accuracy, but we did not find the converse, where FD would perform better than the MAC.

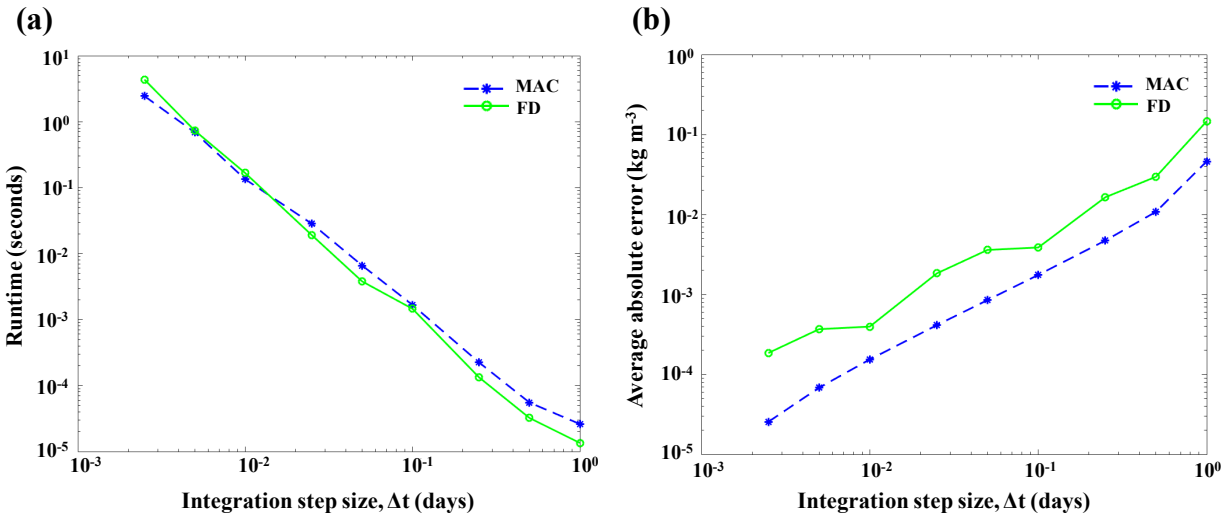

Figure 8: Comparing the method of alternating characteristics (MAC) to finite differences (FD) across a range of integration step sizes.
Comparing the method of alternating characteristics (MAC; dashed lines) to finite differences (FD; solid lines) for the example given in equation (14) using a range of integration step sizes. Both the MAC and FD are implemented with first-order, implicit integration schemes of ordinary and partial derivatives, respectively. The time step Δt is shown, while Δx is predefined for MAC by the nature of the method and thus, the same Δx was adopted for FD to ensure a fair comparison at the same resolution. (*a*) Simulation runtime and (*b*) average absolute value of the error for each Δt compared to the true solution (using an exceedingly small Δt = 0.0005 days where both methods converge to the same solution). The comparison of CPU time is made on a MacBook Air 2.2 GHz Intel Core i7 processor. For any given accuracy, the MAC can use a significantly larger time step than FD resulting in a faster runtime.

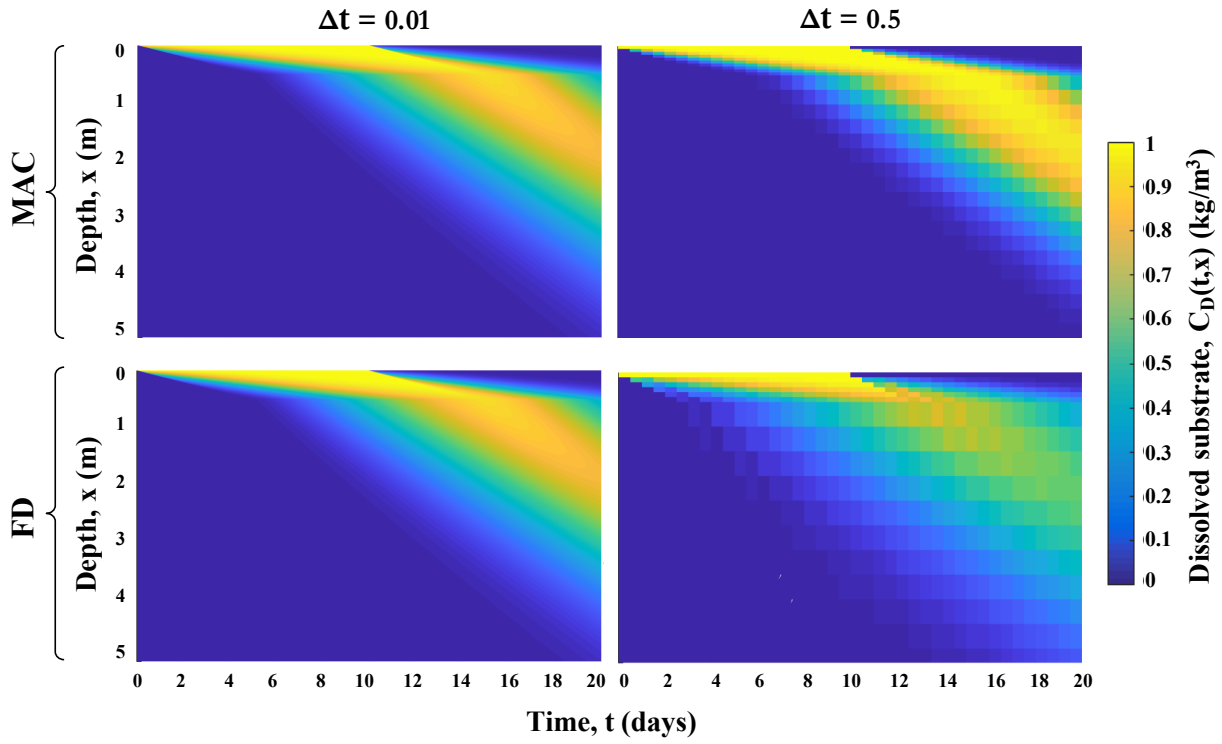

Figure 9: Solving a system undergoing an abrupt change in advection velocity with depth using the MAC and FD.
Solving the system in equation (14) with an abrupt change in advection velocity with depth (from $c = 0.1$ m day^{-1} to $c = 0.5$ m day^{-1} at 0.5m depth) using the MAC (top panels) and FD (bottom panels), both with first-order, implicit integration schemes of ordinary and partial derivatives, respectively. The solutions are compared for increasing integration time steps Δt, and corresponding Δx as defined by the MAC, from (left) Δt = 0.01 to (right) 0.5 days. Significantly more numerical dispersion is observed in the FD solution, especially for steep gradients and larger integration time steps.

While we have thus far explored a numerical example with constant advective velocity, the properties of the medium (e.g., mineralogy and porosity of soil) generally vary with depth [1, 36]. It is also possible to have rough coefficients with depth, for example, in distinct soil horizons (i.e., layers) [30, 36]. A system with heterogeneous coefficients may be more naturally handled by taking advantage of the physics in the MAC solution. A numerical example is presented in Fig. 9, where an abrupt change in the advective velocity occurs with depth. The FD solution results in significant numerical dispersion, especially with steep velocities and large time steps, as seen by comparing the right-hand panels of Fig. 9.

Depth-resolved biogeochemical cycling in soil

We now apply the MAC to a depth-resolved soil carbon model that includes four pools of organic carbon to a depth of 1 meter. These pools include the carbon in *polymeric soil organic matter* (C_S), *dissolved organic matter* (C_D) that leaches down the soil profile with a water transport velocity (c), *microbial biomass carbon* (C_B), and *mineral-associated organic matter* (C_q). The temporal and spatial evolution of these four dependent variables is dictated by

$$\frac{\partial C_S(t,x)}{\partial t} = \underbrace{-\left(\frac{V_{max}\, C_B\, C_S}{K_m + C_S}\right)}_{\text{decomposition}} + \underbrace{k_B C_B}_{\text{mortality}} \tag{15a}$$

$$\frac{\partial C_D(t,x)}{\partial t} = \underbrace{\left(\frac{V_{max}\, C_B\, C_S}{K_m + C_S}\right)}_{\text{decomposition}} - \underbrace{\left(\frac{V_{max,U}\, C_B\, C_D}{K_{m,U} + C_D}\right)}_{\text{uptake}} - \underbrace{k_{ads}\, C_D\, (q_{max} - C_q)}_{\text{adsorption}} + \underbrace{k_{des}\, C_q}_{\text{desorption}} - \underbrace{c\, \frac{\partial (C_D)}{\partial x}}_{\text{leaching}} \tag{15b}$$

$$\frac{\partial C_B(t,x)}{\partial t} = \underbrace{\varepsilon \left(\frac{V_{max,U}\, C_B\, C_D}{K_{m,U} + C_D}\right)}_{\text{uptake}} - \underbrace{k_B C_B}_{\text{mortality}} \tag{15c}$$

$$\frac{\partial C_q(t,x)}{\partial t} = \underbrace{k_{ads}\, C_D\, (q_{max} - C_q)}_{\text{adsorption}} - \underbrace{k_{des}\, C_q}_{\text{desorption}} \tag{15d}$$

where all functions depend on time t and depth x. The nonlinear functions of C_S, C_D, C_B, and C_q represent various chemical and biological reactions, including soil organic matter decomposition, uptake of dissolved organic matter into microbial biomass, and organo-mineral adsorption (see schematic in Fig. 10).

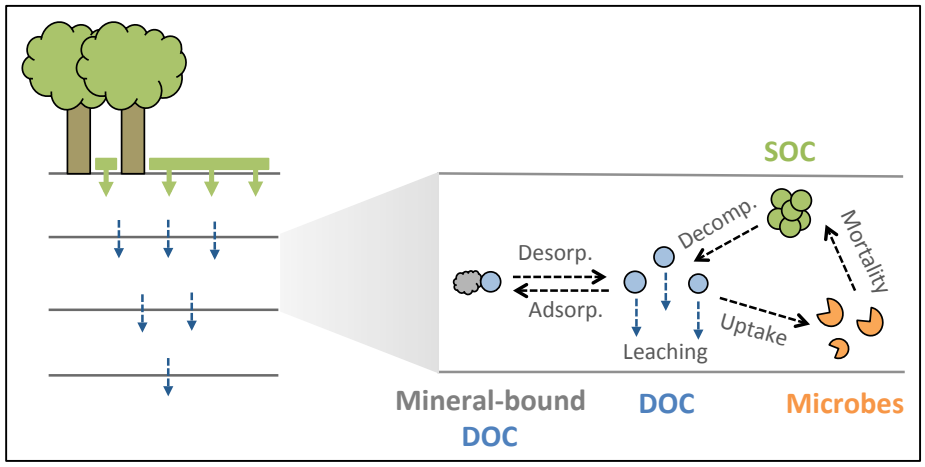

Figure 10: Schematic of depth-resolved soil carbon cycling.
Schematic of depth-resolved soil carbon cycling with dissolved organic carbon (DOC) leaching vertically through the soil profile while undergoing various chemical (i.e., desorption and adsorption with minerals) and biological (e.g., decomposition and uptake by microbial and enzymatic activity) reactions. The key constituents depicted and modeled here in addition to DOC are mineral-bound DOC, soil organic carbon (SOC), and microbial biomass. See equation (15) for details, including the functional form and parameters of each reaction.

We can observe that the system is, in fact, of the same form as the previous example and that of equation (1). Here u and v can be thought of as vector-valued with $\boldsymbol{u} = [C_D]$ and $\boldsymbol{v} = [C_S, C_B, C_q]$, so that there are, again, two corresponding characteristics $\dot{x}^u = c$ and $\dot{x}^v = 0$, respectively. Without loss of generality, we assume values of the parameters as reported in the literature (e.g., [1] and [27]) noting that the relative importance of each term in equation (15), as dictated by the

values of the parameters, does not affect our conclusions. The parameters V_{max}, K_m, $V_{max,U}$, $K_{m,U}$, k_B, ε, k_{ads}, k_{des}, q_{max}, and c take values of 1 day^{-1}, 250 mg C g^{-1} soil, 0.1 day^{-1}, 0.26 mg g^{-1}, 0.005 day^{-1}, 0.31, 1 (mg/g)$^{-1}$ day^{-1}, 0.02 day^{-1}, 1.5 mg g^{-1}, 0.5 m day^{-1}, respectively (Table 1) [1, 27, 30]. Most of these parameters are derived from laboratory incubations (e.g., k_{ads}, k_{des}, and q_{max} via sorption isotherm experiments [30] and ε via measurements of microbial growth and respiration [40]) and the remaining parameters are statistically fit to match overall pool sizes (i.e., C_S, C_D, C_B, and C_q) at the field site of interest [1, 27]. We note that the estimation of these parameters, and the final model structure, depends largely on the application. We therefore use these parameters to illustrate the implementation of this method, and this analysis should be taken in that spirit.

Table 1: Parameters for the model used for depth-resolved soil carbon cycling.
The parameters of the model in equation (15) are V_{max}, K_m, $V_{max,U}$, $K_{m,U}$, k_B, ε, k_{ads}, k_{des}, q_{max}, and c and were, without loss of generality, assumed to take the values given in the table. Here we adopt parameters from recent publications [1, 27, 30] and recognize that in each application these values will be estimated from observations.

Parameter	Description	Value
$\boldsymbol{V_{max}}$	Maximum decomposition (depolymerization) rate	1 day^{-1}
$\boldsymbol{K_m}$	Half-saturation constant for decomposition	250 mg g^{-1}
$\boldsymbol{V_{max,U}}$	Maximum assimilation rate	0.1 day^{-1}
$\boldsymbol{K_{m,U}}$	Half-saturation constant for assimilation	0.26 mg g^{-1}
$\boldsymbol{k_B}$	Mortality rate of microbes	0.005 day^{-1}
$\boldsymbol{\varepsilon}$	Carbon use efficiency of microbes	0.31
$\boldsymbol{k_{ads}}$	Adsorption rate	1 (mg/g)$^{-1}$ day^{-1}
$\boldsymbol{k_{des}}$	Desorption rate	0.02 day^{-1}
$\boldsymbol{q_{max}}$	Maximum adsorption capacity	1.5 mg g^{-1}
$\boldsymbol{c}$	Average pore water velocity	0.5 m day^{-1}

Integrating equation (15) with MAC and FD (both with first-order integration schemes of ordinary and partial derivatives, respectively) across a range of time steps (Δt = 0.01, 0.05, 0.1, 0.25, 0.5) with corresponding spatial steps (Δx) as defined by MAC, we show the resulting transient and steady-state total soil carbon ($C_S + C_D + C_B + C_q$) profiles in Fig. 11. It is clear that the MAC approaches the steady-state faster and with greater accuracy than FD. This is also illustrated in Fig. 12 and Fig. 13, where we show the percent absolute error of the MAC and FD solutions as compared to the true solution (i.e., $100 \cdot |\text{estimated} - \text{true}|/\text{true}$) for a range of time steps Δt. For this example, we conclude that the MAC outperforms FD in accuracy, stability, and speed, especially at larger time steps.

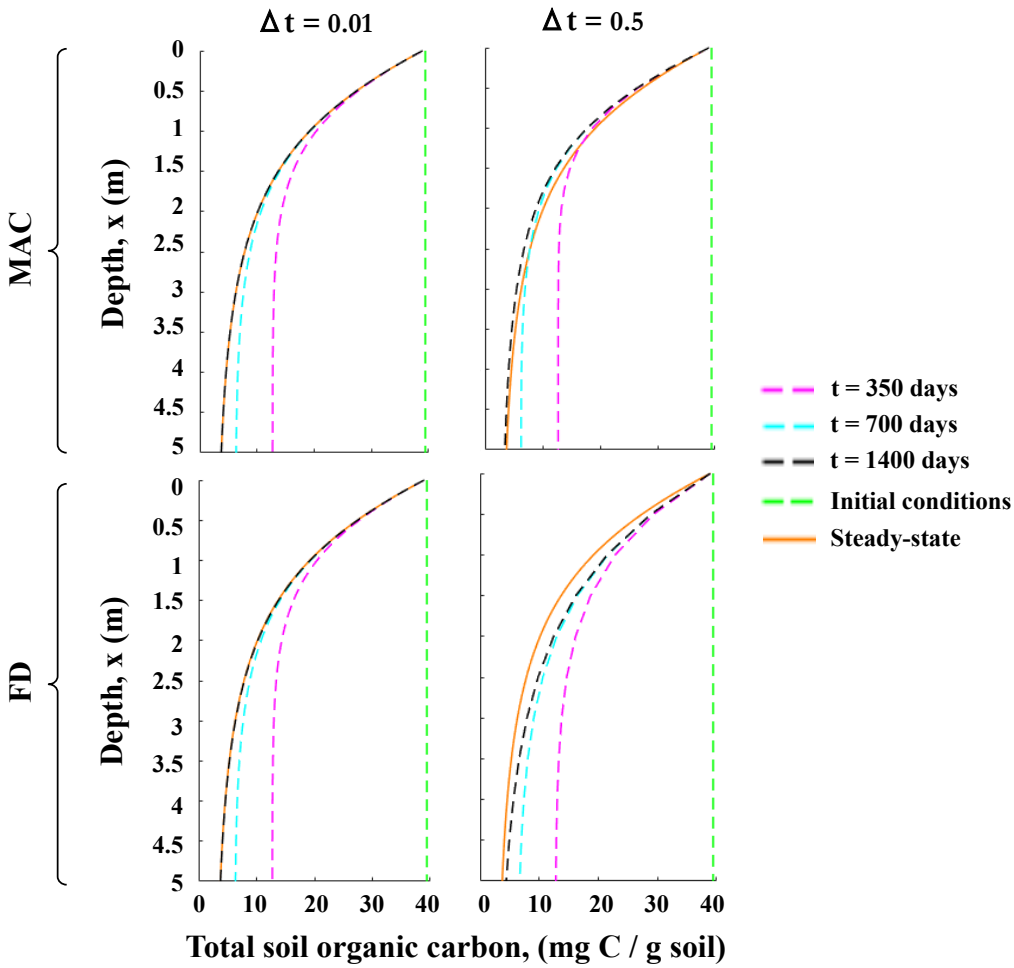

Figure 11: Total soil organic carbon profile as integrated with the MAC and FD.
Total soil organic carbon ($C_S + C_D + C_B + C_q$) profile at t = 350, 700, 1150, and 1400 days, as integrated from equation (15) with the MAC and FD for Δt = 0.01 and 0.5 days, and corresponding Δx as defined by the MAC. Both the MAC and FD are implemented with first-order, implicit integration schemes of ordinary and partial derivatives, respectively, to allow for a direct comparison. Initial conditions and the steady-state solution are shown for reference.

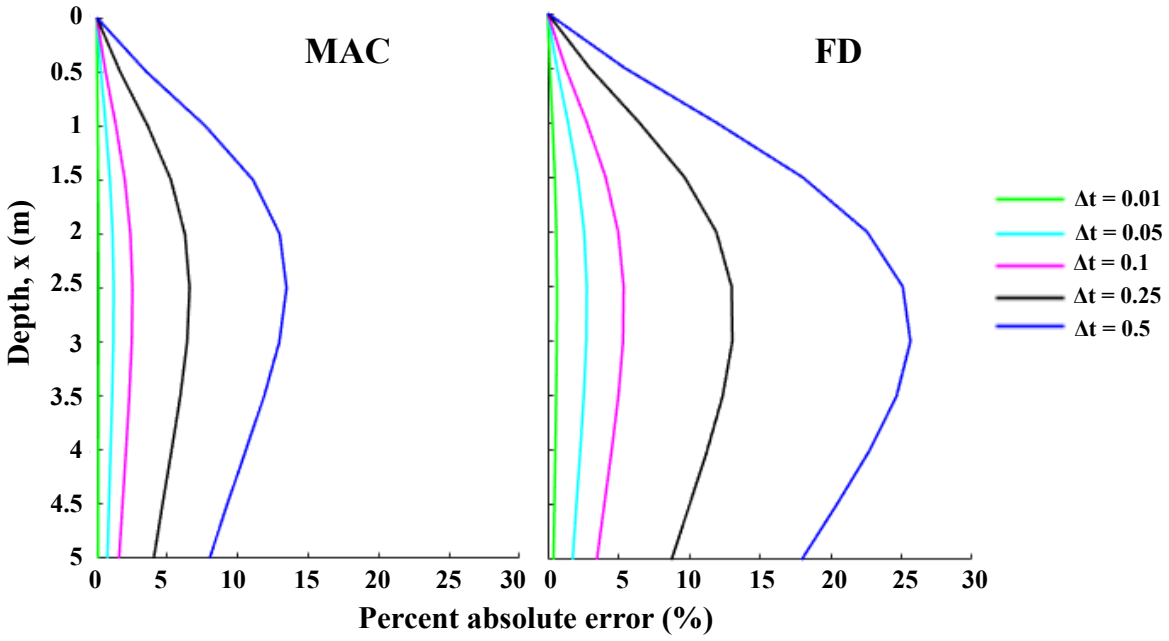

Figure 12: Percent absolute errors obtained from comparing the MAC and FD solutions of the total soil organic carbon profile to the true solution.

Percent absolute errors obtained from comparing the MAC and FD solutions of the total soil organic carbon ($C_S + C_D + C_B + C_q$) profile to the true solution at t = 1400 days. The methods converge to the same solution at small enough time steps Δt < 0.005 days and, therefore, this is considered as the true solution and is used to compare the methods across increasing Δt = 0.01, 0.05, 0.1, 0.25, 0.5 day integration time steps, with the corresponding Δx as defined by the MAC. Both the MAC and FD are implemented with first-order, implicit integration schemes.

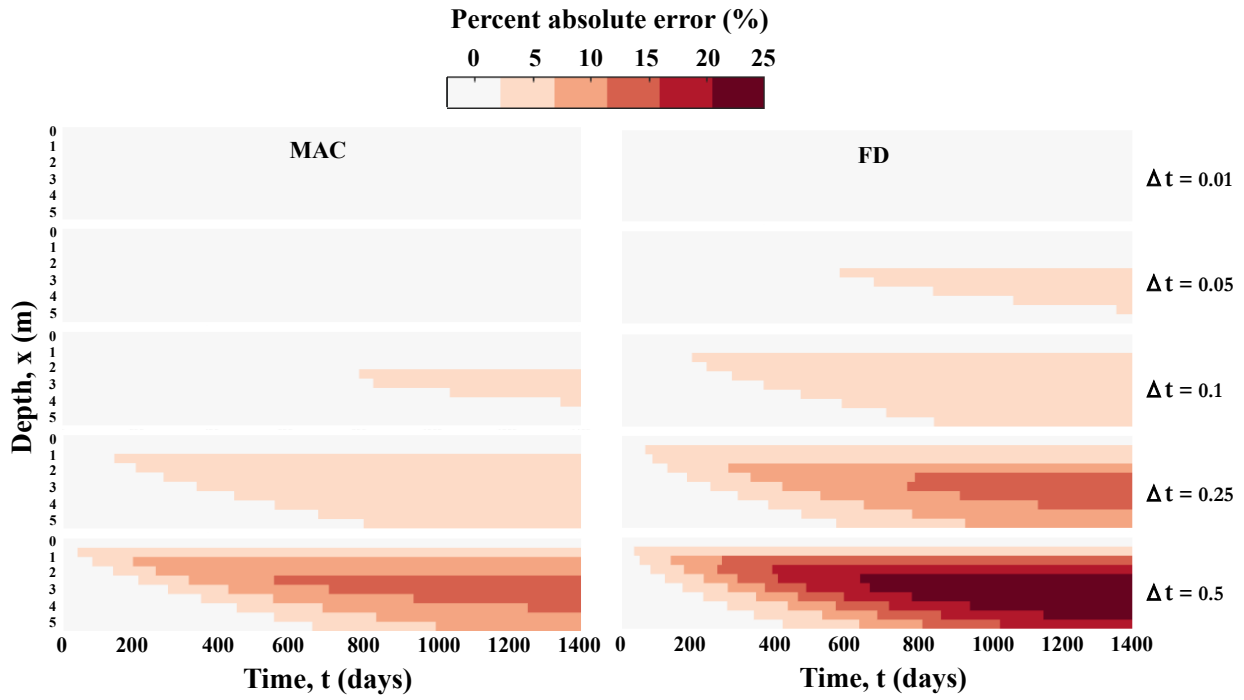

Figure 13: Spatiotemporal evolution of percent absolute error of the first-order, implicit MAC and FD across space and time.
Spatiotemporal evolution of percent absolute error of MAC and FD, calculated by comparing the total soil organic carbon ($C_S + C_D + C_B + C_q$) across space and time to the true solution. The two methods were implemented with Δt = 0.01, 0.05, 0.1, 0.25, 0.5 day time steps and corresponding Δx as defined by the MAC. All solutions are shown on a $(\Delta x, \Delta t)$ = (0.5m, 0.5day) grid for direct comparison.

Discussion & Conclusions

We have presented a method for solving systems of advection-dominated PDEs in which all partial derivatives appear in linear expressions, as in many reactive transport models. The proposed method, termed the *Method of Alternating Characteristics* (MAC), is based on alternating between characteristic directions of the equations, such that a system of PDEs can be sequentially integrated, one step at a time, as ODEs along corresponding directions. We described extensions of this method to systems with two or more characteristics, spatially- and temporally- varying characteristics, and more than one spatial dimension. Finally, we presented two numerical examples, including applications to contaminant transport with mineral adsorption in a porous medium and to soil carbon cycling. The key is that only a subset of the chemical constituents undergo advection, while the remaining constituents are stationary. This scenario arises naturally when a compound can be leached through a porous medium in its dissolved state, for example, but cannot be advected once adsorbed to the surrounding medium.

We compared the MAC using the first-order, implicit Euler method for ODE integration to the standard first-order, implicit upwind finite-difference scheme for PDE integration in space and time [12, 33], and demonstrated that the MAC is substantially more accurate for a given grid resolution or simulation runtime (Fig. 8). More specifically, because the solutions of advection-dominated PDEs are smoother along their characteristics than in the time direction, the MAC can

use larger time steps while maintaining stability and accuracy. This fact is especially true for situations with steep concentration profiles. For such a case, we found that the MAC has a significant advantage in performance with regards to simulation time as well.

In implementing finite-difference schemes, we have not implemented additional advances, e.g., that improve stability [9, 18, 28, 31, 39]. Further, besides stability, when implementing finite-difference schemes, it is also important to preserve conserved quantities if that is the case [19, 26, 34]. This last point has not been considered in the current paper either. However, we anticipate that both, improved stability and conservation, can be suitably addressed since MAC in essence reduces to integration of ODEs. This is a topic of current interest and research.

Our point in the present paper has been to highlight the potential advantages of the proposed method and underscore the suitability for advection-dominated environmental systems with biogeochemical reactions. We expect that the proposed MAC will be useful to other fields of study in which time-dependent advection-dominated PDEs arise, such as air pollution (e.g., atmospheric pollutant transport), geomorphology and geochemistry (e.g., sediment and contaminant transport [5-6, 16, 41]), ecology (e.g., population densities of drift-prone aquatic species [10]), and engineering applications.

References

[1] Ahrens, B., Braakhekke, M.C., Guggenberger, G., Schrumpf, M., Reichstein, M.: Contribution of sorption, DOC transport and microbial interactions to the 14C age of a soil organic carbon profile: Insights from a calibrated process model. Soil Biol. & Biochem. **88**, 390-402 (2015)

[2] Allison, S.D., Wallenstein, M.D., Bradford, M.A.: Soil-carbon response to warming dependent on microbial physiology. Nature Geosci. **3**, 336-340 (2010)

[3] Arbogast, T., Wheeler, M.F.: A characteristics-mixed finite element method for advection-dominated transport problems, SIAM J. Numer. Anal. **32**, 404–424 (1995)

[4] Arnold, D.N.: Stability, consistency, and convergence of numerical discretizations. Encyclopedia of App. and Comput. Mathematics. Springer-Verlag, pp. 1358-1364 (2015)

[5] Centler, F., Shao, H., Park, C.-H., de Biase, C., Kolditz, O., Thullner, M.: GeoSysBRNS – a flexible multi-dimensional reactive transport model for simulating biogeochemical subsurface processes. Comput. Geosci. **36**, 397–405 (2010)

[6] Chiang, C.Y., Wheeler, M.F., Bedient, P.B.: A modified method of characteristics technique and mixed finite elements method for simulation of groundwater solute transport. Water Resour. Res. **25**, 1541-1549 (1989)

[7] Douglas Jr., J.: Simulation of miscible displacement in porous media by a modified method of characteristic procedure, in: Numerical Analysis, Springer, Berlin/Heidelberg, pp. 64–70 (1982)

[8] Douglas Jr., J., Russell, T.F.: Numerical methods for convection-dominated diffusion problems based on combining the method of characteristics with finite element or finite difference procedures, SIAM J. Numer. Anal. **19**, 871–885 (1982)

[9] Donea, J., Quartapelle, L.: An introduction to finite element methods for transient advection problems. Comp. Methods in App. Mech. and Eng., **95**, 169-203 (1992)

[10] Downes, B.J., Lancaster, J.: Does dispersal control population densities in advection-dominated systems? A fresh look at critical assumptions and a direct test. Journal of Animal Ecology. **79**, 235-248 (2010)

[11] Ewing, R.E.: Simulation of multiphase flows in porous media. Transport in Porous Media. **6**, 479-499 (1991)

[12] Ewing, R.E., Wang, H.: A summary of numerical methods for time-dependent advection-dominated partial differential equations. Journal of Computational and Applied Mathematics. **128**, 423-445 (2001)

[13] Ewing, R.E., Russell, T.F., Wheeler, M.F.: Convergence analysis of an approximation of miscible displacement in porous media by mixed finite elements and a modified method of characteristics. Comput. Methods Appl. Mech. Eng. **47** 73–92 (1984)

[14] Fang, Y.L., Yabusaki, S.B., Yeh, G.T.: A general simulator for reaction-based biogeochemical processes. Comput. Geosci. **32**, 64–72 (2006)

[15] Frei, S., Knorr, K.H., Peiffer, S., Fleckenstein, J.H.: Surface micro-topography causes hot spots of biogeochemical activity in wetland systems: A virtual modeling experiment. J. of Geophys. Res. **117**, 1-18 (2012)

[16] Gruber, J.: Contaminant accumulation during transport through porous media. Water Resour. Res. **26**, 99-107 (1990)

[17] Hararuk, O., Smith, M.J., Luo Y. Microbial models with data-driven parameters predict stronger soil carbon responses to climate change. Global Change Biol. **21**, 2439–2453 (2015)

[18] Harten, A., Engquist, B., Osher, S., Chakravarthy, S.R.: Uniformly high order accurate non-oscillatory schemes, III. J. of Comput. Phys., **71**, 231-303 (1987)
[19] Ham, F. E., Lien, F. S., Strong, A. B.: A Fully Conservative Second-Order Finite Difference Scheme for Incompressible Flow on Nonuniform Grids. J. of Comput. Phys. **177,** 117–133 (2002)
[20] Holstad, A.: A mathematical and numerical model for reactive fluid flow systems. Comput. Geosci. **4**, 103-139 (2000)
[21] Knabner P.: Finite-element-approximation of solute transport in porous media with general adsorption processes. In: Flow and Transport in Porous Media, (ed.) S.-T. Xiao, pp. 223-292, World Scientific Publishing, Singapore (1992)
[22] Knabner, P., Totsche K.U., Kögel-Knabner, I.: The modeling of reactive solute transport with sorption to mobile and immobile sorbents. 1. Experimental evidence and model development. Water Resour. Res. **32**, 1611-1622 (1996)
[23] Knabner, P., Igler, B. A., Totsche, K. U., DuChateau, P.: Unbiased identification of nonlinear sorption characteristics by soil column breakthrough experiments. Comput. Geosci. **9**, 203-217 (2005)
[24] Lakoba, T.: Method of characteristics for solving hyperbolic PDEs, University of Vermont. http://www.cems.uvm.edu/~tlakoba/math337/notes_17.pdf. Accessed 11 April 2016.
[25] Lele, S.K.: Compact finite difference schemes with spectral-like resolution. J. of Comput. Phys. **103**, 16-42 (1992)
[26] Leveque R.: Finite volume methods for hyperbolic problems. Cambridge University Press (2002)
[27] Li, J., Wang, G., Allison, S.D., Mayes, M.A., Luo ,Y.: Soil carbon sensitivity to temperature and carbon use efficiency compared across microbial-ecosystem models of varying complexity. Biogeochem. **119**, 67-84 (2014)
[28] Liu, X.D., Osher, S., Chan, T.: Weighted essentially non-oscillatory schemes. J. of Comput. Phys., **115**, 200-212 (1994)
[29] Matzner, E., Zuber, T., Alewell, C. Lischeid, G., Moritz, K.: Trends in deposition and canopy leaching of mineral elements as indicated by bulk deposition and throughfall measurements. In: Matzner, E. (Ed.) Biogeochemistry of Forested Catchments in a Changing Environment. Springer, Berlin Heidelberg, pp. 233-250 (2014)
[30] Mayes, M.A., Heal, K.R., Brandt, C.C., Phillips, J.R., Jardine, P.M.: Relation between soil order and sorption of dissolved organic carbon in temperate subsoils. Soil Sci. Soc. of Am. J. **76**, 1027-1037 (2011)
[31] Mazzia, A., Putti, M.: High order Godunov mixed methods on tetrahedral meshes for density driven flow simulations in porous media. J. of Comput. Phys., **208**, 154-174 (2005)
[32] Meysman, F.J.R., Boudreau, B.P., Middelburg, J.J.: Modeling reactive transport in sediments subject to bioturbation and compaction. Geochimica et Cosmochimica Acta. **69**, 3601-3617 (2005)
[33] Olver, P.J.: Introduction to partial differential equations, Chapters 2 and 5. Springer (2014)
[34] Osher, S., Solomon, F.: Upwind Difference Schemes for Hyperbolic Systems of Conservation Laws. Mathematics of Comput. **38**, 339-374 (1982)
[35] Russel, T.F., Wheeler M.F.: Finite element and finite difference methods for continuous flow in porous media. In: The mathematics of reservoir simulation, R.E. Ewing (Ed.), SIAM, Philadelphia, PA, pp. 35-106 (1984)

[36] Riley, W.J., Maggi, F., Kleber, M., Torn, M.S., Tang, J.Y., Dwivedi, D., Guerry N.: Long residence times of rapidly decomposable soil organic matter: application of a multi-phase, multi-component, and vertically resolved model (BAMS1) to soil carbon dynamics. Geosci. Model Dev. **7**, 1335-1355 (2014)
[37] Rinaldo, A., Beven, K.J., Bertuzzo, E., Nicotina, L., Davies, J., Fiori, A., Russo, D., Botter, G. Catchment travel time distributions and water flow through in soils. Water Resour. Res. **47**, 1-13 (2011)
[38] Scovazzi, G., Wheeler, M.F., Mikelić, A., Lee, S.: Analytical and variational numerical methods for unstable miscible displacement flows in porous media. J. of Comput. Phys., **335**, 444-496 (2017)
[39] Shu, C.W., Osher, S.: Efficient implementation of essentially non-oscillatory shock-capturing schemes. J. of Comput. Phys., **77**, 439-471 (1988)
[40] Sinsabaugh, R. L., Mazoni, S., Moorhead, D. L., Richter, A.: Carbon use efficiency of microbial communities: stoichiometry, methodology and modelling. Ecology Letters, **16**, 930–939 (2013)
[41] Steefel, C.I., DePaolo, D., Lichtner, P.C.: Reactive transport modeling: An essential tool and a new research approach for the Earth sciences. Earth Planet. Sci. Lett. **240**, 539–558 (2005)
[42] Steefel, C. I., Appelo, C. A. J., Arora B. et al.: Reactive transport codes for subsurface environmental simulation. Comput. Geosci. **19**, 445–478 (2015)
[43] Strikwerda, J. C.: Finite difference schemes and partial differential equations. Wadsworth and Brooks/Cole, Pacific Grove, CA (1989)
[44] Tadmor, E.: A review of numerical methods for nonlinear partial differential equations. Bulletin of the American Mathematical Society, **49**, 507-554 (2012)
[45] Tang, J.Y., Riley, W.J., Koven, C.D., Subin, Z.M.: CLM4-BeTR, a generic biogeochemical transport and reaction module for CLM4: model development, evaluation, and application. Geosci. Model Dev. **6**, 127-140 (2013)
[46] Todd-Brown, K.E.O., et al.: Changes in soil organic carbon storage predicted by Earth system models during the 21st century. Biogeosci. **11**, 2341–2356 (2014)
[47] Weill, S., Mazzia, A.M., Putti, M., Paniconi, C.: Coupling water flow and solute transport into a physically-based surface–subsurface hydrological model. Adv. in Water Res. **34**, 128-136 (2011)
[48] Wieder, W.R., Allison, S.D., Davidson, E.A., et al.: Explicitly representing soil microbial processes in Earth system models. Global Biogeochem. Cycles. **29**, 1782-1800 (2015)
[49] Wiggert D.C., Wylie E.B.: Numerical predictions of two-dimensional transient groundwater flow by the method of characteristics. Water Resour. Res. **12**, 971-977 (1976)

CHAPTER 7: CONCLUSIONS

CONCLUSIONS

It is an exciting time to be a soil scientist. Soil is essential to life, and understanding how carbon and nutrients are cycled and stabilized is critical for informing sustainable management practices and mitigation and conservation policies. Soil can be a potential solution or a positive feedback to rising temperatures and atmospheric CO_2 concentrations. It is our responsibility to understand and maintain this critical resource for our own well-being and for the generations to come.

Below I provide additional context that highlights the broad importance and applications of this growing field, and I briefly outline plans for upcoming work.

Broader implications

"The nation that destroys its soil, destroys itself." - *Franklin Delano Roosevelt* (1937)

By 2060, the U.S. population is expected to increase from 319 million in 2014 to 417 million (U.S. Census Bureau, 2015), and with that, so will emissions and the demand for food production. Maintaining healthy soils is not only crucial to long-term environmental sustainability, but carbon sequestered in soils also has the potential to mitigate emissions. Throughout my interactions with students and the broader public, I have been heartened to see a widespread interest in soils across the political and socio-economic spectrum, and an innate understanding that soil conservation is paramount to environmental prosperity. From students to home-gardeners, ranchers, engineers, and stakeholders alike, the significance of soils is tangible. Fostering public awareness and disseminating research findings to regional and national stakeholders (e.g., through the California Healthy Soils Initiative) is key in maintaining this critical resource and leveraging it as a potential solution in carbon sequestration.

Future work

Upscaling micro-scale interactions to macro-scale models

Overarching question: How do micro-scale interactions modulate macro-scale soil C cycling?

Soil is organizationally complex and spatially heterogeneous with exceptional microbiological diversity that varies in time and space (Jackson and Caldwell, 1993; Petridis *et al.*, 2014; Mishra and Riley, 2015). Hotspots of microbial activity (e.g., in the rhizosphere; Kuzyakov and Blagodatskaya, 2015) are prevalent, yet they are patchy and periodic and it is intractable to represent this level of detail in macro-scale models. Most macro-scale microbial models have, therefore, been focused on exploring theory and capturing select processes in a simplified way. Process representations are often borrowed from micro-scales, without concern for effective, upscaled equations and parameterizations applicable at macro-scales (Fig. 1). Indeed, even key process representations are still debated (e.g., *Michaelis-Menten* versus *reverse Michaelis-Menten* kinetics for SOC decomposition; Wieder *et al.*, 2015a) and the relevant relationships may in fact depend on the intended scale. Thus, there is a need for continuum models that integrate across scales and can make process-based predictions of emergent feedbacks. Currently, the bridge between these scales is lacking.

While previous modeling studies have adopted mathematical formulations using bulk microbial biomass from a micro-scale understanding of microbial physiology (Allison, Wallenstein and Bradford, 2010; Wieder, Bonan and Allison, 2013), the mechanisms (and consequent effective equations) that operate at the community-level have not been sufficiently explored. In this dissertation, I showed that microbial community-level interactions (e.g., density-dependent microbial turnover) are essential for capturing the response of bulk SOC stocks to long-term litter manipulations, and that simply extrapolating process representations from micro- to macro-scale models can lead to unrealistic behaviors. These findings motivate additional research on scaling, and illustrate the large implications that scale-dependent formulations can have on global carbon-concentration feedbacks. I will continue to explore how soil microbial processes regulate macro-scale SOC cycling through integrating empirical and computational insights across spatiotemporal scales to bridge the gap between micro- and macro-scale soil biogeochemical models.

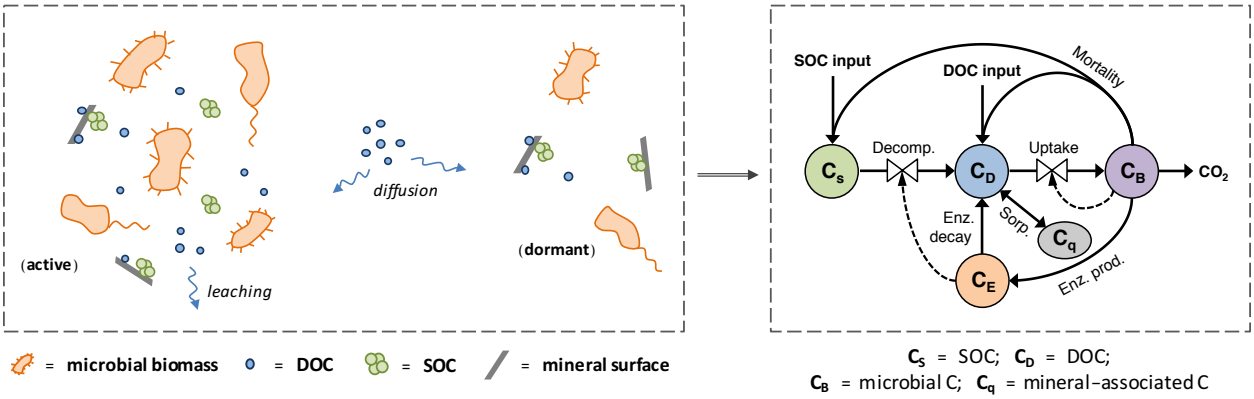

Figure 1: Scaling considerations and challenges in soil C modeling.
There is an urgent need to bridge the gap between our micro-scale understanding (left panel) and effective representations in bulk, pool-based models (right panel).

References

Allison, S. D., Wallenstein, M. D. and Bradford, M. A. (2010) 'Soil-carbon response to warming dependent on microbial physiology', *Nature Geoscience*. Nature Publishing Group, 3(5), pp. 336–340. doi: 10.1038/ngeo846.

Jackson, R. B. and Caldwell, M. M. (1993) 'Geostatistical patterns of soil heterogeneity around individual perennial plants', *Journal of Ecology*, 81(81), pp. 683–692. doi: 10.2307/2261666.

Kuzyakov, Y. and Blagodatskaya, E. (2015) 'Microbial hotspots and hot moments in soil: Concept & review', *Soil Biology and Biochemistry*. Elsevier Ltd, 83, pp. 184–199. doi: 10.1016/j.soilbio.2015.01.025.

Mishra, U. and Riley, W. J. (2015) 'Scaling impacts on environmental controls and spatial heterogeneity of soil organic carbon stocks', *Biogeosciences*, 12(13), pp. 3993–4004. doi: 10.5194/bg-12-3993-2015.

Petridis, L., Ambaye, H., Jagadamma, S., Kilbey, S. M., Lokitz, B. S., Lauter, V. and Mayes, M. A. (2014) 'Spatial arrangement of organic compounds on a model mineral surface: Implications for soil organic matter stabilization', *Environmental Science and Technology*, 48(1), pp. 79–84. doi: 10.1021/es403430k.

Wieder, W. R., Allison, S. D., Davidson, E. A., Georgiou, K. and Hararuk, O. (2015) 'Explicitly representing soil microbial processes in Earth system models', *Global Biogeochemical Cycles*, 29, pp. 1782–1800.

Wieder, W. R., Bonan, G. B. and Allison, S. D. (2013) 'Global soil carbon projections are improved by modelling microbial processes', *Nature Climate Change*, pp. 1–7.